GoNEXUS
Integrated solutions for water, energy, food and ecosystems

Reference Basin scale WEFE nexus evidence

Deliverable D5.6 – WP5, August 2024

www.gonexus.eu

Version 4.0

August, 2024

Deliverable D5.6: Reference Basin scale WEFE nexus evidence

Lead by ETH Zurich

ETHZ, UPV, ULAVAL, POLIMI, UU, ADELPHI, UPM, ZAMCOM, UCAD, OMVS, FAMIFE

Dissemination level of document

Public.

Abstract

This deliverable reports the first results of task 5.4, presenting relevant WEFE evidence for the reference scenario (current climate and policies) at the local and river basin scales.

Version history

Version	Date	Author(s)	Comment
V0.1	2023-11-15	S. Sinclair (ETHZ)	Initial draft outline
V0.2	2024-07-14	P. Burlando (ETHZ)	Added additional content (various sections)
	2024-07	H. Macian Sorribes, D Martinez Domingo, I.G. Lagos Castro (UPV), A. Tilmant (ULAVAL), D. Mayer, S. Sinclair (ETHZ), R. van Beek (UU)	Added content for sections on Senegal, Jucar, Tagus-Segura River, Zambezi, Lake Como and Danube case studies.
V1.0	2024-07-30	P. Burlando (ETHZ)	Harmonisation of contributions, review and highlight of missing content
V1.0	2024-08-09	R. van Beek (UU)	Review and commenting
V2.0	2024-08-11	P. Burlando (ETHZ)	Harmonisation of contributions
V2.0	2024-08-12	M. Häfliger, S. Sinclair (ETHZ)	Added content on Lake Como
V3.0	2024-08-14	P. Burlando (ETHZ)	Harmonisation of contributions
V3.0	2024-08-22	H. Macian Sorribes, D Martinez Domingo, I.G. Lagos Castro (UPV)	Update of contribution for sections on Senegal, Jucar, Tagus-Segura River
V4.0	2024-08-23	P. Burlando (ETHZ)	Finalisation of the deliverable

Table of contents

1 Introduction

This deliverable reports the first results of task 5.4. It includes the evidence for the reference scenario (current climate and policies) at the local and river basin scales using the Solutions Assessment Framework (SAF) to characterize the WEFE nexus from a multi-attribute perspective, revealing trade-offs and synergies existing in the reference basin-scale scenario. The target audiences are the GoNEXUS partners, scientists working on basin-scale WEFE modelling, and regional and local WEFE stakeholders. The content of this report will be used in Tasks 6.1 and 6.2 to inform the dialogues, in particular to discuss the portfolio of solutions to improve the management of WEFE issues that emerged from the evidence analysis.

2 Description of reference period and scenarios

The basin scale WEFE evidence reported here uses the terminology of a "Reference Period" instead of "Baseline" to avoid confusion with observed history or reanalysis, and in an effort to be more consistent with the definitions used by the IPCC Sixth Assessment Report (IPCC, 2022). During the reference period, the basin models are forced by down-scaled climate data based on the historical simulations of CMIP6 GCMs (1979-2014), which refers to the historical period simulated with GCMs, not simulated with observed/re-analysis data. It includes historical changes in demands in the models. Figure 1 provides a visual characterisation of the scenarios used to drive the evidence modelling reported in this deliverable.

In some case studies where the modelling efforts are sufficiently advanced, the reference period evidence is contrasted with evidence from future global socio-economic scenarios (SSP186, SSP370 and SSP585 in Figure 1) that do not yet include solutions (evidence from the full suite of future scenarios, both with and without solutions, will be reported in deliverable D5.7). Moreover, some of the case studies adopted scenario variants that slightly deviate from the common reference as detailed in the specific sections of each case study. This was deemed to be appropriate to cope better with the challenges emerged from the dialogues than it would have been possible with a strict use of reference scenarios.

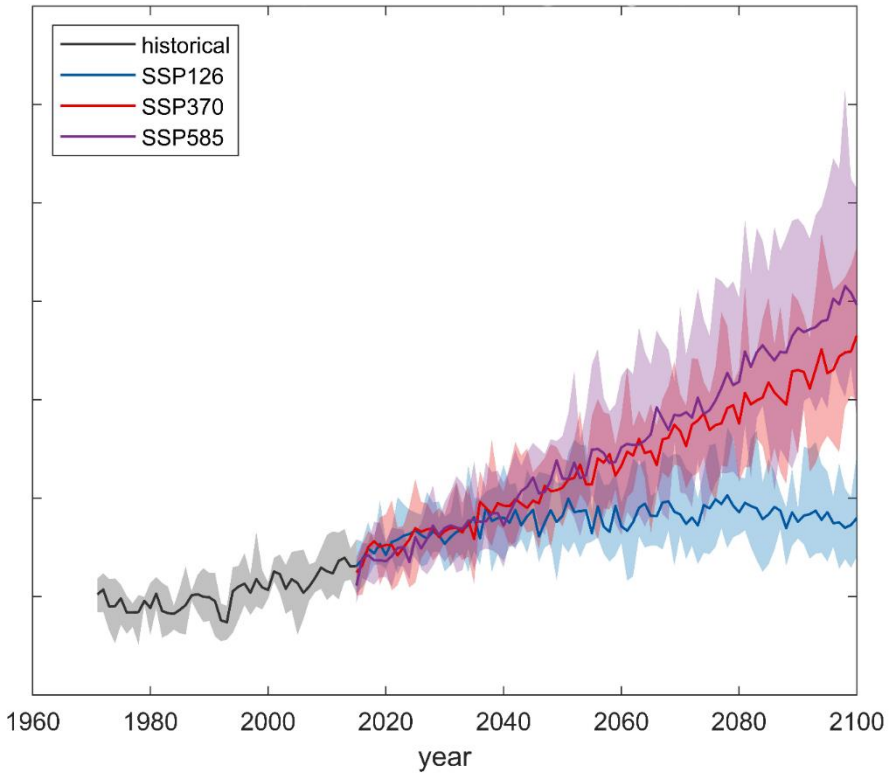

Figure 1. Illustration of the GoNEXUS reference period – historical period climate simulations from selected CMIP6 models, downscaled for the basin case studies using appropriate methodologies depending on the case study (solid black line model mean, and grey shaded region model spread). Also illustrated SSP126, SSP370, and SSP585 as examples of scenarios with WEFE indicators that can be contrasted with equivalent indicators from the reference period (solid lines mean across models, and shaded regions model spread).

3 Basin scale WEFE evidence

The WEFE evidence at basin scale was investigated for the six case studies using the different models from GoNEXUS' model toolbox. In the following sections we summarise for each case study the key elements characterising the case study and the most significant results from the evidence simulation, also providing a summary of the key evidence that will lead, respectively led, to the identification of solutions, which will be implemented in the next round of simulations to investigate their impact on the WEFE challenges.

3.1 Zambezi Watercourse

The Zambezi Watercourse is located in south-eastern Africa, originates in eastern Angola and northwest Zambia, spans an extensive 1.4 million square kilometres and flows for 2,700 km through plains, gorges, and marshlands, with an average annual discharge of 2,600 m^3/s into the delta in Mozambique. It is the fourth largest basin of Africa, is shared by eight countries (Angola, Botswana, Malawi, Mozambique, Namibia, Tanzania, Zambia, and Zimbabwe) and

populated by around 40 million inhabitants (Figure 2) The climate of the Zambezi Watercourse follows a seasonal pattern associated with the Intertropical Convergence Zone: a rainy season from November to April and a dry season from May to October. While the average annual rainfall in the basin is high (950 mm/year), it is unevenly distributed across the basin, Moreover, the interannual variability is substantial: up to 1,400 mm/year are observed in the northern and eastern parts of the basin, whereas 400 mm/year characterizes the southern and western regions. A large amount of water is lost by evaporation due to the high evaporation rates. Whereas the source of the Zambezi is in the humid tropical climate zones and hence discharges water on a continuous basis, the pronounced seasonality of rainfall at more southern latitudes introduces greater variability of the seasonal discharge regime. Information on groundwater resources in the Zambezi Watercourse is relatively scarce so that water availability from groundwater bodies cannot be properly quantified even at coarse temporal and spatial scales. Finally, the basin is home to many wetlands, which provide a broad range of ecosystem services. The basin has a large hydropower potential and the world's largest artificial reservoir, Lake Kariba. The basin's management operates internationally under the cooperative 2004 ZAMCOM agreement and a sustainable water resources management is vital.

Figure 2. Four dams and six power plants currently in operation and 8 irrigation abstraction locations representing 182,000 ha of irrigated areas in the Zambezi Watercourse (Giuliani et al., 2022).

3.1.1 Overview of Challenges, Models, and Indicators

Based on outcomes from the former EU project DAFNE and on exchange with stakeholders during the first and second dialogue the main challenges were identified in relation to (*i*) flood risks throughout the entire basin and at specific locations, (*ii*) water scarcity and drought risk in the main agricultural districts and at hydropower systems, (*iii*) deforestation and soil erosion following harvesting of trees to produce charcoal, and (*iv*) impact of streamflow regulation on aquatic ecosystems. All of the challenges point at the strong nexus among the key

water users and at the importance of modelling and analysing the trade-offs, searching for a sustainable management of the resource nexus. More specific challenge details – e.g. critical locations – are reported in the deliverable D5.1.

The sustainable development in the Zambezi basin requires the consideration of various WEFE nexus issues and trade-offs. Three modelling approaches – High Resolution WEFE Modelling (Topwatch), Many-Objective Robust Decision Making (MORDM), and System Dynamics (SD) Modelling – are applied to evaluate the WEFE nexus. MORDM and Topwatch represent a joint modelling system in that MORDM is an optimization based strategic model, which operates on a coarse scale and focusing on key sectoral indicators with the purpose of identifying the most suitable management policies, whereas Topwatch is a spatially distributed, physically explicit and high space-time resolution model, which is able to simulate the impact of the MORDM selected policies in great spatial and temporal detail and computing a broader set of indicators. The SD model developed for the Zambezi Watercourse is intended to represent water management using simple reservoir operating rules. The use of simple operating rules could provide an alternative to the use of more complex functions, given that they could be easier to communicate to the stakeholders and to be implemented by the reservoir managers. Details of the models are provided in deliverable D4.1.

3.1.2 Evidence simulations results

A set of main indicators was selected from a wider pool from previous projects during the first dialogue and confirmed during the second dialogue. These indicators directly address key WEFE challenges. Some of them represent strategic metrics that were used in the optimisation runs of MORDM to quantify the nexus across the main water use sectors. A broader set was conversely selected for use with Topwatch and aiming to evaluate the impact of selected policies at those key locations in the basin, which were highlighted by stakeholders in the two dialogues as hotspots. The main sectors targeted by the indicators are related to hydropower production, agriculture, hydrologic risks (floods and droughts), sediment dynamics and environmental flow indicators. A comprehensive list and description is available in D5.1 "Indicators and Sustainability Assessment Framework"

For the reference evidence simulations in the Zambezi Watercourse reported here we focus mainly on evidence for the flood and drought challenges, based on high-resolution Topwatch simulations driven by the reference scenario and the current water management strategy. The evidence derived from MORDM planning and operations policies will feature more heavily in the evidence simulations that include solutions (i.e. water management and allocation strategies and implementation actions) to be reported in deliverable D5.7.

Flood frequency under climate change

The flood frequency analysis was performed following the U.S. Geological Survey Guidelines for "Determining Flood Flow Frequency - Bulletin 17C" (England et al., 2018). The dataset for each of the five climate models under the three scenarios was divided into three distinct periods: historical reference (1980-2013), mid-century (2016-2057), and end-century (2058-2099). Separate flood frequency analyses were carried out for each period in accordance with the guidelines. To improve the trend analysis, each future period was later further divided

into two intervals. As all data were simulated, no quality control procedures were considered necessary.

Table 1. Daily streamflow calibration and validation periods used for the Great East Road and Itezhi Tezhi sub-catchments.

	Calibration period	Validation period
Great East Road	01.01.1981 - 31.12.1986	01.01.1987 - 31.12.1993
Itezhi Tezhi	01.01.1981 - 31.12.1997	01.01.1998 - 30.01.2018

The models were calibrated to observed daily streamflow records (see Table 1 for the relevant periods, more details of the calibration and validation results are reported in deliverable D3.3). However, since the flood frequency distributions were only fitted to the annual maxima of daily flows, an independent verification was carried out as shown in Figure 3. The frequency distributions for observed annual maxima were compared with those simulated during the historical reference period for each down-scaled climate model to check whether the climate model driven simulations could capture a reasonable distribution of flood peaks compared to that derived from observations.

For Great East Road the climate models are able to approximate the discharge magnitude, with the observed maxima sequence falling within the range of the climate model-based simulations, as illustrated in Figure 3(a). Flood magnitudes were captured well over a broad range of exceedance probability; however the highest frequency floods were overestimated by all the climate models. Since these more common events are of lower magnitude and therefore have less consequences, this was considered as reasonable. In Itezhi Tezhi, the flood frequency distribution of the observed discharge falls within the range of those simulated by different climate models for most exceedance probabilities (see Figure 3(b)). Most models predict higher flood magnitudes than observed, for both high and low frequency events. Climate models "mpi-esm1-2-hr" and "mri-esm2-0" show the closest agreement with observed peak flows. This gives greater confidence in their predictions for Itezhi Tehzi, compared with simulations by the other climate models.

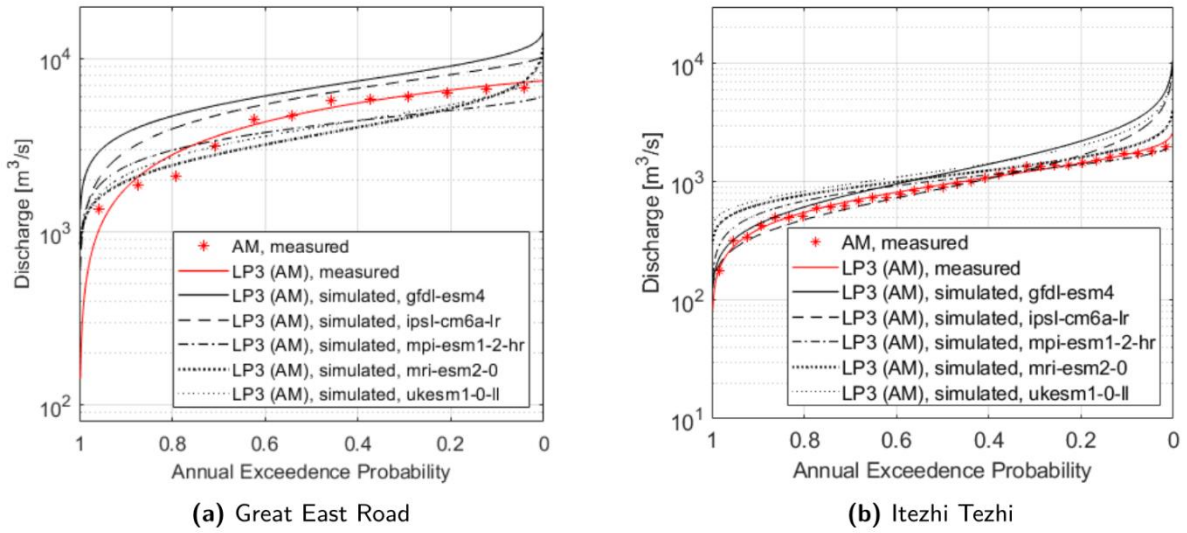

Figure 3. Comparison of the simulated (black) and observed (red) flood frequency distribution for the historical period of Great East Road and Itezhi Tezhi. Included are all the years, with at least 80% data availability during the wet season in the period of 1980 - 1992 for Great East Road and the period of 1980 - 2013 for Itezhi Tezhi. The flood frequency analysis was conducted by fitting a Log-Pearson Type-lll (LP3) to the annual maximum AM of each year.

Since the historical reference period flood frequency distributions give a good representation of observed conditions, it was feasible to compare the reference to future distributions for mid- and late-century over the three climate scenarios. The results are shown in Figure 4 for Great East Road, and Figure 5 for Itezhi Tezhi.

The common behaviour shown in Figure 4 and in Figure 5 is a tendency towards lower flood magnitudes for the most common (high exceedance probability) events across all models at mid-century. This effect intensifies in the end of century time period.

The second impact under all climate scenarios (but stronger for certain models, and under SSP370/SSP585 forcing), is an increase in the magnitude of the least frequent flood events (low exceedance probability).

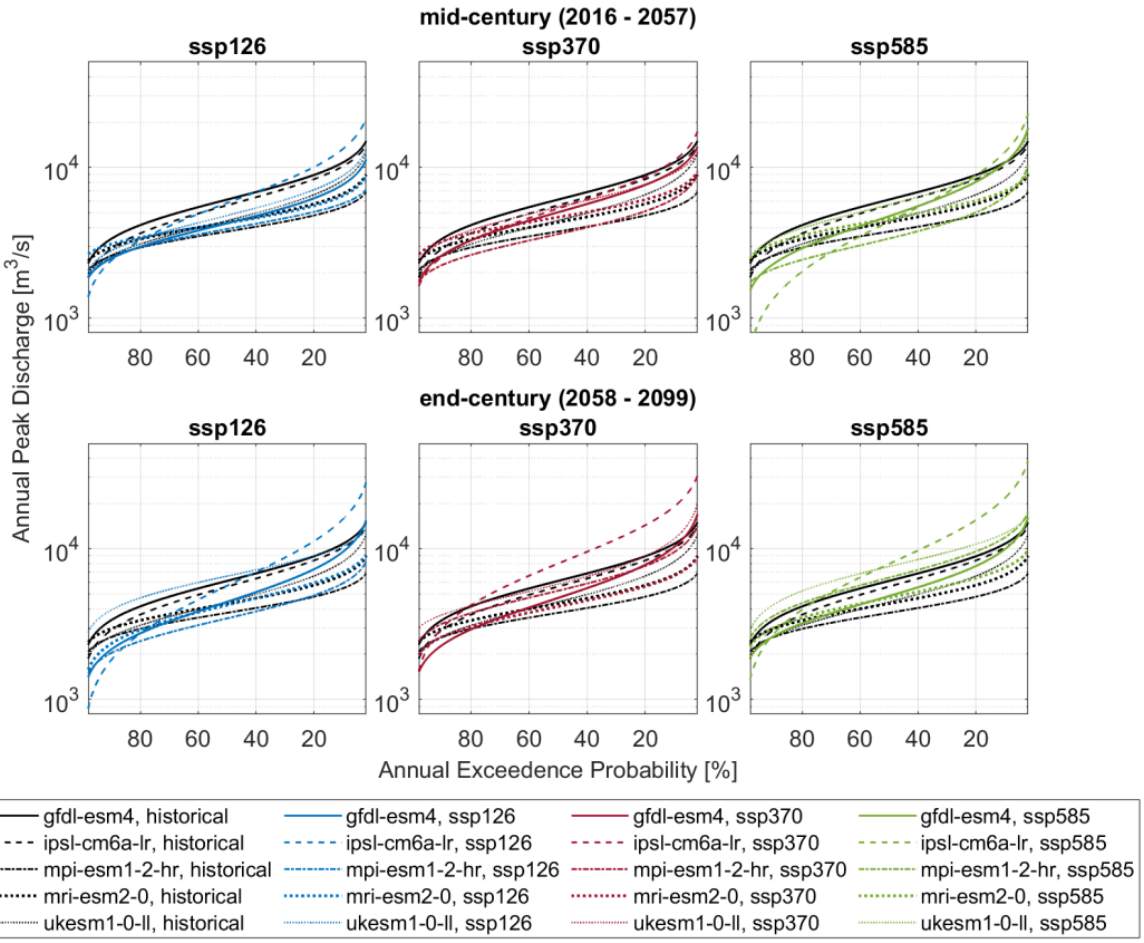

Figure 4. Mid- and end-century flood frequency distribution of the simulated future discharge (blue, green and red) of the five climate models and three climate scenarios, compared to the distribution of simulated historical discharge (black) of all climate scenarios at the outlet of the Great East Road catchment. The discharge on the y-axis is displayed in log-scale.

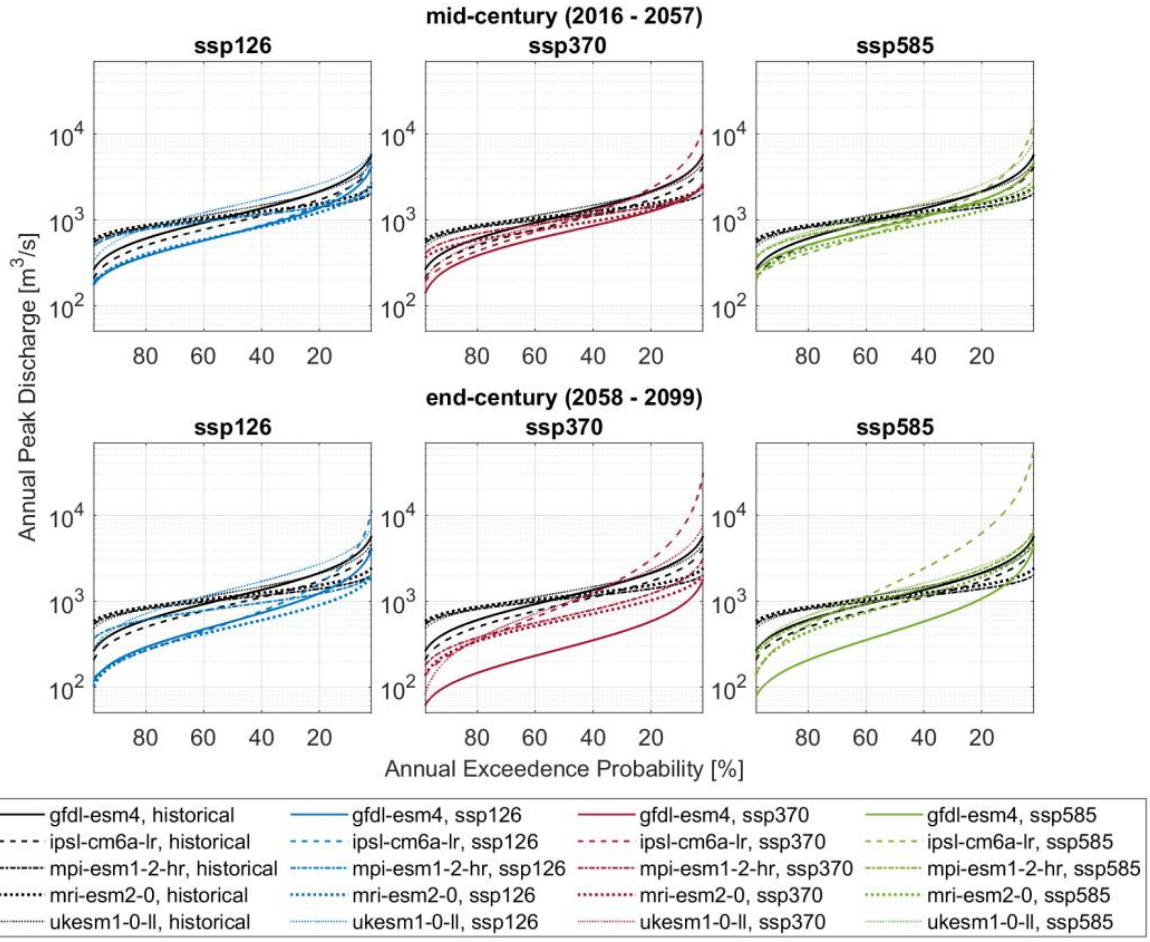

Figure 5. Mid- and end-century flood frequency distribution of the simulated future discharge (blue, green and red), compared to the distribution of simulated historical discharge (black) at the outlet of Itezhi Tezhi.

Drought and flow distribution indices

The second ranked challenge identified during the process of engaging stakeholders during the dialogues was that of drought. To demonstrate the modelling toolchain's capability of assessing drought related indicators, we include here both a spatially lumped and spatially distributed example of the evidence that can be developed using the modelling approach.

Figure 6 and Figure 7compare the changes in the proportion of daily flows in the 25th percentile, 25th-75th, 75th – 95th, and above the 95th percentile of simulated flows during the historical reference period. The comparison is done at mid- and late-century for each model and climate scenario.

There is an evident trend across all models, and for each climate scenario, towards an increasing proportion of low flows compared with the reference period. This can have impacts in many sectors including hydropower and water availability for irrigation.

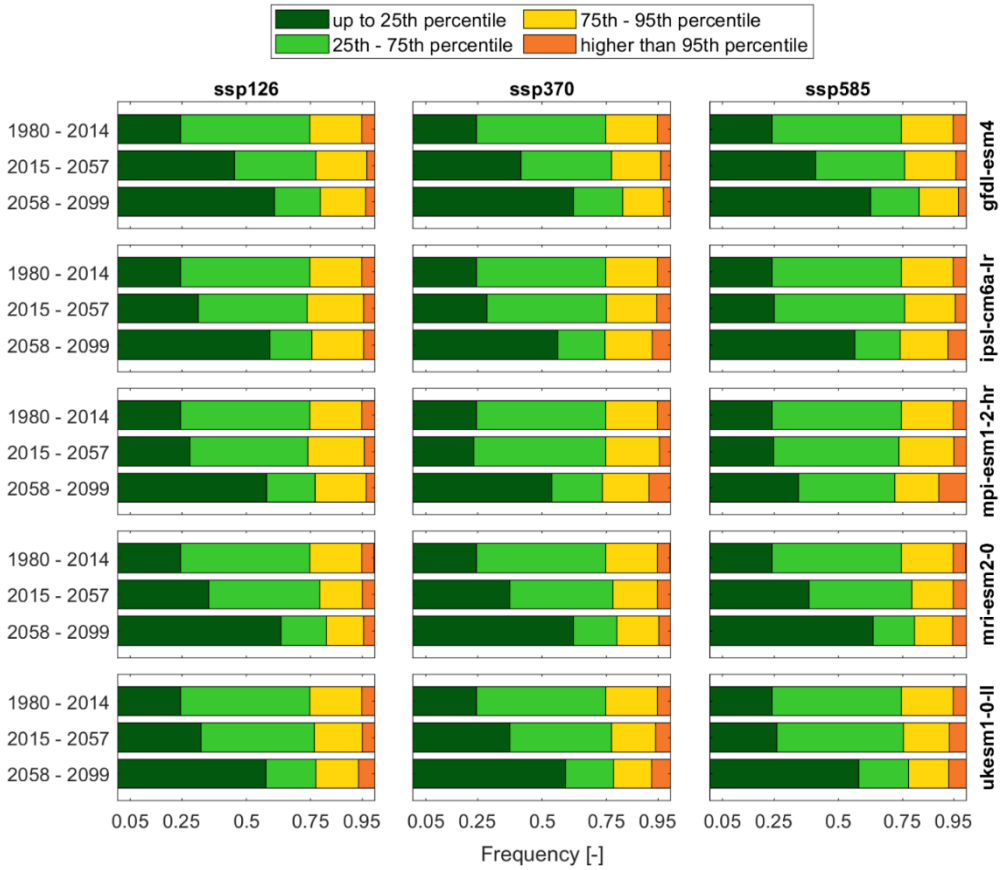

Figure 6. Change in frequency of low flow (dark green), medium flow (light green), high flows (yellow) and extreme flows (orange) from the historical reference period (1980 - 2014) to the mid-century (2015 - 2057) and the end-century (2058 - 2099) period at the outlet of the Great East Road catchment.

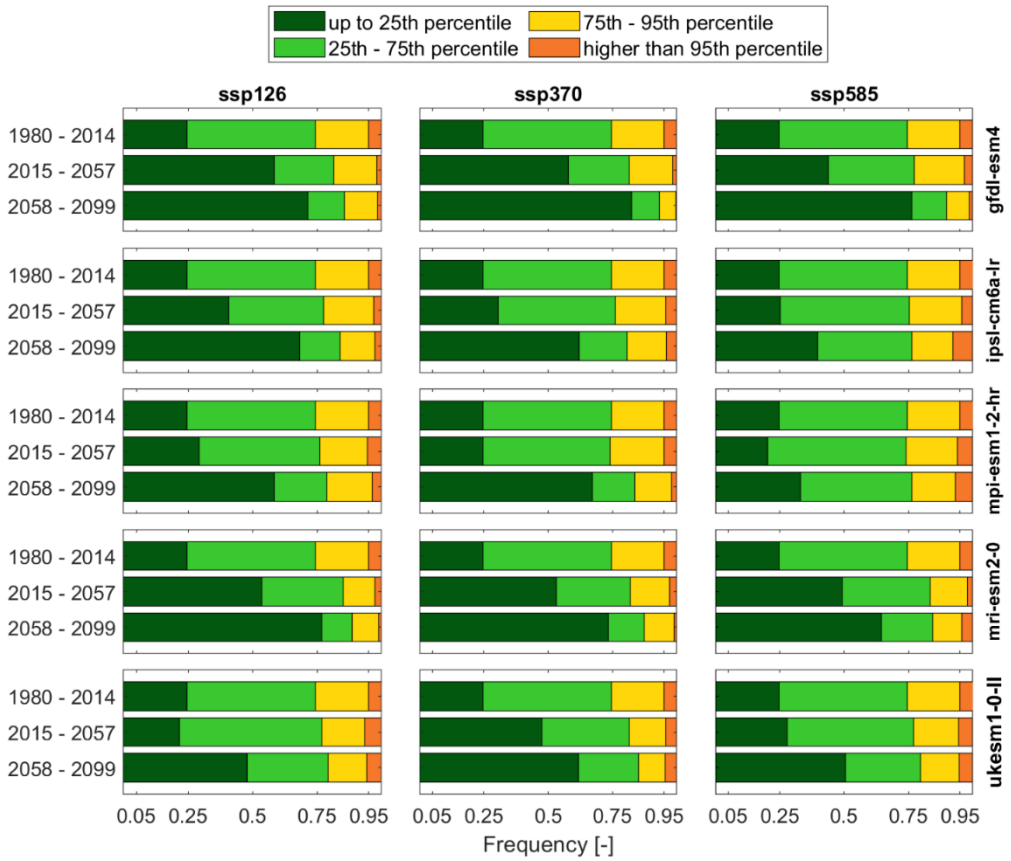

Figure 7. Change in frequency of low flow (dark green), medium flow (light green), high flows (yellow) and extreme flows (orange) from the historical reference period (1980 - 2014) to the mid-century (2015 -2057) and the end-century (2058 - 2099) period at the outlet of the Itezhi Tezhi catchment.

In Figure 8 and Figure 9 we show the tendency towards an increase in water stress using the ratio between potential and actual evapotranspiration as an indicator. This impact is largely controlled by the increasing temperatures during the future climate scenarios, without a significant shift in the average rainfall. However, as shown in Figure 10, these impacts are highly variable in space, with neighbouring areas showing opposite trends and gradients.

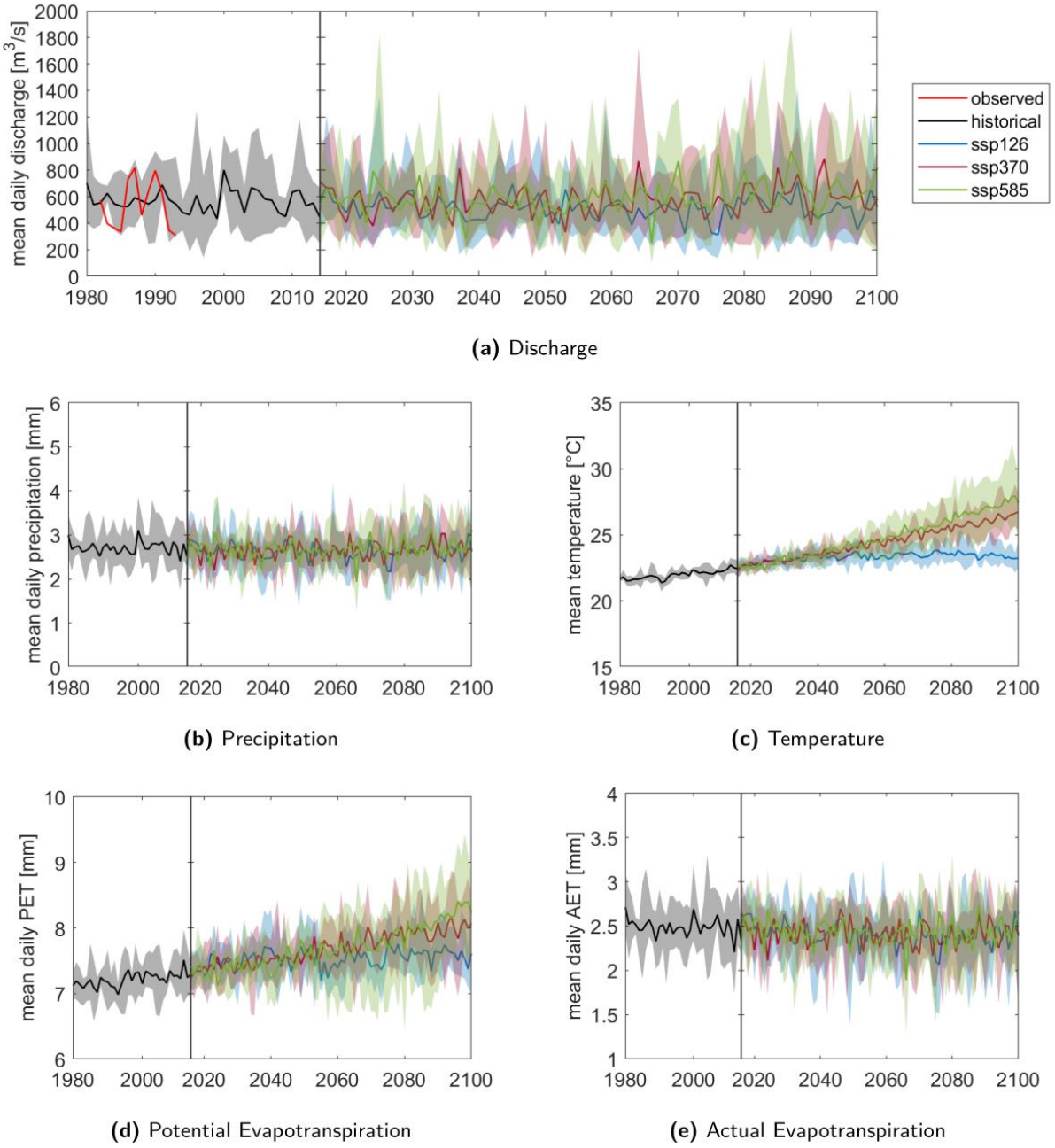

Figure 8. Change in annual average daily discharge (a), precipitation (b), temperature (c), potential and actual evapotranspiration (d and e) averaged over the catchment of Great East Road. The shaded area represents the range between the minimum and maximum annual averages of the five climate models, while the solid line illustrates the mean of the models.

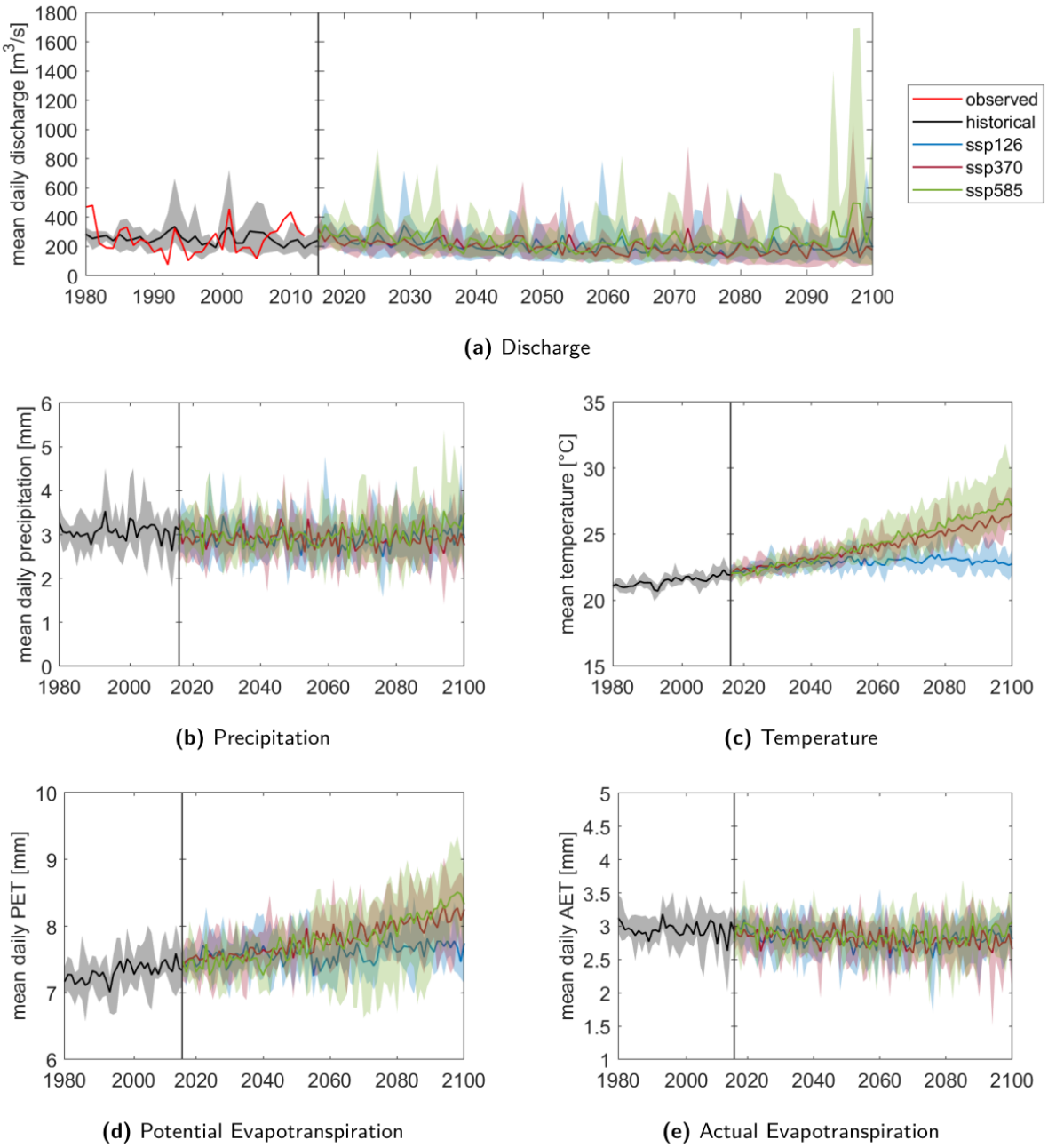

Figure 9. Change in annual average daily discharge (a), precipitation (b), temperature (c), potential and actual evapotranspiration (d and e) averaged over the catchment of Itezhi Tezhi. The shaded area represents the range between the minimum and maximum annual averages of the five climate models, while the solid line illustrates the mean of the models.

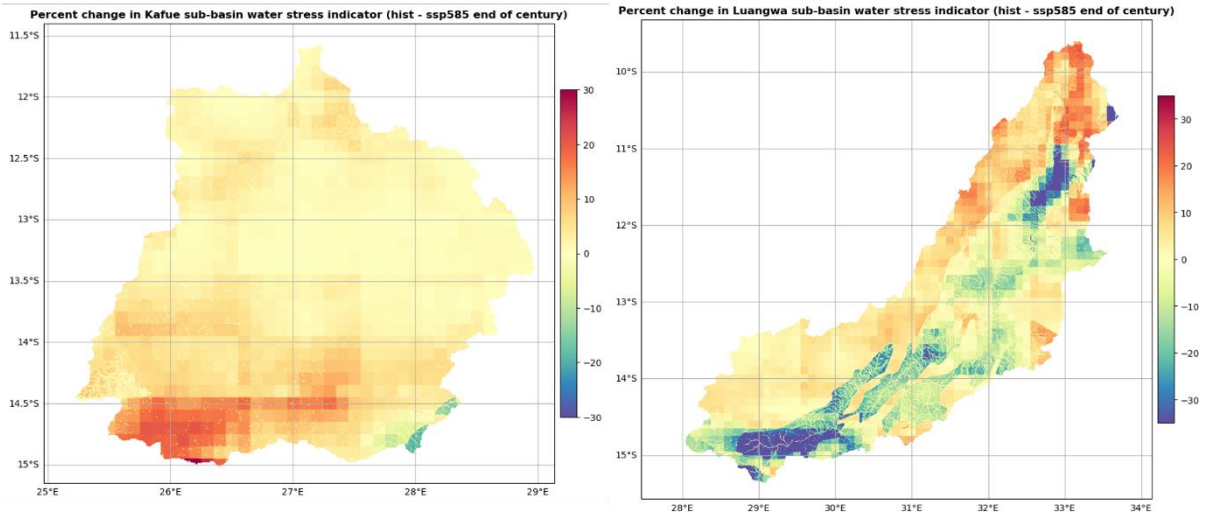

Figure 10. Example of impacts on drought proxy indicators (water stress) for different climate and socio-economic forcing scenarios in two sub-catchments of the Zambezi watercourse. The water stress indicator is defined as the ratio between actual and potential evapotranspiration (ETa/ETp) during the given period (i.e. higher values closer to 1 have less stress). As a result, the colour scale shows percentage improvement in water stress indicator in blue (negative values), and vice versa for more stress indicated in red colours. The spatial variation and direction of change depends strongly on location, highlighting the benefit of evidence modelling in a spatially distributed manner.

3.1.3 Summary of key evidence

The key evidence indicates a tendency towards reduced magnitude of the high-frequency flood events in the future. This tendency is consistent across all models and future scenarios, with an intensification of the effect during the end of century time period. On the contrary, the evidence simulations indicate an increase in the magnitude of rarer (low exceedance frequency) flood events. However, this impact is not as clear as the reduction in magnitude for the frequent events.

In respect of droughts and water availability there is a clear tendency towards a higher proportion of flows below the 25th percentile of the reference simulations. There is also a clear tendency for increasing water stress (ratio of potential to actual evapotranspiration) overall, but with a highly variable spatial distribution.

3.2 Lake Como

Located in the Italian Alps, Lake Como's basin spans 4,500 km² and includes a large, regulated lake. Known as a popular tourist destination, the lake also supports irrigation and powers 16 hydropower plants. The lake's management must balance between irrigation water supply and flood control along the shores. The lake plays a critical role in meeting the peak summer water demand. Interests in hydropower, navigation, fishing, tourism, and ecosystems pose challenges to existing water management strategies.

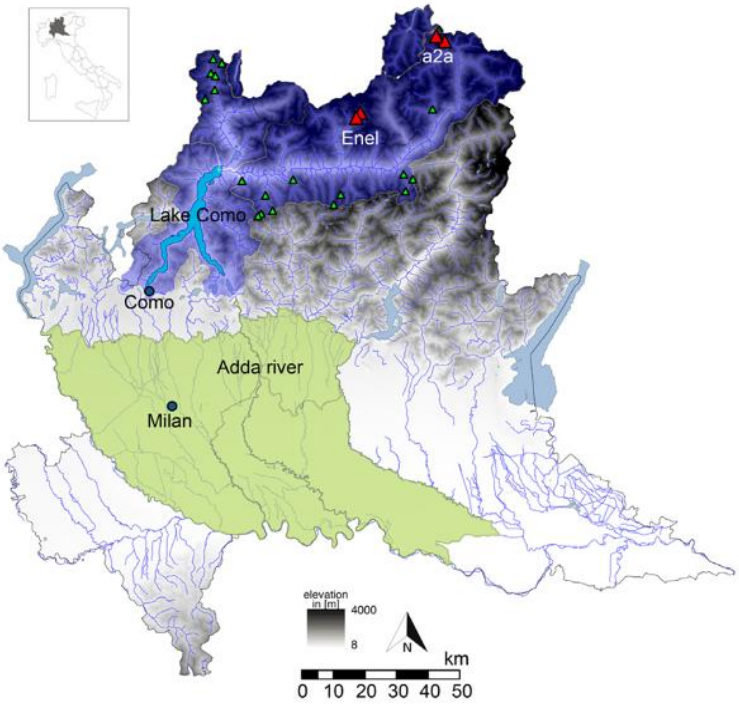

Figure 11. Map of the Lake Como basin: Lake Como, the catchment area (violet) and downstream agricultural districts (green). The triangles denote hydropower reservoirs with the red ones being the main ones (Denaro et al., 2017).

3.2.1 Overview of Challenges, Models, and Indicators

The main nexus challenges for Lake Como are: (*i*) the conflicts over seasonal allocation of water across the WEFE Nexus sectors for food and energy production, flood control and irrigation supply, and ecosystem preservation, (*ii*) the observed increase in drought events requiring new management strategies to cope with water scarcity, and (*iii*) the projected increase in climate change induced extreme events requiring the exploration of novel financial tools (e.g., index-based insurances) to hedge the risk. More details are reported in D5.1.

Similarly to the Zambezi Watercourse case study, the Lake Como case study was modelled by combining the cascade loop model consisting of the optimisation model MORDM, which combines many-objective evolutionary optimization (MOEA) and robust decision making (RDM) into a framework for planning and management of complex human-environmental systems under deep uncertainty, with the Topwatch model, which is a high-resolution physically explicit, spatially distributed hydrological model that can simulate both the hydrological response of a basin under the influence of operation of water infrastructures. More details are reported in D4.1.

To quantify the above-mentioned challenges the selected models were used to compute a set of relevant indicators, which were identified for their capacity to characterise the basin functioning and were confirmed by the stakeholders during the first two dialogues. The selected set of indicators include metrics related to hydropower production and revenue, impact on ecosystems (e.g. fish population) and ecosystem services (e.g. recreation and tourism) and agriculture (downstream irrigation deficit). Further details are found in D5.1.

3.2.2 Evidence simulations results

Due to unavoidable challenges that delayed the timely preparation of the Topwatch model configuration and calibration in the lake Como case study, the evidence in this report focusses on the impact of climate change on seasonal water availability resulting from snowmelt and glacier contributions. The extended evidence obtained by the downstream impact models described in deliverable D4.1 will be simulated and reported along with the solutions in the upcoming deliverable D5.7.

The magnitude and timing of snowmelt has a significant impact on water availability in the alpine catchment of lake Como. In Figure 12 the snow-covered area is presented as an indicator of potential snow water, while Figure 13 shows the actual melt volume. In the left-hand panel of Figure 12 the snow extent is reduced for all forcing scenarios, but significantly more so for the late century period and scenarios SSP370 and SSP585. The overall reduction in snow extent is also reflected in the volume of snowmelt, but with a tendency towards earlier melt runoff, especially evident for the late century period and scenarios SSP370 and SSP585. The right-hand panel of Figure 12 shows the evolution of snow extent in time for each scenario, with the most notable feature being a levelling off under the scenario SSP126, suggesting that impacts could be easier to manage if global solutions lead to an emissions trajectory close to that in SSP126.

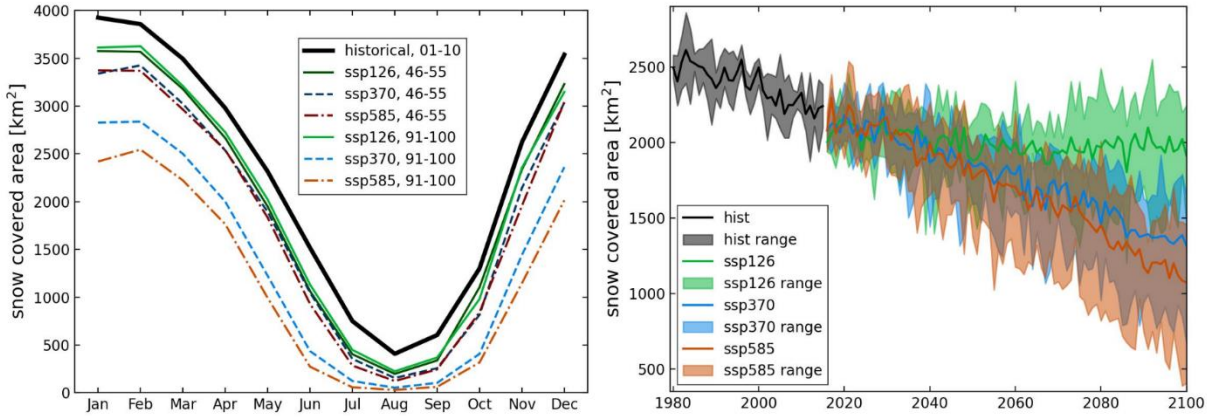

Figure 12. On the left side the snow-covered area over the months is represented for a historical reference period (2001-2010) and for three future scenarios at the middle and at the end of the century (a). On the right side the annual average of the snow-covered area is shown, where the line represents the average of the five climate models. The corresponding range was determined by the minimum and the maximum of snow-covered area of the climate models for each year.

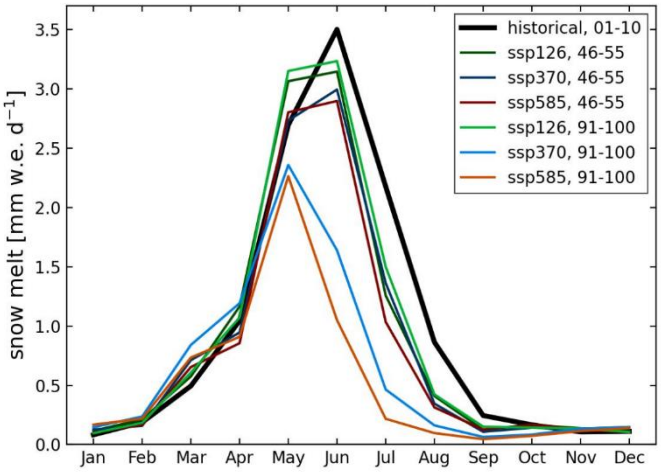

Figure 13. Seasonal cycle of snow melt averaged over a historical period (2001-2010) and over two periods in the future period (2046-2055, 2091-2100) for all three future scenarios. The extent of the range was established based on the annual minimum and maximum snow melt derived from the climate models. The unit is given in mm w.e. d−1 , where w.e. stands for water equivalent.

The time evolution of simulated total glacier volume is shown in Figure 14. All of the historical and the future simulations were initialized with the same ice thickness, resulting in the same initial total glacier volume for both time periods as shown by the step change in Figure 14 at 2018. In the historical period, there was an initial substantial increase in glacier volume, which later reached almost a constant volume for the last decade of the historical simulation, with a limited variance among the climate models. In contrast, all of the future simulations decrease until 2050. While the scenarios SSP370 and SSP585 exhibit a continued substantial decline until the end of the century, the decline of glacier volume of the scenario SSP126 reduces until 2060 and commences to increase after 2070. The recovery of glacier volume in SSP126 after 2070 is confirmed by all climate models, as the top and the bottom of the model spread has rising values as well (Figure 14). The extent of the range of all scenarios is gradually growing over the entire future period, largest for SSP585, illustrating the large uncertainties despite a very clear general indication.

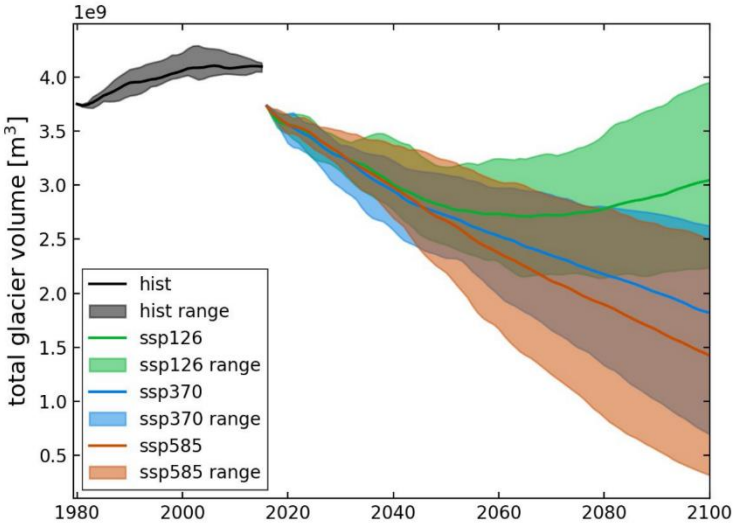

Figure 14. Total annual glacier volume over the entire catchment averaged over the five climate models is shown for the historic and the future period. In the future the three scenarios and their corresponding range are illustrated, where the range was determined by the annual minimum and maximum of glacier volume from all the climate models.

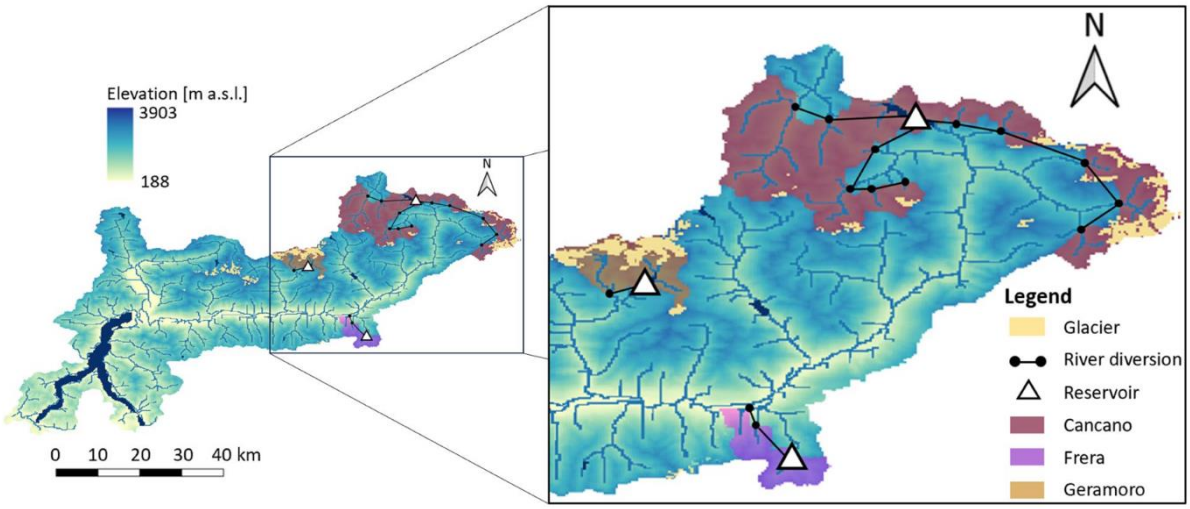

Figure 15. Overview of the catchment with the Digital elevation model (DEM) in the background. In the zoom image on the right the reservoirs and the river diversion are shown, as well as the three subcatchments Cancano, Frera and Geramoro.

Figure 16, Figure 17 and Figure 18 show the partitioning of inflows to the main hydropower generation reservoir complexes Geramoro (Enel) Cancano (A2A), and Frera (Edison), with the system illustrated in Figure 15. The results are averaged over the different climate models and annual periods during mid-/late-century, while Figure 19, Figure 20 and Figure 21 distribute the partitioning as monthly averages to highlight seasonal shifts in the timing of inflow volumes.

The evidence illustrates two key features consistent with the catchment average behaviour from earlier figures 1) the general trend towards reduced reservoir inflows from the reduction in snow and icemelt contributions, which worsens towards the end of the century; 2) a tendency for an earlier onset of snowmelt. The impact is much less for the Frera reservoir complex as the proportional contribution to inflows from snowmelt is much less than for the

Geramoro and Cancano complexes. The impact will be on the planning and management of reservoir operation policies designed to address the challenge of conflicts over seasonal allocation of water across the WEFE Nexus sectors.

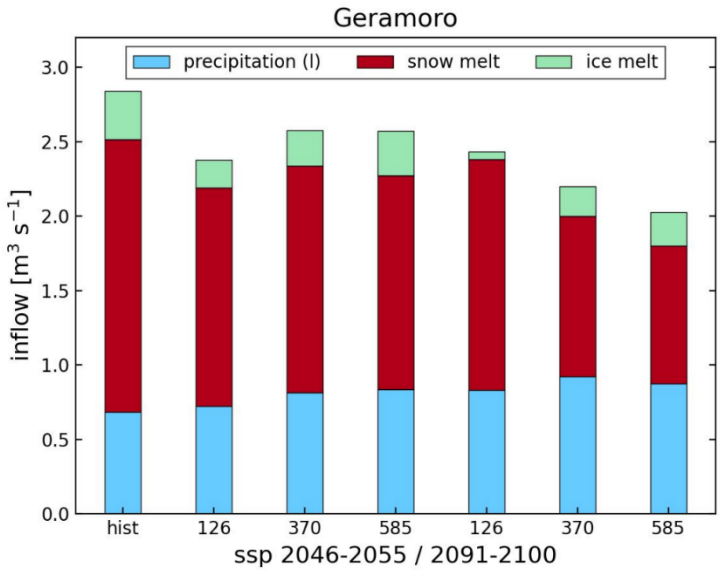

Figure 16. Flow partition of the inflow into the Geramoro reservoir into the liquid precipitation, snow melt and ice melt for the historic period (hist, 2001-2010) and for future periods for all three scenarios at half century (2046-2055, left side to centre) and at the end the of century (2091-2100, right side).

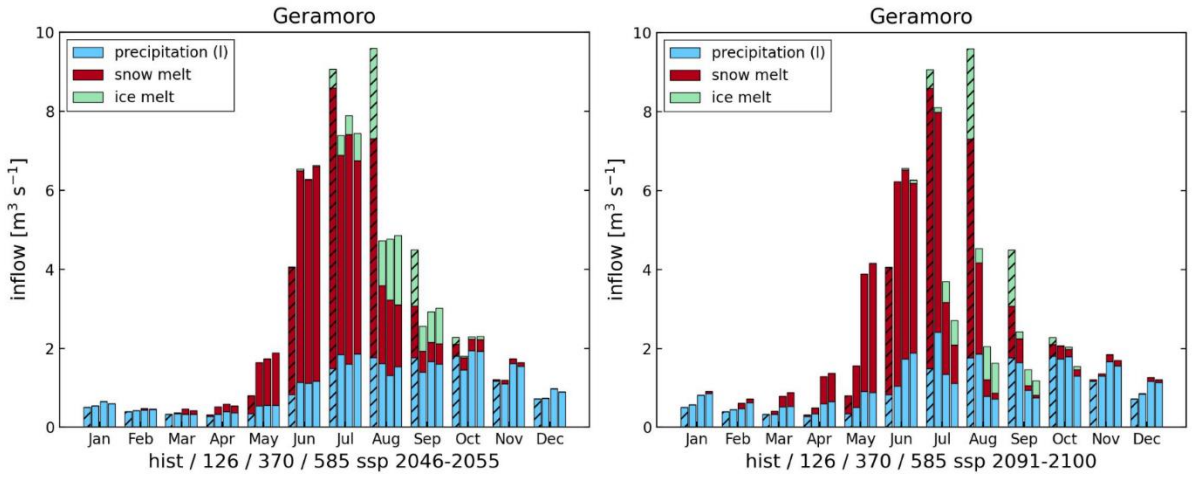

(a) Monthly flow partition at half century(2046-2055). **(b)** Monthly flow partition at end of century(2091-2100).

Figure 17. Seasonal cycle of flow partition of the inflow into the Geramoro reservoir averaged over all five climate models for the historic period (2001-2010, inclined lines) and for all three SSPs at half century (a) and at the end of the century (b).

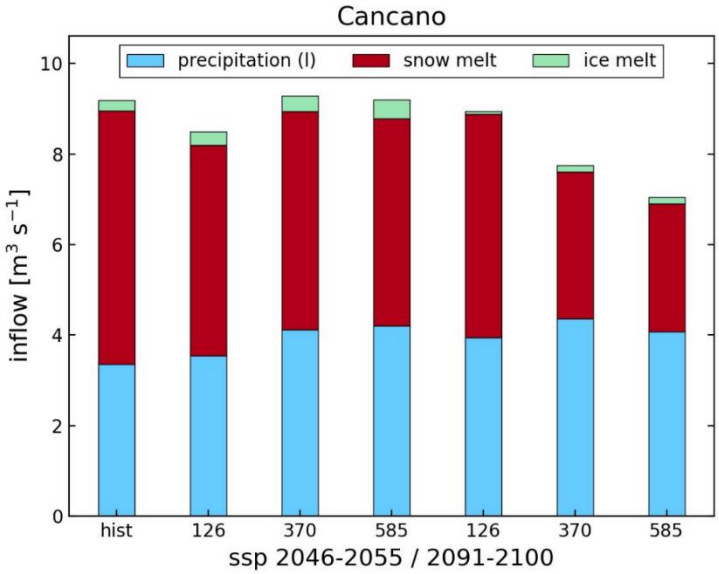

Figure 18. Flow partition of the inflow into the Cancano reservoir into the liquid precipitation, snow melt and ice melt for the historic period (hist, 2001-2010) and for future periods for all three scenarios at half century (2046-2055, left side to centre) and at the end the of century (2091-2100, right side).

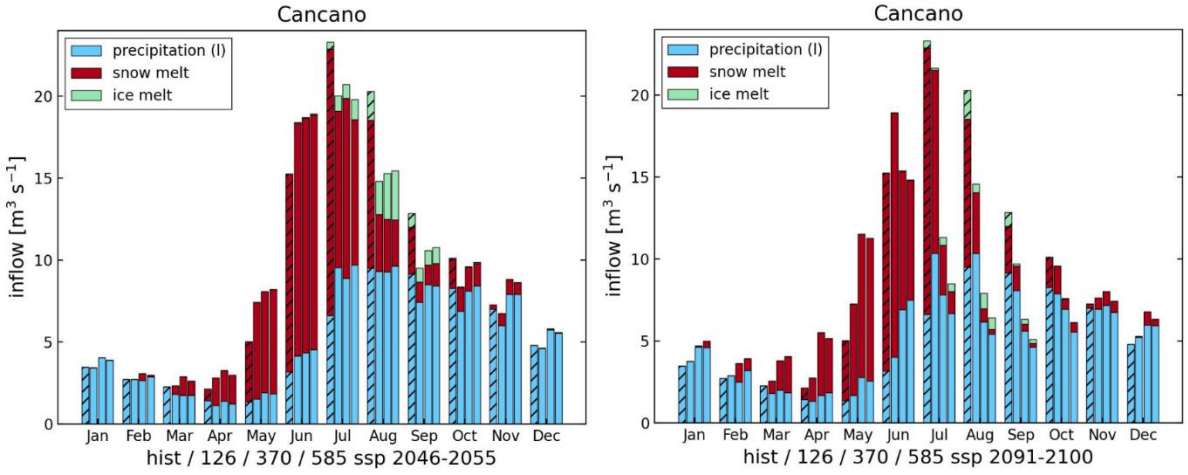

(a) Monthly flow partition at half century(2046-2055). **(b)** Monthly flow partition at end of century(2091-2100).

Figure 19. Seasonal cycle of flow partition of the inflow into the Cancano reservoir averaged over all five climate models for the historic period (2001-2010, inclined lines) and for all three SSPs at half century (a) and at the end of the century (b).

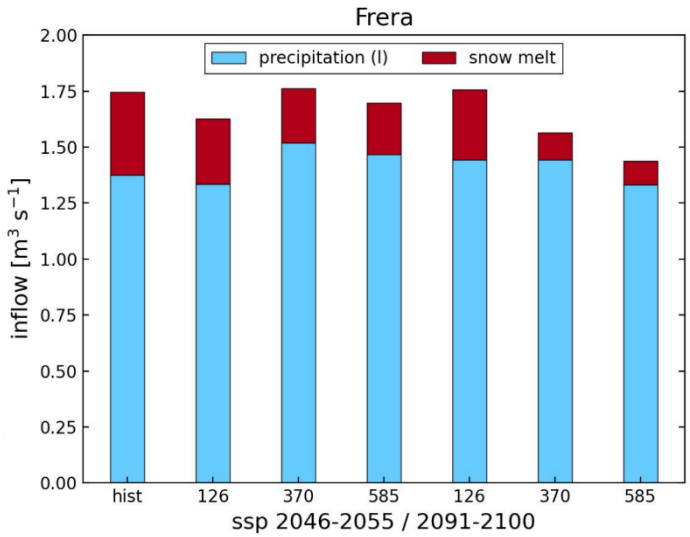

Figure 20. Flow partition of the inflow into the Cancano reservoir into the liquid precipitation and snow melt for the historic period (hist, 2001-2010) and for future periods for all three scenarios at half century (2046-2055, left side to centre) and at the end the of century (2091-2100, right side).

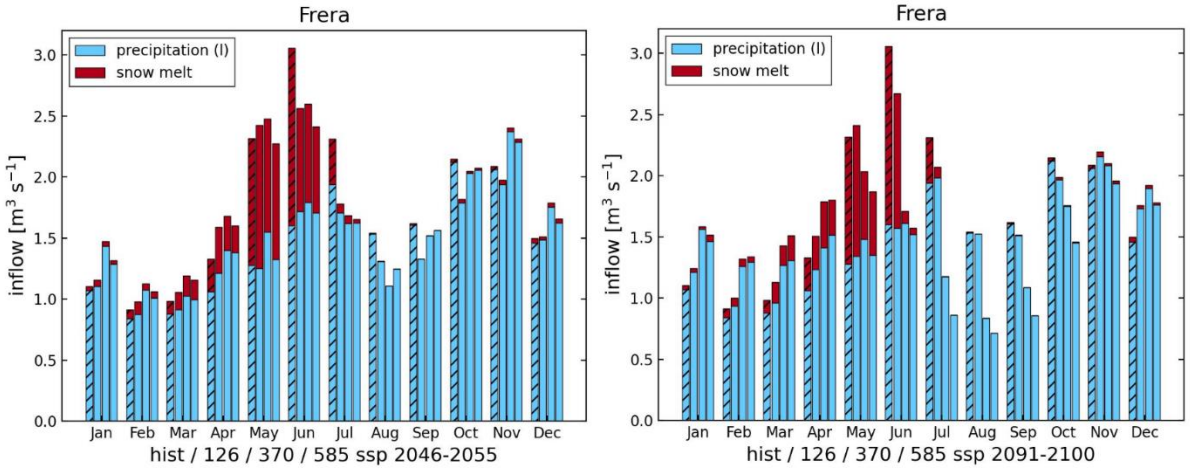

(a) Monthly flow partition at half century(2046-2055). **(b)** Monthly flow partition at end of century(2091-2100).

Figure 21. Seasonal cycle of flow partition of the inflow into the Frera reservoir averaged over all five climate models for the historic period (2001-2010, inclined lines) and for all three SSPs at half century (a) and at the end of the century (b).

3.2.3 Summary of key evidence

The evidence from the reference simulations carried out in the lake Como basin show an expected general trend towards a reduction in water availability from snow and ice melt largely driven by increasing temperatures in the future. There is also evidence of a shift in seasonal timing of the water available, likely to induce impacts in planning and generation of hydropower, and irrigation scheduling among others.

3.3 Júcar

The Júcar River Basin (JRB) is a semi-arid area that covers 22,261 km², with the Júcar stream (512 km long) being one of the most important rivers in Eastern Spain. The river flows along two Spanish regions (Castilla – La Mancha and Comunitat Valenciana) and three provinces (Cuenca, Albacete and Valencia) until it meets the Mediterranean Sea. Its annual precipitation ranges between 309 and 717 mm, averaging 473 mm, with a Mediterranean pattern: high rainfall in autumn (especially in October), a second peak in April–May, and very little precipitation during summer. According to the last Jucar River Basin Management Plan, the average annual surface resources (including groundwater discharge to water bodies) are equal to 1,456 Mm3/year, while demands combine together to a total value of 1,484.2 Mm3/year. The most significant amount of water use is for agricultural use (89%), followed by urban (9%) and industrial uses (2%). This weak equilibrium, combined together with long-term drought periods, has been traditionally addressed by groundwater pumping and conjunctive use strategies. In order to address drought periods, the Jucar River has a distinct regulation capacity mainly due to its dams and reservoirs: the Alarcon (1,118 Mm^3 of useful capacity), Contreras (852 Mm^3 that in practice cannot be more than 440 Mm^3 due to dam stability issues) and Tous (378 Mm^3 but subject to strict limits on its storage limit due to flood protection). The Júcar River system also holds 31 hydropower plants with a total installed capacity of 1,272 MW).

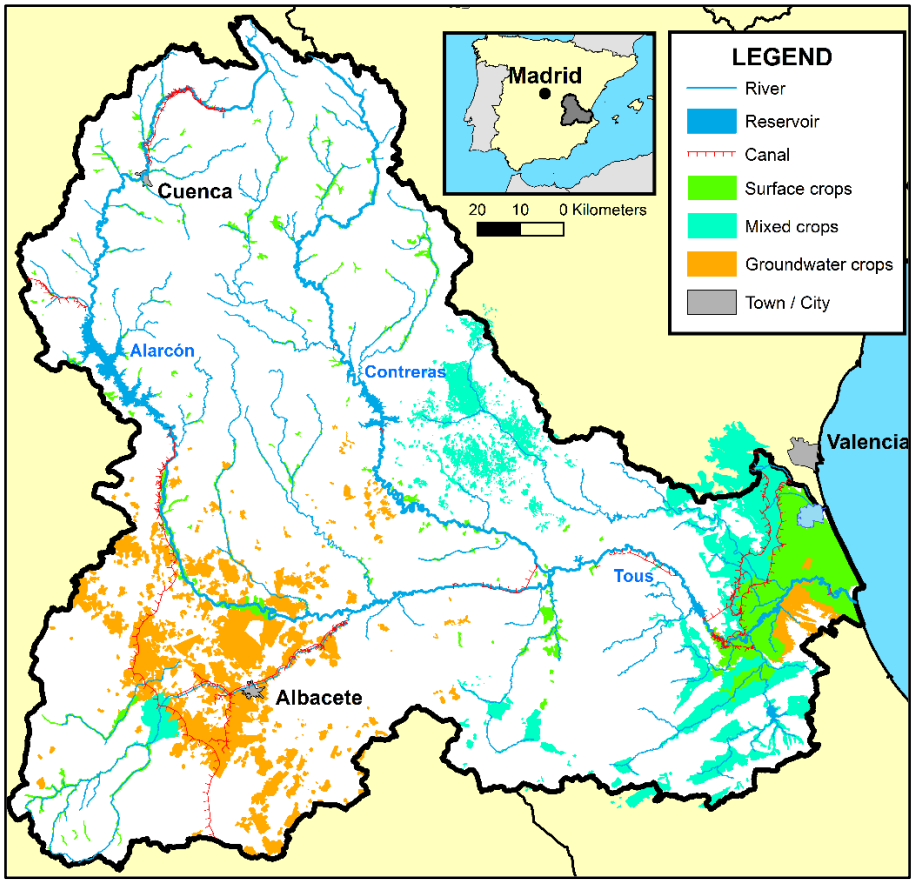

Figure 22. the Jucar River system (modified from Macian-Sorribes, 2017).

The Júcar is the primary source of urban water supply to Valencia and its metropolitan area (about 1,500,000 inhabitants, third-largest municipality in Spain) together with the Turia. In a normal scenario, 75% of the water allocated to Valencia is supplied from the Jucar and 25% from the Turia. These percentages are adjusted during droughts, depending on how drought impacts materialize in both basins. Agricultural demands are concentrated in two main areas. The coastal plain holds the most ancient surface irrigation users (from Middle Age) while the middle Jucar has the main groundwater use district of the Mancha Oriental irrigated area, developed in the 20th century thanks to groundwater pumping. Concerning ecosystems, the Jucar River system has minimum streamflow prescribed in selected river streams in order to preserve the habitat of native fish species, while its downstream part holds the Albufera lake and wetland, one of the most iconic protected areas in Spain.

3.3.1 Overview of Challenges, Models, and Indicators

According to D5.1, the main WEFE nexus challenges, together with prospected solutions identified beforehand, based on the review of technical documentation by the Jucar River Basin Agency, are presented in Table 2.

Table 2. WEFE nexus challenges of the Jucar River basin

Challenge	Prospected solutions
Water scarcity due to prolonged episodes of drought and growing demand	Supporting the implementation of efficient water-use processes; Improving existing infrastructure, particularly irrigation; Including effective purification and reuse of water to reduce consumption
Energy transition: Effective implementation and integration of renewable energies, while ensuring a fairer, more accessible, and efficient model	Spreading implementation costs and encouraging self-consumption of renewable energy
Environmental sustainability: Preserving the ecological integrity of the Jucar River basin and its associated ecosystems	Increasing investment in hydrological and forestry restoration; Evaluating ecological flows; Implementing stricter control measures on exploitative activities and discharges
Agri-food sustainability: Transitioning to an efficient, ecological, and profitable production model that prioritises sustainability	Promoting rain-fed agriculture and local markets Leveraging new technologies such as an early warning system for crops
Enhancing sustainability management by strengthening multi-sectoral coordination and improving social awareness	Investing more in environmental education and participatory governance processes

The modelling chain used to build evidence based on the scenarios developed in WP2 (see D2.2 and D2.3) is shown in Figure 23. It pivots around two models: the eco-hydrological TETIS model and the STIG-CROPROD hydroeconomic IWRM model. More details about both models can be found in D4.4.

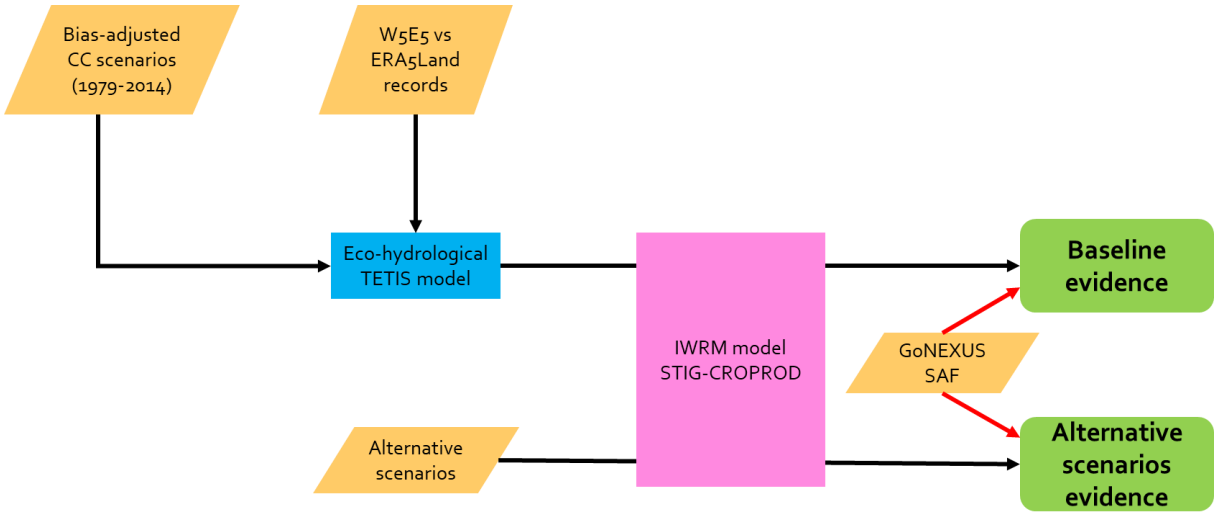

Figure 23. the GoNEXUS modelling chain to provide evidence on the Jucar River basin

The combination of both models enables a thorough analysis of the spatial and temporal distribution of the hydrological impacts of climate and socioeconomic change (thanks to the

fully distributed modelling strategy used by TETIS) and a comprehensive evaluation of their impacts for the economic and environmental uses of water resources (by using the STIG-CROPROD hydroeconomic simulation model). In particular, the modelling chain computes hydrological discharges, streamflows, reservoir storages and releases, groundwater storage, pumping rates and discharges to stream-aquifer interaction for selected aquifers, deliveries, crop productions, energy consumption and revenues in consumptive demands, energy production and benefits in hydropower plants, inflows to the Albufera lake, and habitat for selected fish species and streams.

In addition to the previous variables, the modelling chain facilitates the computation of WEFE indicators from the GoNEXUS SAF. From the indicator list provided in D5.1, the following ones have been selected to describe the evidence in the Jucar case study from the modelling chain.

Table 3. Computed WEFE indicators of the GoNEXUS SAF

ID or Name	Additional information	Unit	Scale
Water			
WAT_15	Total Freshwater withdrawals	Mm³/year	Sum of all sectors
WAT_18	Freshwater withdrawn per sector	Mm³/year	Urban and agricultural
WAT_20	Groundwater Table Depth (inferred from model suite)	Mm³/year	Not tables, but change of storage in aquifer elements
WAT_22	Total Groundwater withdrawal	Mm³/year	Sum over all aquifers
WAT_23	Groundwater withdrawn per sector	Mm³/year	Urban and agricultural
WAT_30	Amount of wastewater recycled in agriculture	Mm³/year	The only sector involved is agriculture
Food			
FD_23	Water productivity of irrigated crop	m³/kg & m³/€	Irrigation district
FD_28	Energy consumption per crop (energy to put water on the field)	kWh	Irrigation district (particular values for each crop not possible)
FD_29	Total energy used in agricultural practices	kWh	Sum over all irrigation districts
Energy			
ENG_2	Cost of Energy	M€/year	Per demand / pumping station
ENG_8	Energy production from hydropower - river basin	GWh/year	All plants with installed capacity higher than 3.5 MW
ENG_9	Energy production from a specific hydropower plant	GWh/year	Every plant with installed capacity higher than 3.5 MW
Ecosystems			

ID or Name	Additional information	Unit	Scale
ECO_3	Wetland Extent	Mm^3/year (inferred from inflows measured by the model)	L'Albufera wetland
ECO_4	Size of key biodiversity areas/habitats	Percentage of optimal habitat area	5 selected locations along the Jucar and Cabriel rivers
Socio-economic			
SOCIO_40	Income from hydropower	M€/year	Sum over all hydropower plants

3.3.2 Evidence simulations results

The evidence simulations cover the reference period (1979-2014) of the five climate change scenarios defined in D2.2. For each scenario, variables and indicators referring to the WEFE nexus are computed for this period to provide a broad and coherent picture of how the WEFE nexus performs, both per scenario and to compare the whole set of them and evaluate how performance and trade-offs across the WEFE nexus behave. As an example, the evidence provided by the GFDL.ESM4 climate model for variables is shown in Figure 23 in the form of box-whisker plots. This figure depicts the "baseline" evidence, in the sense that it corresponds to the model setup that represents the historical conditions of the 1979-2014 period, as contrasted during the calibration of the model (see D4.1 for more details).

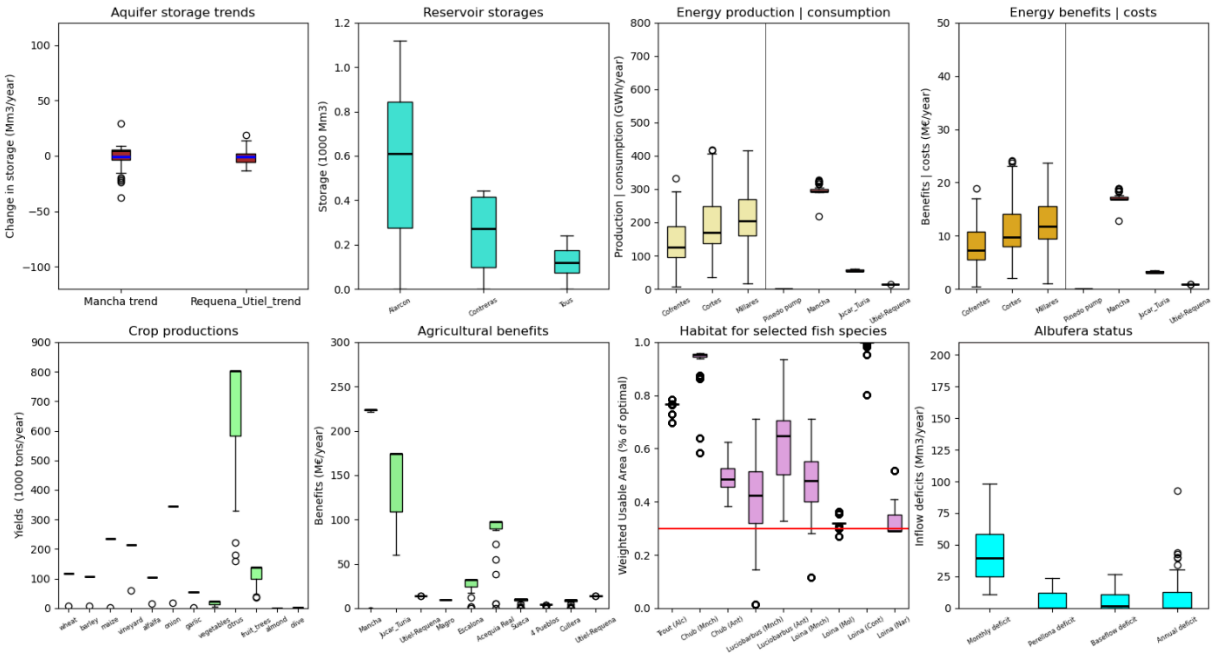

Figure 24. Jucar evidence computed by the GFDL-ESM4 model simulations for the reference scenario and selected variables

According to the storage component, the Mancha Oriental and Requena-Utiel aquifers (the ones with overexploitation issues in the past) would show fluctuations in the amount of water stored in them, although no significant long-term trend is noticed, since the average values (blue lines) are close to zero. Surface reservoirs, as expected, show larger fluctuations covering from being empty to being full, although most of the time the storage levels are far from compromising the system performance. The lower limits of the boxes show no less than 300 Mm^3 in Alarcon, 100 Mm^3 in Contreras and 100 Mm^3 in Tous. This implies that at least 75% of the time there are more than 300 Mm^3 stored and thus the system demands and environmental flows are not compromised. However, the situations in which reservoirs are empty means that the system is compromised during extreme events.

This absence of drought impacts during the majority of the period is reinforced by the box-whisker plots associated with irrigated agriculture demands. Crop productions for most of the crops are constant and optimal, with the exception of one year in which most of them show no production. This situation is caused by the fact that most of the crop types present in the Jucar (all the herbaceous crops, vineyards, almonds and olive trees) are cultivated in the Mancha Oriental and the Requena – Utiel areas, whose main source is groundwater. Consequently, their allocation is usually independent from the surface water availability, unless an extreme drought event endangers the fulfilment of the minimum streamflows in the middle Jucar. Under this situation, the model severely constrains groundwater pumping to increase the streamflows of the middle Jucar thanks to stream-aquifer interactions. This model behaviour is in line with the policy actions taken by the Jucar River Basin Agency during the 2005-2008 drought, in which groundwater abstractions were distinctly reduced to guarantee a minimum streamflow in the Jucar (Garcia-Molla et al, 2016). This is also reflected in the box-whisker plot of the Mancha irrigation district, which shows generally (?) very small changes but for one year in which no profit is achieved. In contrast, citrus, vegetables and fruit trees (and the demands in which they are the main use) show larger changes in crop production and benefits due to being subject to surface water availability. However, in most years their water supplies are not curtailed, so most of the time the system is not subject to drought impacts. When they occur, they concentrate in the Jucar-Turia irrigation demand, which does not possess senior rights on surface water use and thus is curtailed more often than the rest of the downstream water uses.

Concerning energy, results show that energy production in the Jucar River through hydropower plants is, on a broader view, higher than its consumption through groundwater pumping, implying that the Jucar river has a positive energy budget. However, energy consumption and costs are stable, while its generation is subject to significant fluctuations, meaning that in drought events the system's behaviour inverts, and it moves to a net energy consumer. This behaviour is fully transferred to the costs (upper right plot of figure 24), since intra and inter-annual cos patterns do not show a significant variability and thus energy revenues and costs are dominated by their production / consumption instead of their unitary amount.

In terms of ecosystems, the GFDL-ESM4 scenario shows in general a fair status of fish habitat, with most of the native fish species showing median habitat values above 50% of the maximum Weighted Usable Area (WUA). The only issues are found for Luciobarbus and Loina in the Mancha Oriental streams, with habitat values below the minimum threshold of 30% imposed by the Spanish law; and for Loina downstream of the Naranjero reservoir, in which

habitat values fall slightly below the 30% threshold. Regarding the status of the Albufera wetland, failures on the minimum requirements are found for all years at the monthly scale, more than 50% of them during the baseflow (summer) season and between 25% and 50% during the "*Perellonà*" (winter) season and at the annual scale. However, both the monthly and the seasonal requirements were set recently by the Jucar River Basin Agency, and they were not binding during the 1979-2014 period. Since the minimum annual required inflows to the Albufera were set at 210 Mm^3/year, deficits are far from critical except for one year in which they reach a value close to 50%.

GFDL-ESM4 evidence provided by the SAF indicators are shown in Figure 25. Part of the evidence built from indicators overlaps with the one of variables given that most of the main variables computed are included in the SAF. Water abstraction indicators show that surface resources are the main origin of water supplies (although groundwater resources assume 40% of the total deliveries in agriculture). Concerning water productivity indicators, the most productive irrigated agriculture demands in m^3/kg are the ones in which groundwater is involved (Mancha Oriental, Jucar-Turia, Magro and Utiel-Requena), due to having the highest irrigation efficiencies. On the other hand, the lowest ones are found in the lower basin, given its relatively low irrigation efficiencies, in particular the ones of the Cullera irrigation district. Furthermore, these demands are exposed to productivity shocks during drought periods. This equally applies to irrigated area on Jucar-Turia coastal plain that depends on both surface and groundwater allocation.

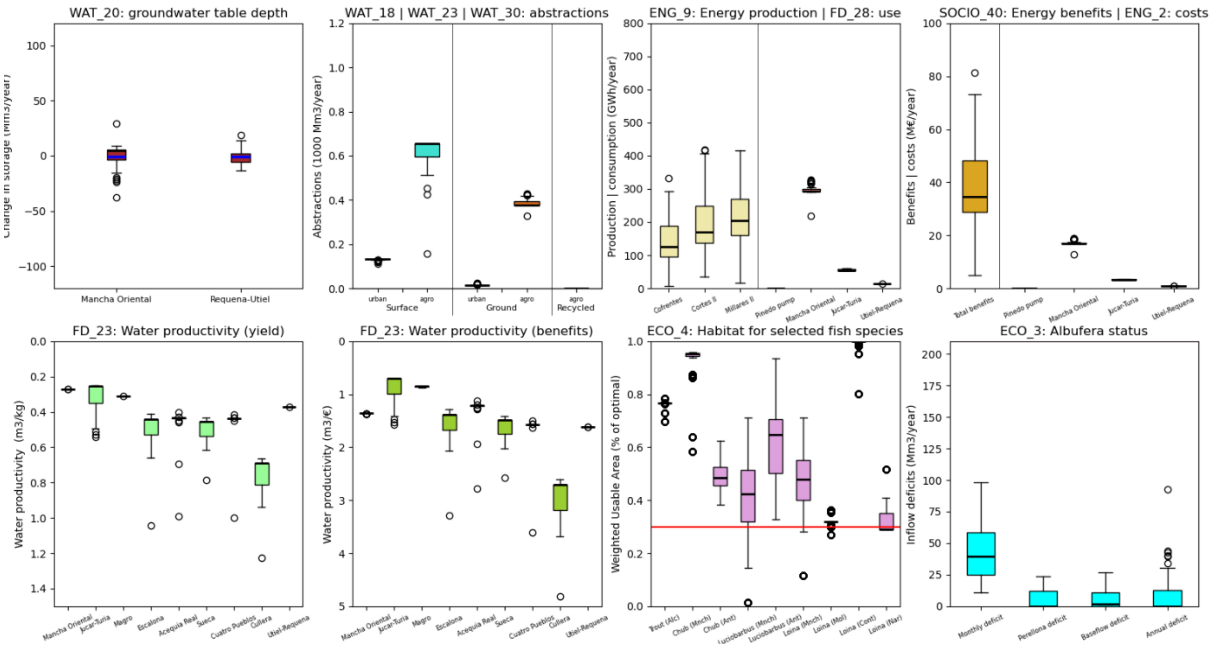

Figure 25. Jucar evidence computed by the GFDL-ESM4 model simulations for the reference scenario and for selected indicators.

The m^3/€ ratio in irrigated agricultural demands shows distinct differences compared to the previous metric. In particular, Jucar-Turia shows the highest ratios unless drought conditions are found, in which the Magro is the one with the highest ones. Although possessing a lower

ratio in m^3/kg, the Acequia Real demand has a higher m^3/€ ratio than the Mancha Oriental. Oppositely, the Utiel-Requena performs worse in m^3/€ than in m^3/kg, showing even lower values than the lower basin demands unless drought years. The Cullera demand, however, shows the worst results for both kg-based and €-based metrics. These results highlight the importance of considering economic indicators and, in more practical terms, the strong influence played by market prices, which in some cases collides with yield. This situation implies that, for some irrigation districts, the crop price is a driver stronger than irrigation efficiency in their decision-making processes.

The baseline evidence provided by the whole set of climate models is summarised in Figure 26 (variables) and Figure 27 (SAF indicators). On a broader view, all models provide a consistent and similar picture of the Jucar River basin performance, although there are significant differences in some particular aspect. The IPSL-CM6A scenario is the most optimistic for water and agriculture although its hydrological discharge is not the highest one. However, this scenario is the one showing the highest values for low-flow periods, implying less severe droughts. This is also reflected in the energy and fish habitat variables and indicators, in which this scenario offers the highest minimum values and the most stable performance levels across years, despite not showing the best values on average. This highlights the distinct role played by water regulation, which is able to absorb the impact of mild droughts and favours the least drought-prone scenarios over other trajectories with higher average values but also exposed to higher variability in water resources. In fact, the GFDL-ESM3 scenario offers the highest median values, but it is also subject to the highest inflow variability and thus yields a less optimistic vision than ISPL-CM6A and MRI-ESM2_0, which offers the second-best performance in water and agriculture and the best performance in energy and for the inflows to the Albufera.

On the contrary, the UKESM_0_11 model offers the most pessimistic vision in water, energy and agriculture, achieving in the latter a significantly different performance compared to the rest. It also offers the worst fish habitat for Loina in Mancha Oriental and Luciobarbus in Antella, although yielding the highest habitat for Chub in Antella and being in the middle in terms of the inflows to Albufera. Since its hydrological discharge does not show a significant change in its cumulative probability function compared to the rest, this reinforces the argument pointed before: the Jucar River system is not quite sensitive to average values of hydrological discharge, but it is sensitive to its lower extremes, and in particular to their repetition over several years. It can also be stated that there are strong interconnections between water, energy and agriculture, but their bonds with ecosystems, in particular with the Albufera, is less evident. The reason behind this could be the different treatment given by the model to ecosystems compared to the rest of the WEFE nexus components. Since the minimum streamflows or inflows to sustain ecosystems are considered as constraints, the model usually does not move above those thresholds, in contrast to consumptive uses, to which water allocation is always favoured.

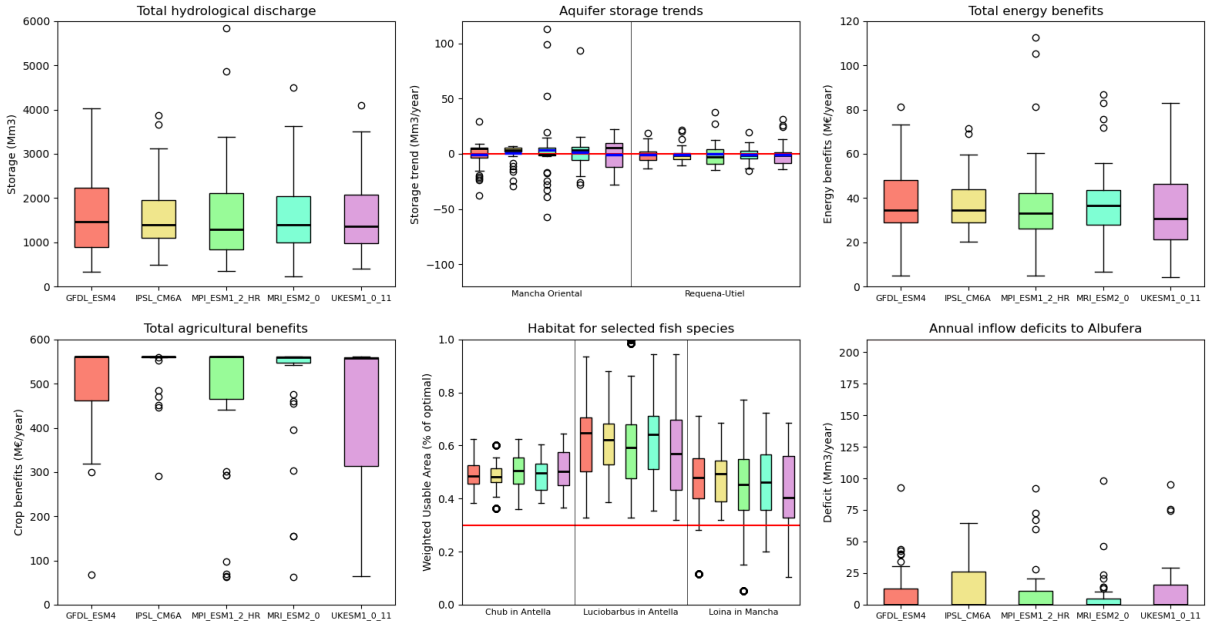

Figure 26. Jucar evidence computed by the whole model ensemble for the reference scenario and for selected variables

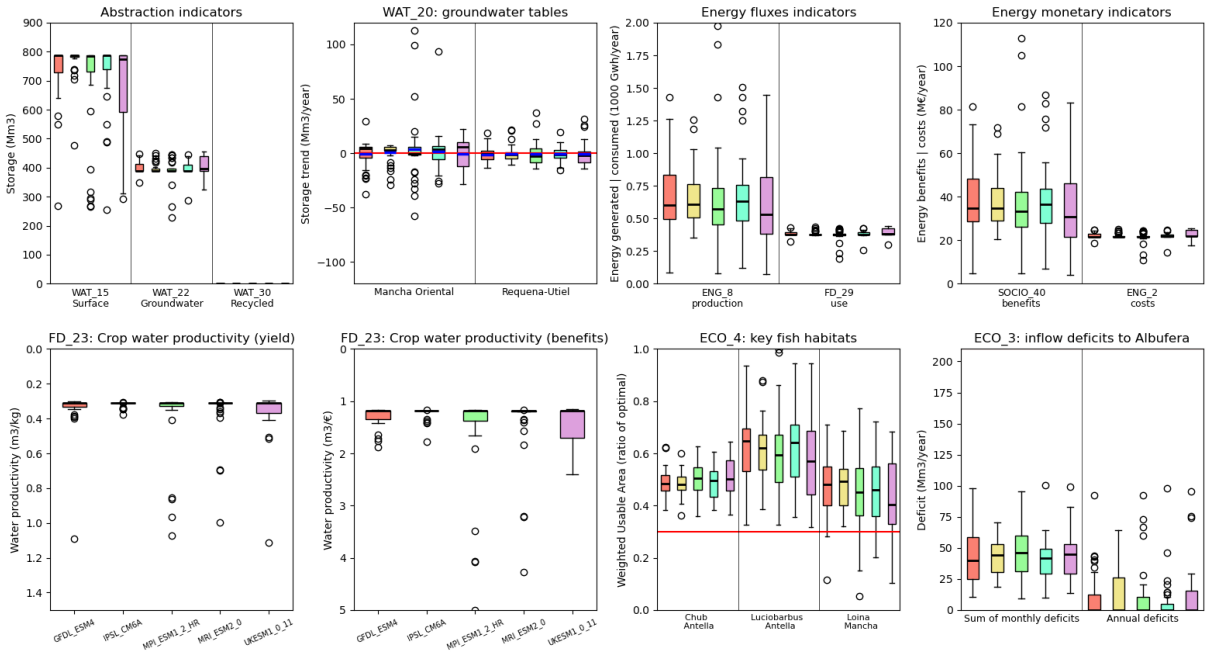

Figure 27: Jucar evidence computed by the whole model ensemble for the reference scenario and for selected indicators.

Above any difference among climate change models, the baseline evidence highlighted some of the current issues in the Jucar River basin, the resolution of which is being addressed: the recovery of the Mancha Oriental aquifer and the improvement of the Albufera status. In this regard, no model shows a clear recovery trend in the Mancha Oriental aquifer while all of them point to non-negligible deficits in the fulfilment of the Albufera requirements. In order to work out these issues, the Jucar River Basin Agency already sets or plans to set in the short-

term some measures. Concerning the Mancha Oriental aquifer, a shift of water origins from groundwater to surface water resources has been established, curtailing pumping up to 275 Mm^3/year and provide the same amount via surface water (up to 80 Mm^3/year). Although not belonging to the 1979-2014 period, these measures are currently under implementation and they will be in place in the near future, so any further WEFE nexus solution should be evaluated on top of them. The evidence provided under this scenario is shown in Figure 28 (variables) and Figure 29 (indicators).

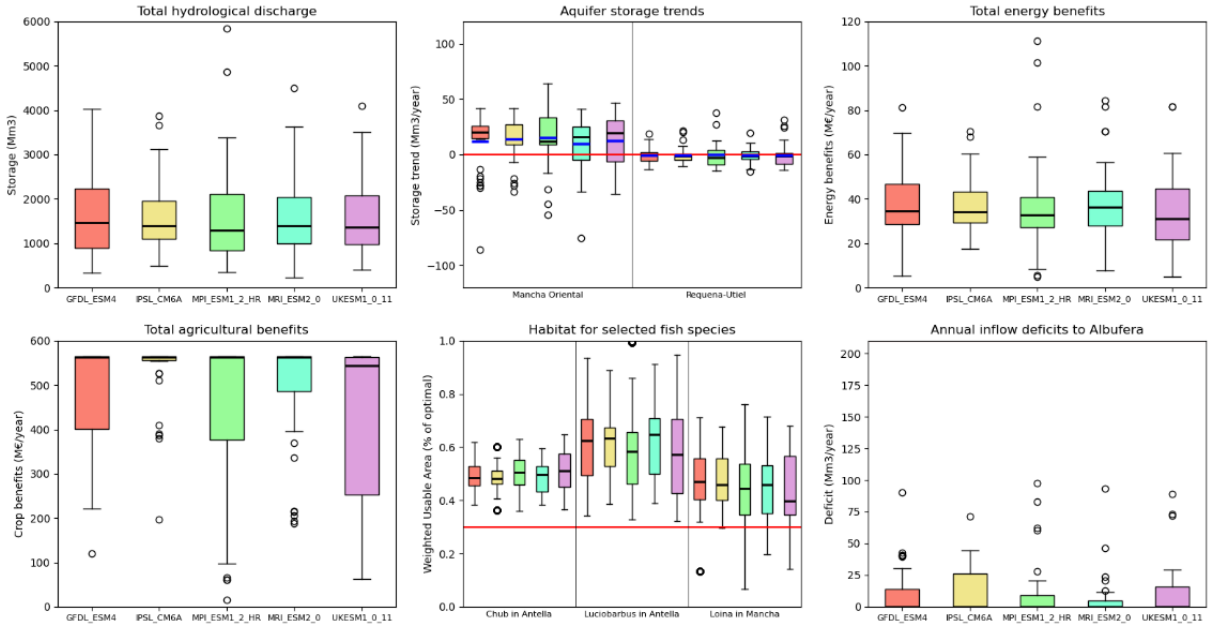

Figure 28. Jucar evidence computed by the whole model ensemble for the Mancha Oriental source shift socio-economic scenario across selected variables.

The partial switch of the Mancha Oriental water source from groundwater to surface has a positive impact on groundwater storage for all the scenarios, which show a clear increasing trend. This comes at the cost of increasing surface water allocation for most of the years as noticed by the abstraction indicators. This situation is reflected in the agricultural variables and indicators, which show a poorer performance compared to the baseline scenario. Such behaviour matches the expectations because substituting groundwater by surface resources implies the integration of the Mancha Oriental users into the surface allocation procedures of the Jucar River basin, in which they would not have senior rights and thus would be subject to curtailments if the groundwater pumping cap is set at the same level regardless of the surface hydrology. However, the impacts differ depending on the climate model considered. With the exception of the most pessimistic UKESM1_0_11 scenario, in which negative impacts would be found between 50% and 75% of years, the median values of agricultural benefits and crop productivities remain stable, implying that most of the time there will be no impacts on agriculture. Nevertheless, they are found during dry years in all scenarios. The most optimistic scenario, IPSL-CM6A, shows impacts only in the driest periods (below 25% of years) with economic losses up to 100 M€/year. The remaining scenarios show an impact up to 50 M€/year for the drier half of the analysis period, which could worsen up to 100

M€/year for 25% of the period (with the exception of UKESM1_0_11). On the other hand, impacts on energy are also positive, with a decrease in energy use and costs, while ecosystem impacts are negligible. It can be concluded that the switch of origins for the Mancha Oriental users would have a positive impact in energy consumption and costs, as well as a distinct positive impact in groundwater storage in the Mancha Oriental aquifer, although farmers would be exposed to higher economic losses during droughts.

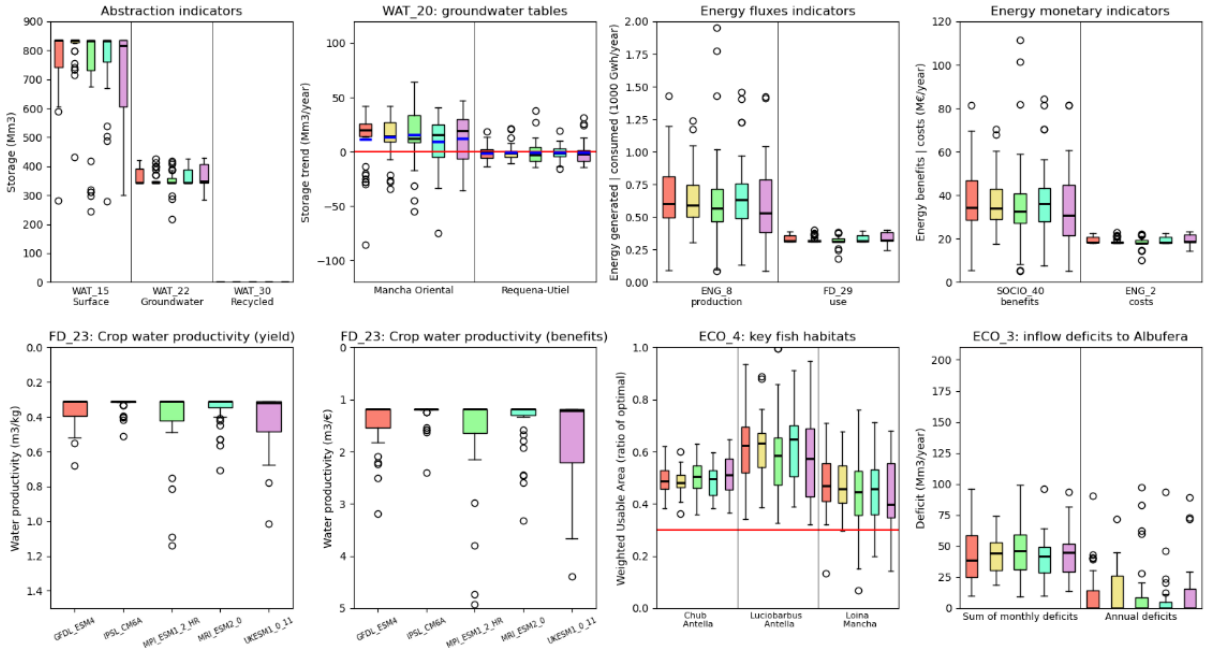

Figure 29. Jucar evidence computed by the whole model ensemble for the Mancha Oriental source shift socio-economic scenario across selected indicators.

On top of the switch of Mancha Oriental water sources, another action highlighted by the Jucar River Basin Agency, which is currently under implementation, consists in directly allocating water to the Albufera, which traditionally was fed from irrigation returns and groundwater discharge. The impact of this measure on the WEFE nexus is presented in Figure 30 and Figure 31. All models point to the fact that the deficits noticed in previous scenarios would be eliminated but during the most extreme situations. This change does not affect energy generation nor consumption during the system, while showing very slow impacts in groundwater storage. Both situations were expected, since the Albufera is placed downstream of all hydropower plants and the cap put on the Mancha Oriental aquifer prevents increasing its exploitation compared to the previous scenario.

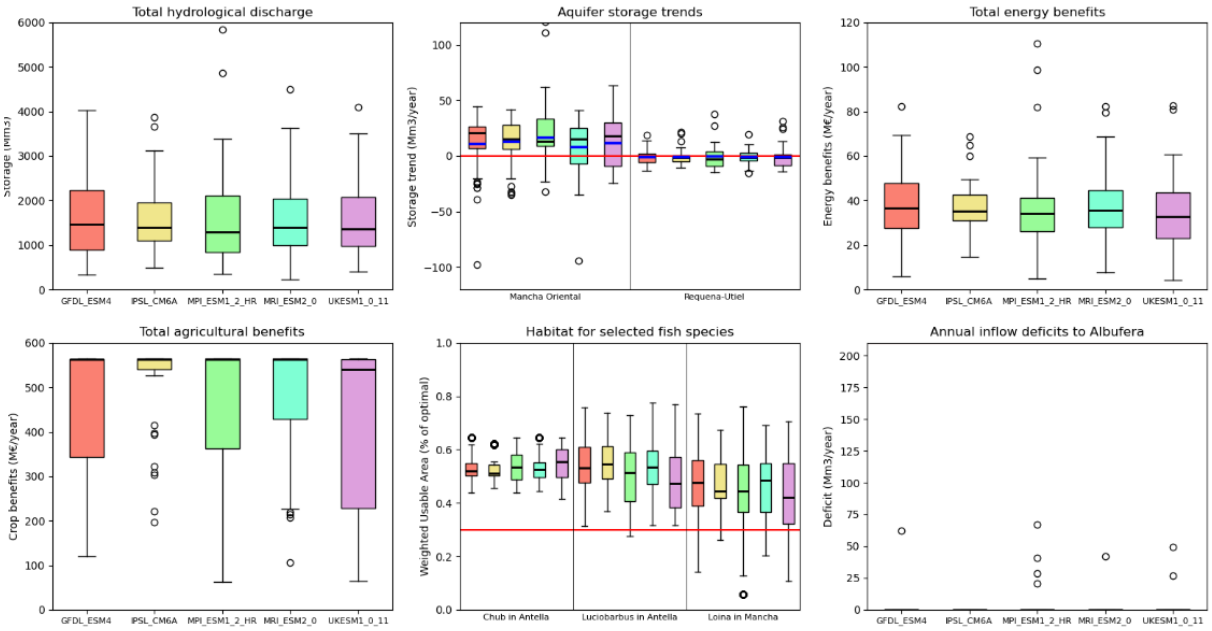

Figure 30. Jucar evidence computed by the whole model ensemble for the socio-economic scenarios (i) Mancha Oriental source switch and (ii) direct allocation to Albufera across selected variables.

Directly allocating water to the Albufera would have a negative impact in water abstractions for agriculture and thus in agricultural benefits. As found in the previous scenario, these impacts materialise only during the driest half of the years. Depending on the scenario, surface abstraction could reduce between 25 and 50 Mm³/year during mildly dry years (25% to 50% probability), and from 50 to 100 Mm³ during extremely dry years (less than 25% probability). Agricultural benefits also suffer decreases, with a loss of profit up to 50 M€/year during mildly dry years, although the impacts of extreme years remain similar but for the MPI_ESM1_2_HR and the MRI_ESM2_0 scenarios. The UKESM1_0_11 is the scenario with lower impacts compared to the situation in which only the Mancha switch of origins is applied. Concerning fish habitat, the direct allocation of water to the Albufera decreases the fish habitat suitability for the Luciobarbus in Antella, decreases the habitat suitability variability for the Chub in Antella and further aggravates the habitat status for the Loina in the Mancha Oriental area during the extreme dry years, falling below the threshold of 30% for all scenarios. In summary, directly allocating water to the Albufera could have a distinct positive impact in its status without affecting hydropower nor aquifer storage, but it would negatively impact surface abstractions, agricultural benefits and fish habitat.

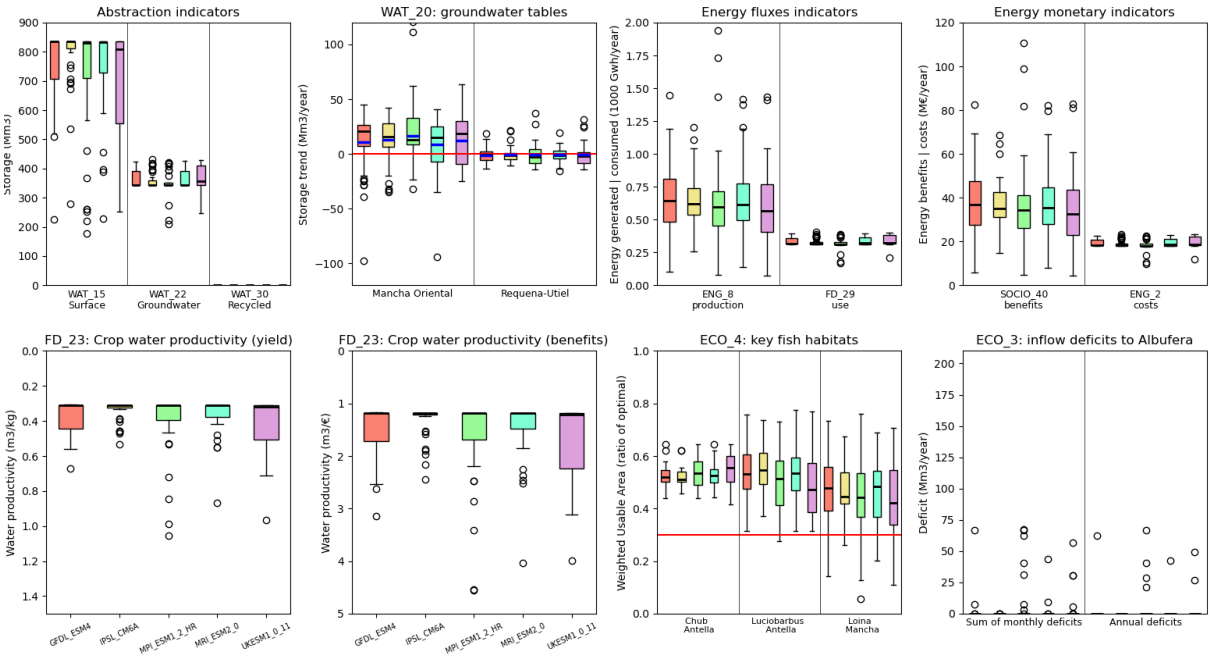

Figure 31. Jucar evidence computed by the whole model ensemble for the socio-economic scenarios (i) Mancha Oriental source switch and (ii) direct allocation to Albufera across selected indicators.

3.3.3 Summary of key evidence

The five climate scenarios (ensemble of five models), baseline and alternative (shift of Mancha Oriental water sources and direct allocation to the Albufera) socio-economic scenarios and policy options analysed in the Jucar River basin demonstrate the interconnections between the WEFE sectors. In this regard, energy production does not appear to be sensitive to the actions proposed, while energy costs vary according to aquifer storages. Aquifer storages in turn are related to agricultural productivity and benefits, since improving its status implies a decrease in crop yields and benefits. The ecological status of the Albufera, on the other hand, is negatively correlated to agricultural benefits and fish habitat, although the impact on the latter is relatively small. The alternative scenarios analysed (switch of the Mancha Oriental origins and direct allocation to the Albufera) would have a distinct impact on the WEFE sectors they address and, in the case of the switch of origins, on energy consumption and costs. Nevertheless, they would have negative side impacts on agricultural production, together with negative impacts on fish habitat in the case of the direct allocation to the Albufera.

3.4 Tagus-Segura

The Tagus-Segura system comprises two basins linked by an aqueduct through which the Tagus basin transfers water to the Segura basin (Figure 32). However, the two basins have

strongly different policy, physical, and management contexts. The nexus governance challenge is particularly trying in transboundary systems, as many stakeholders and other policy sectors must accept any action.

The Tagus basin's central axis is the Tagus River, the longest in the Spanish part of the Iberian Peninsula, stretching over 1092 km. Significant elevation, climate, and geology variability lead to a heterogeneous landscape. The basin climate is Mediterranean with continental features. It is the most populated basin in Spain, with almost 8 million inhabitants, and it is home to 11.8 million people and two European capitals (Madrid and Lisbon), which are important economic hubs. Cropland, found mostly on the plains close to the Tagus River, is the second most significant land use in terms of surface area (32% of the basin). In comparison, grassland covers 39% of the territory, this being the predominant land cover (Mezger et al., 2022). Aquifers are mostly seen as a strategic water source during severe droughts or to meet local water needs. The upper part of the TRB is less populated, and the primary source of water transfers to the Segura River on the Mediterranean coast. Water is diverted from the Entrepeñas and Buendía reservoirs, with a total storage capacity of 2,518 hm³ (23% of the total reservoir capacity in the basin).

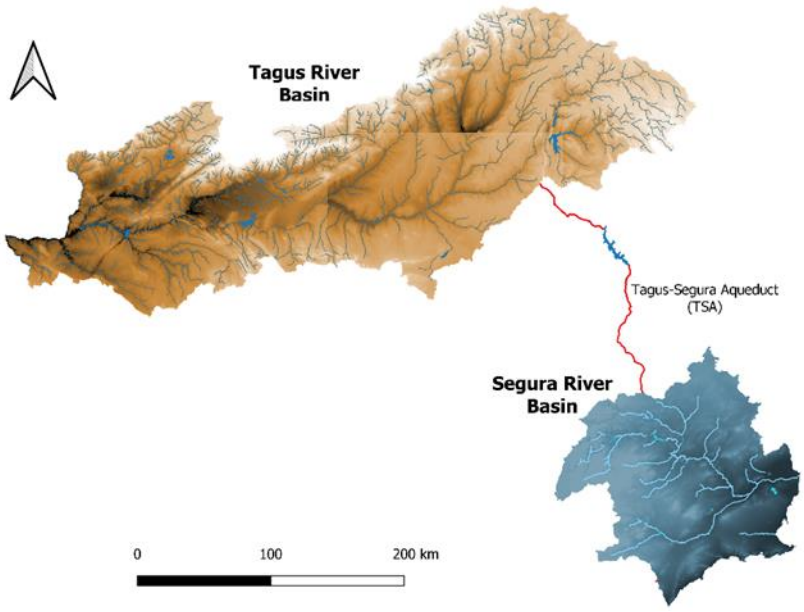

Figure 32. Map of the Tagus and Segura River basins and their connection through the water transfer system (TSA).

On the other hand, the Segura River Basin (SRB) district is in south-eastern Spain and covers an area of 18740 km^2. The co-existence of good-quality soils, a semi-arid climate and water resources, both surface and groundwater, has fostered the development of one of Europe's most productive irrigated agriculture systems (Pellicer-Martinez and Martínez-Paz, 2015). Given the elevated participation of the agricultural and tourism sectors in the water-use activity of the basin, the water demands are highly seasonal, the summer being the period when greater volumes are required (Perni & Martínez-Paz, 2017). However, the natural water resources, mainly originating in winter and spring, are at their lowest levels in summer. This

seasonal gap and frequent droughts in the basin have promoted the construction of important hydraulic infrastructures since the beginning of the 20th century. Although the capacity of the reservoirs (over 1,100 Mm3) is greater than the mean annual surface water resources (1,010 Mm3), the supply problems have not yet been solved. Due to this, transfers from other basins (TRB) and a large group of coastal desalination plants are implemented at the SRB.

3.4.1 Overview of Challenges, Models, and Indicators

Relevant challenges were identified based on the first GoNEXUS Dialogues performed with the stakeholders of both basins. In Table 4 challenges are shown, and preliminary solutions are identified for each.

Table 4. WEFE nexus challenges and preliminary solutions of the Tagus-Segura case study.

Challenge	Solution
Water deficit due to recurrent drought episodes and growing water scarcity.	Monitoring the water resource and adapting production models based on availability; Improving purification methods to promote water reuse.
Energy transition: Implementing a renewable, sustainable, and profitable energy model.	Actively prioritising the implementation of renewable energies and self-consumption practices to reduce carbon emissions and promote sustainability.
Environmental sustainability: Aligning economic activities with ecological health to protect ecosystems.	Prioritising the implementation of ecological flows based on nature and exercising greater control over resource use and pollution hotspots
Agri-food sustainability: Enhancing the agricultural sector and implementing sustainable models that ensure food security.	Providing training and technical support to producers for crop diversification that meets local and seasonal needs. Adopting modern and technological production systems.

Although the challenges identified are a joint reflection of the two basins, it was necessary to propose two different modelling methodologies to obtain the evidence in each case due to the geographical and operational heterogeneity between the basins.

In the case of the Tagus basin, a chain of two models was used. (1) A hydrological model in SWAT for hydrological modelling of the system based on meteorological scenarios according to the scenarios described in Chapter 2, and (2) a VENSIM system dynamics model for operational simulation of the system. Three models were used for the Segura basin case. (1) A fully distributed eco-hydrological model in TETIS for hydrological simulation, (2) a hydro-economic model in STIG-CROPROD for economic and operational simulation of the system, and (3) a system dynamics model in VENSIM that is coupled with the Tagus basin and that complements the results of the hydro-economic model. A more detailed description of these model chains can be found in D4.1.

For the Tagus basin, the SWAT model was calibrated at a monthly scale in Cedillo (outlet in the Spanish part) for the period from 2002-2018. Data used for calibration includes wet, average, and dry years. Calibration was carried out for discharge with naturalized series from

the Tagus River Basin Authority. For model warm-up, years from 2002 to 2005 were used for calibration, 2006 to 2012, and 2013 to 2019 were used for validation. Parallel, a SWAT+ is currently being calibrated, but due to lack of time, only results for the SWAT are shown in this deliverable and have been used as input for the SDM. The idea for D5.7 is to use the results of SWAT+ since it introduces several improvements and enhancements over the original SWAT model. These improvements aim to increase the model's flexibility, accuracy, and usability for hydrological and environmental simulations. Especially, SWAT+ offers more flexible and detailed definitions of Hydrologic Response Units (HRUs) and provides improved connectivity between sub-basins and reaches, supporting more complex routing and better representation of landscape interactions, together with a more detailed groundwater modelling, with enhanced representation of aquifer interactions and subsurface flows. Table 5 and Figure X show model performance in Cedillo. **¡Error! No se encuentra el origen de la referencia.** shows the simulation efficiency through the most widely used statistics tests reported for calibration and validation: R^2, Nash Sutcliffe and KGE.

Table 5 Calibration and validation statistical indexes for the hydrologic modelling in the Tagus River basin

Period	NSE	R2	KGE
Calibration (2006-2012)	0.52	0.63	0.70
Validation (2013-2019)	0.60	0.67	0.55

¡Error! No se encuentra el origen de la referencia. Figure 33 depicts the hydrograph for the observed values against the best simulation obtained.

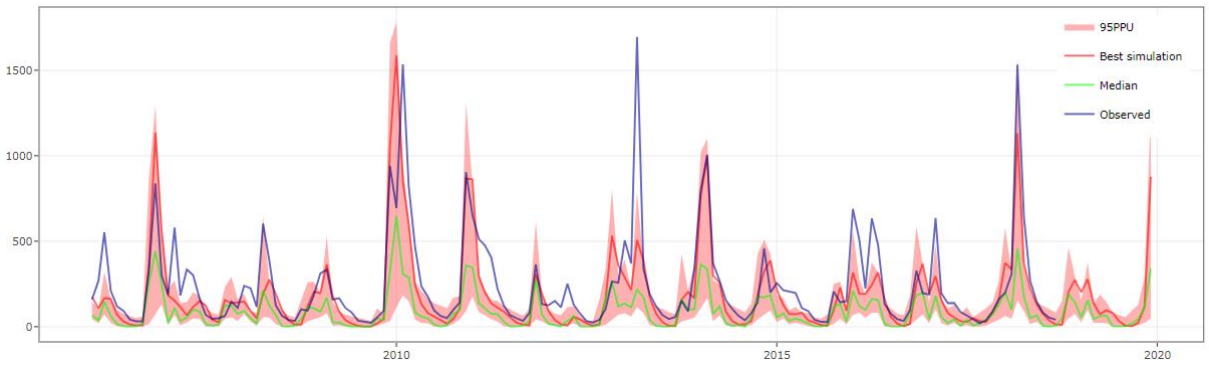

Figure 33. Simulated and observed hydrograph for calibration and validation period. Cedillo station Tagus River basin.

A preliminary list of indicators was defined in D5.1 to synthesise the evidence obtained in each case and facilitate the diagnosis of the basins with a nexus vision. However, a smaller list of indicators most relevant to the study was defined based on the challenges identified in the first dialogues, the exploration of solutions for these challenges, official initiatives already projected, and the characteristics and limitations of the model chains.

Although the Tagus and Segura systems have heterogeneous contexts, the nexus challenges faced by each basin are directly or indirectly related to the transfer of water resources from the upper Tagus River basin to the Segura River basin. The situation of the Tagus-Segura system is contextualised below in Table 6, including the hinge effect of the TSA (Tagus-Segura Aqueduct) between the two basins, the main challenges faced and their interconnection, the indicators that allow diagnosing its status in each case and the possible solutions already being evaluated in the system.

3.4.2 Evidence simulations results

Tagus River basin

The indicator WAT_1 River discharge has been calculated using the five climatic models for the reference period at two river sections, as shown in Figure 34. The Tagus basin has been divided into two sub-basins: Upper and Lower. The Upper part is characterised mainly by the water transfer to the Segura basin and the Madrid city's pressure in the system. The Lower part starts from the Azután reservoir and is a sort of cascade of reservoirs in the main channel for hydropower production until the border with Portugal (Cedillo reservoir). Following the State Official Gazette (Num.179, 2021), the SDM encompasses the rules for transferring water to the Segura basin. The volume of water transferred depends on the combined volume storage of the Bolarque, Entrepeñas and Buendía reservoirs at the beginning of the month, representing the indicator WAT_4 reservoir storage in Figure 35.

Table 6. WEFE main indicators of the GoNEXUS SAF computed for the Tagus-Segura case study.

ASPECT REGARDING THE CASE STUDY	TYPE	SAF INDICATOR
The intensive agricultural activity through irrigation in the Segura basin is a primary component of the social and economic development of the territory. Water scarcity threatens this development.	Contextual Challenge	FD_20 Productivity of irrigated crops FD_23 Water productivity of irrigated crops
The scarcity in the Tagus-Segura system is more pronounced in the Segura basin. This system uses multiple sources of resources, both conventional (surface and underground water, 53%) and non-conventional (reuse, desalination, and transfers, 47%), to reduce the chronic deficit in supply to demands (especially agricultural ones).	Contextual	WAT_18 Freshwater withdrawn per sector WAT_20 Groundwater withdrawn per sector WAT_28 Total treated municipal wastewater WAT_30 Amount of wastewater recycled FD_24 Agricultural dependency on groundwater
Desalination water has represented 10% of the resource available to supply the Segura basin. The future increase in this resource is emerging as one of the most viable solutions to face the challenge of current and future scarcity. However, an effective future increase in the use and availability of desalinated resources for irrigation is inhibited by various factors such as the limitation of infrastructure, low concentrations of nutrients for irrigation, high energy consumption, and high economic costs to the farmer.	Contextual Challenge Solution	WAT_25 Desalinated water use/abstraction FD_28 Energy consumption per crop (Desalination)
The distribution of the energy mix used in the Segura basin to extract underground resources and desalinate seawater represents a considerable load of CO_2 emissions into the atmosphere.	Challenge	FD_32 Total Agricultural Greenhouse Gas Emissions
Reducing agricultural irrigation demand in the Segura basin, supported by improvements in irrigation efficiency or migration to economic sectors with lower water consumption, is another plausible solution to mitigate resource scarcity.	Solution	FD_23 Water productivity of irrigated crops
Water transferred from the Tagus basin has driven agricultural development in the Segura basin for decades. This resource represents 20% of the total resources available to meet agricultural and urban demands.	Contextual	WAT_34 Water transfers

ASPECT REGARDING THE CASE STUDY	TYPE	SAF INDICATOR
Recently, the reduction in the amount of transferable volume and even the existence of transfer itself has been debated. The guarantee of environmental flows in the Tagus basin and the improvement of the quality of the resources are two of the main arguments for seeking the reduction of the transfer.	Contextual Challenge	WAT_1 River discharge WAT_4 Reservoir volume WAT_11 Land Surface runoff WAT_14 Water requirement for habitat and fish migration
The agricultural sector in the Tagus basin is mainly rainfed. However, adverse climate change scenarios could drive a transition to irrigated agriculture. This change could imply the need to increase surface extractions, impacting other nexus components such as energy production or the maintenance of ecological habitats.	Contextual Challenge	FD_2 Cropland extent FD_35 Crop water needs
The generation of hydroelectric energy in the lower Tagus basin is one of the main components of the territory's economic development. The reduction in the availability of surface resources may threaten this development.	Contextual Challenge	ENG_8 Energy production from hydropower - river basin ENG_9 Energy production from a specific hydropower plant

Figure 34 presents a comparison of river discharge at the outlet of the Upper part (Azután) after the water transfer to the Segura (WAT_1 River Discharge Azután PT). The reduction in the flow is significant downstream of the Entrepeñas and Buendia Reservoirs from where the water is taken.

The Indicator WAT11_ Land Surface Runoff is also calculated and shown at the watershed level for the five climatic models.

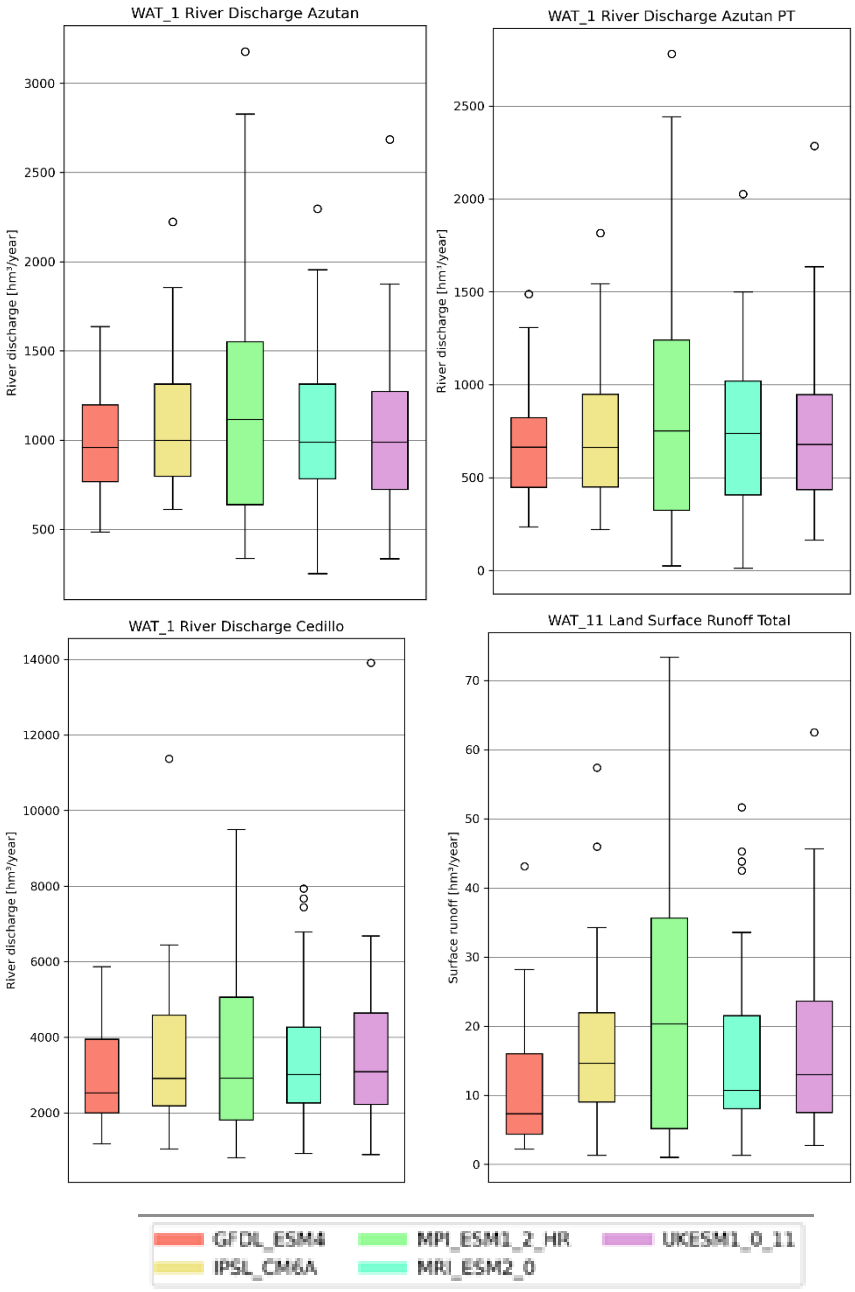

Figure 34. SAF indicator for water availability evaluation in Tagus River basin.

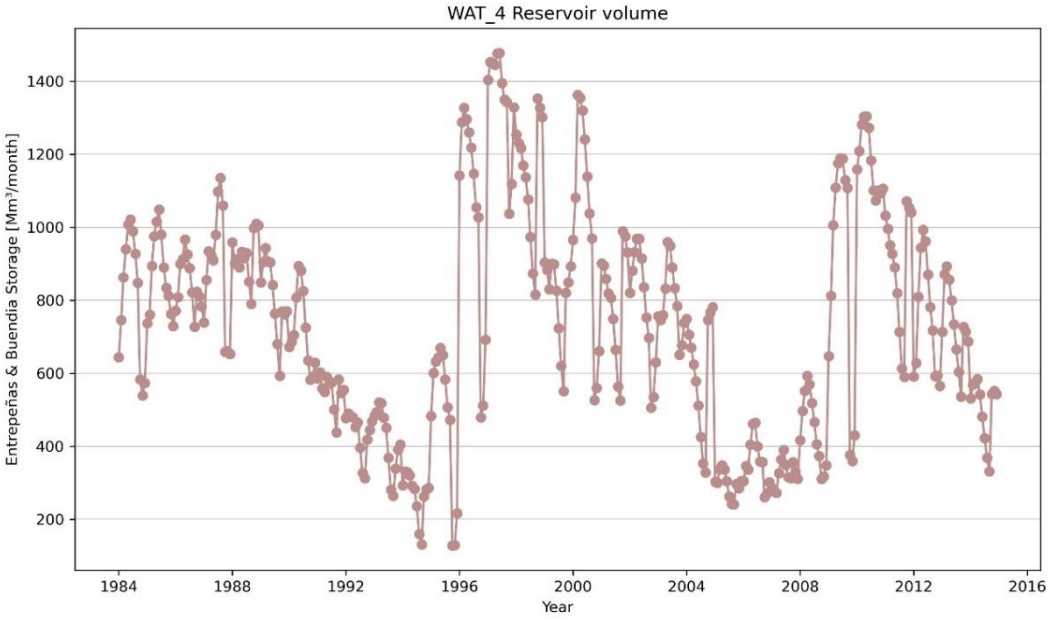

Figure 35. SAF indicator for evaluating water reserves in the upper Tagus River basin.

Regarding Energy Indicators, Figure 36 illustrates the variation in energy production at the main hydroelectric plants in the Tagus Basin. The different climate models show varied predictions in energy production, with the MPI_ESM1_2_HR model consistently exhibiting higher variability and outliers. This model predicts significant fluctuations in hydropower output, indicating potential periods for lower and higher-than-average production.

Assessing this indicator in future climate scenarios is crucial for understanding energy production patterns, given its importance to the Tagus Basin and various economic sectors. This evaluation allows for implementing measures focused on promoting the use of alternative energy sources to mitigate potential decreases in hydroelectric production.

The total hydropower energy generation, as depicted in Figure 36, varies across different climate models. The median values range between approximately 250 and 350 GWh/year, with the MPI_ESM1_2_HR model showing the highest variability and some outliers reaching up to 700 GWh/year. This suggests that the MPI_ESM1_2_HR model predicts significant fluctuations in hydropower output, which could be crucial for planning and management.

The observed variability in energy production underscores the need for robust energy management strategies. The differences in energy production across the models highlight the importance of diversifying energy sources and enhancing storage capabilities to buffer against periods of low hydropower generation. Ensuring energy security in the Tagus Basin requires a flexible and adaptive approach to managing energy resources.

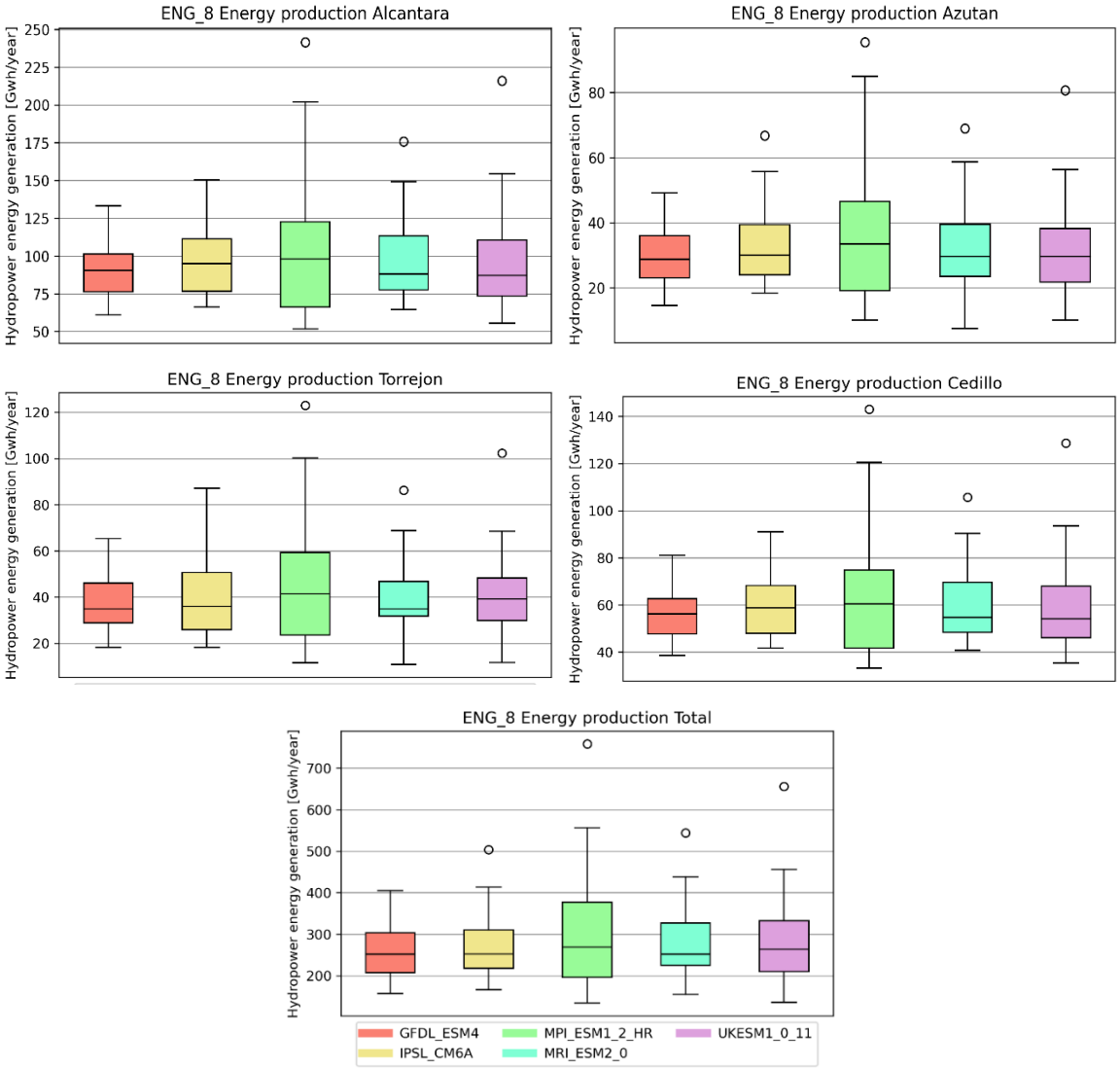

Figure 36. SAF indicator for evaluating energy production in lower Tagus River basin.

In contrast to the Segura, rainfed agriculture dominates the Tagus basin. Cereals such as barley, wheat and oats are the most popular annual crops, followed to a lesser extent by permanent olive groves and vineyards. In Figure 37, Cropland extents (FD_2) are presented, and the share of the different land uses can be observed from 1990 until 2018. Data is extracted from CORINE Land Cover — Copernicus Land Monitoring Service and used as an input into both SWAT and SWAT+ models.

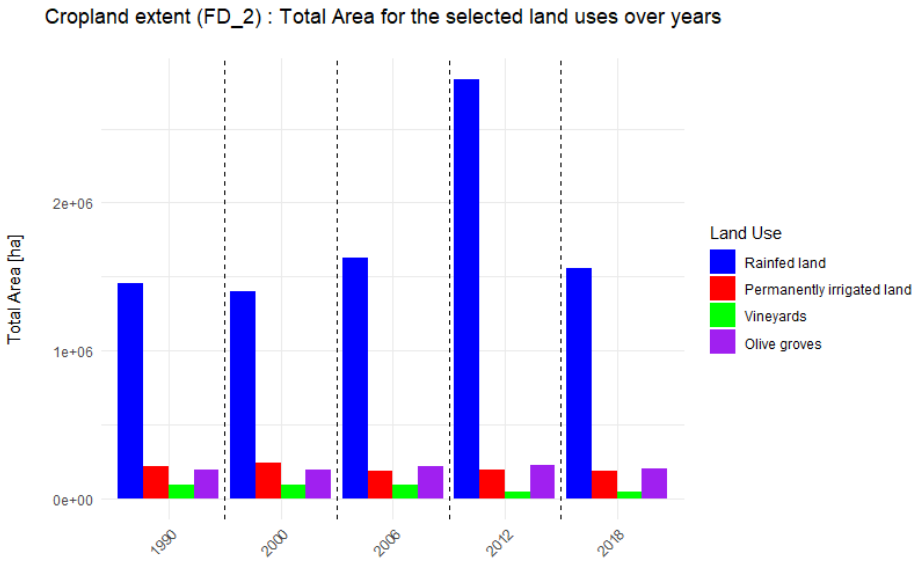

Figure 37. Cropland extent in Tagus River basin.

With the available data ERA5-Land | ECMWF (1981 – 2019), temperature and precipitation trends were calculated to explore rainfed agriculture feasibility. The analysis was performed monthly using the Mann-Kenndall test and Sen's trend slope. The MK-Test allows the detection of significant trends and requires that the data is independent but does not require the data to be normally distributed, so it can be used to analyse trends in climate data, stream flow and water quality data. The Sen's slope allows the detection of the magnitude of trends, estimating the slope or rate of change. In precipitation, significant pixels were not found when a decrease in rainfall intensity was observed. The trend temperatures maps show in Figure 38 in red colour a significant temperature increase in the area, which leads to an increase in evapotranspiration and a potential increase of water stress for some of the crops. The objective was the spatial identification of pixels in the Corine land use maps under rainfed, vineyard and olive groves in 2018, which might have a potential risk of suffering water stress, affecting yields and maybe future crop feasibility (Deliverable D5.7) in the area for traditional crops, due to a clear trend in the increase of temperature, which will lead to an increase in ET since the pixels trends in precipitation remain either with no change or with a decrease (which will even contribute to higher stress).

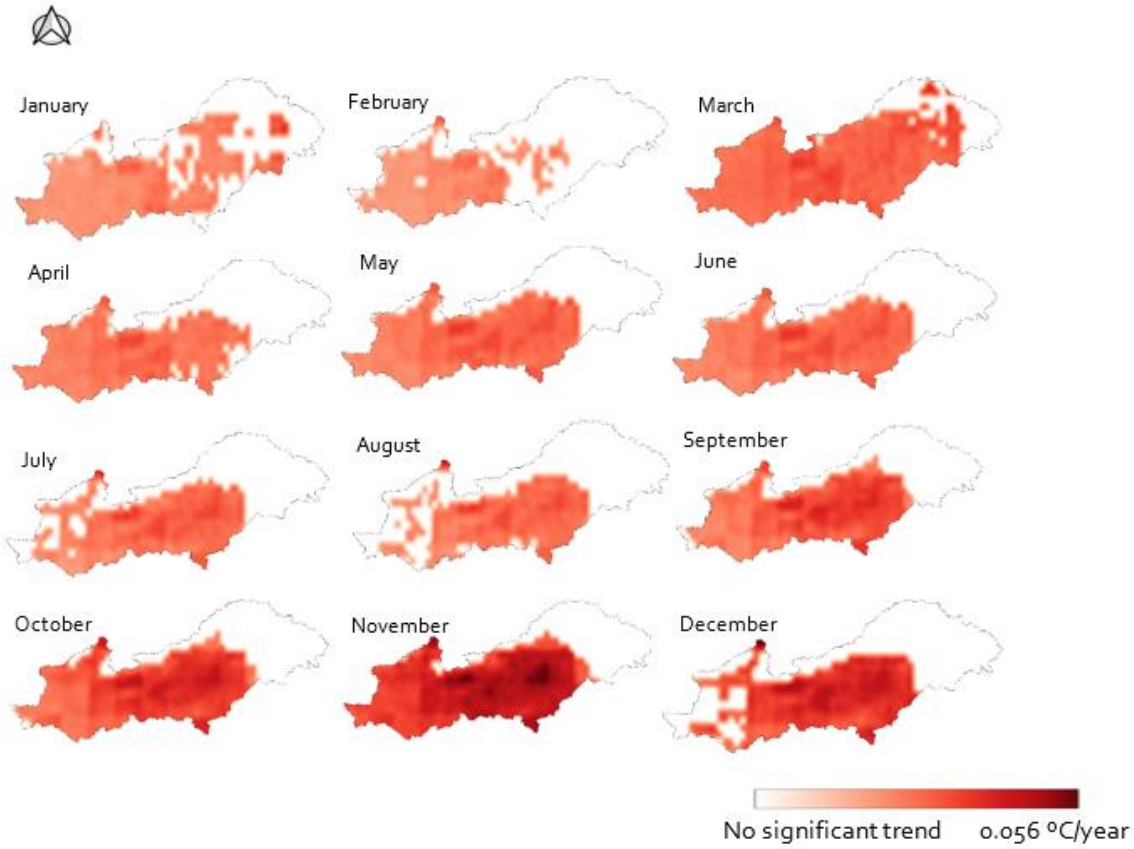

Figure 38. Monthly temperature trend (1981-2019) for Tagus River basin.

The water deficit was calculated as the difference between the water crop needs and the effective rainfall in mm to account for water stress in crops. Figure 39 and Figure 40 show potential pixels that might have gone under water stress for the studied period. This assumption leaves out any potential water uptake from groundwater. Although crops such as olive groves and vineyards with deeper root systems are reaching it, no information was available about the spatial distribution of the water table. The effective rainfall was obtained following FAO Chapter 3: Effective Rainfall (https://www.fao.org/4/s2022e/s2022e03.htm).

Following FAO Chapter 3: Crop water needs,[1] the Blaney-Criddle theoretical method was used to calculate the reference crop evapotranspiration, ETo. The Blaney-Criddle method is simple, using measured data on temperature only. It is, therefore, not very accurate; it provides a rough estimate or "order of magnitude" only. Current parallel methods are being used to gain accuracy in the ETo calculation:

$$ETo = p(0.46T_{mean} + 8) \qquad \textit{Equation 1}$$

where p is monthly precipitation in *mm*, and T_{mean} is the mean monthly temperature in °C.

[1] https://www.fao.org/4/s2022e/s2022e07.htm#3.1.3%20blaney%20criddle%20method

In order to calculate the crop evapotranspiration (crop water needs) ETc, FAO recommendations for crop growing period (Chapter 2: Crop Water needs[2]) and Kc coefficient (Chapter 6: Single Crop Coefficient-Kc[3]) were considered:

$$ETc = ETo * K_c$$ *Equation 2*

The different land use changes were used from Corine data: LU 1990 (we assume it is permanent from 1983 – 1996), LU2000 (1997-2002), LU2006 (2003-2008), LU2012 (2009-2014). Olive groves and vineyards are spatially specified in Corine, but a general category is given for rainfed agriculture. The most representative rainfed crops per province for the different periods above from Spanish national statistics of the Spanish Ministry of Agriculture were analysed, and a homogeneous distribution to check a potential risk of water deficit was assumed. Figure 39 and Figure 40 show the spatial distribution of potential water deficit for olive groves and vineyards.

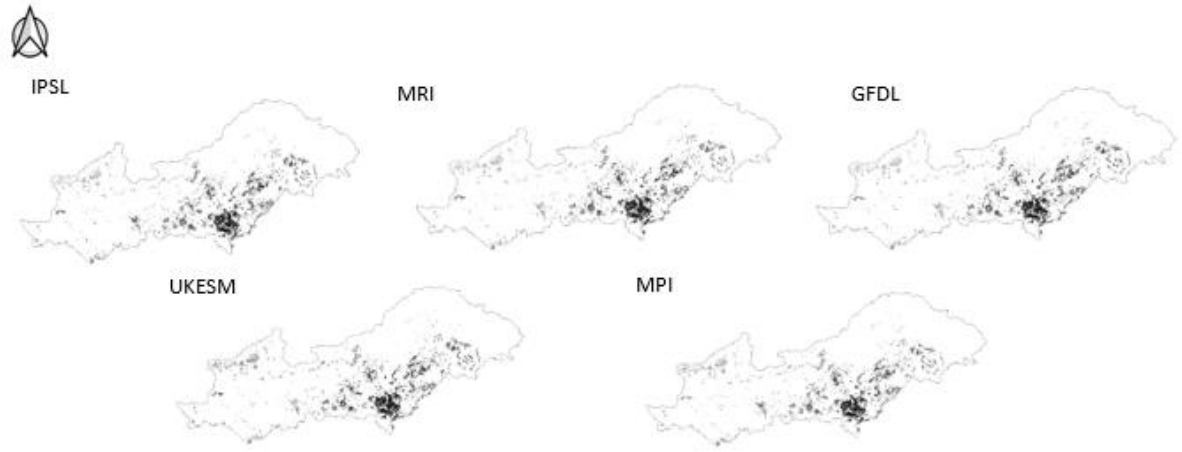

Figure 39. Water deficit in olive groves [mm]

Figure 41Table 7 presents the maximum and minimum values of the potential millimetre water deficit for the selected crops.

[2] https://www.fao.org/4/s2022e/s2022e02.htm#2.4%20determination%20of%20crop%20water%20needs
[3] https://www.fao.org/4/X0490E/x0490e0b.htm

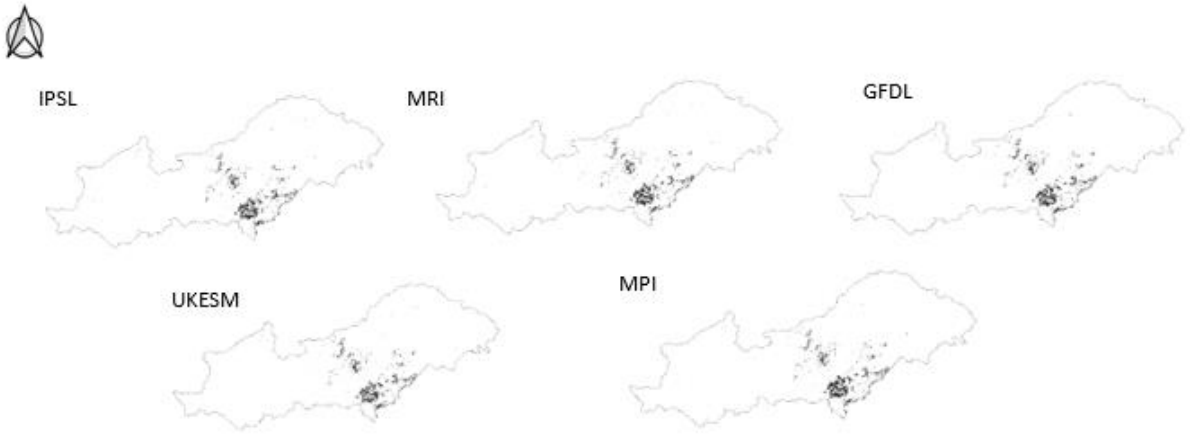

Figure 40. Water deficit in a vineyard [mm]

Table 7. Maximum and minimum water deficit values for olive and vineyard in Tagus River basin.

	IPSL		MRI		GFDL		UKESM		MPI	
	Max	Min	Max	Min	Max	Min	Max	Min	Max	Min
Olive grove (mm)	736.5	238.5	743.2	357.3	715.6	309.2	717.6	229.4	779.7	360
Vineyard (mm)	387.8	47.7	434.2	38.2	406	64	386.5	6.7	389.2	43.2

Figure 42 indicates it for wheat, barley and oat in non-spatial information due to the inconsistency of realistic crop distribution maps. The mean (mm/year) is presented in the water deficit information section for representation purposes in this deliverable.

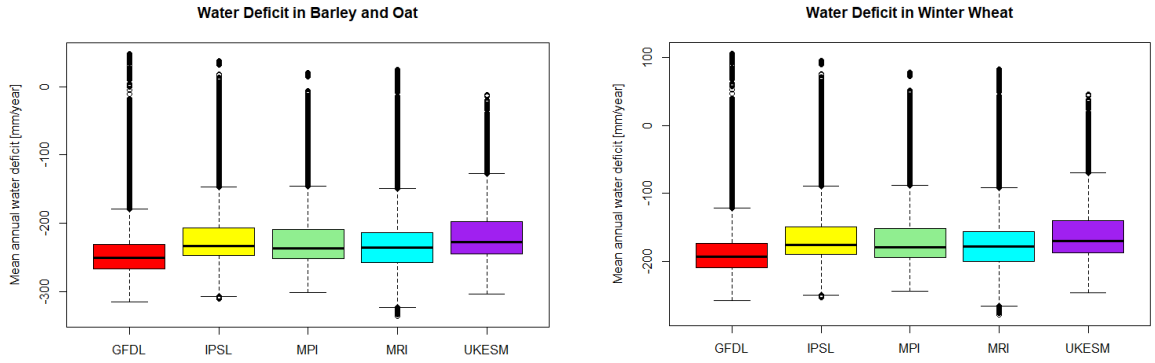

Figure 41. Water deficit of barley/oat and winter wheat in the Tagus River basin

From FAO GAEZ:v4 Data Portal (https://gaez.fao.org/), the gap yield for barley, olive and wheat was available in a raster format of 5 arc-minute for the year 2010. Although water availability is not the only factor affecting crop production, Figure 42 shows the improvement margin for yield (%) for the available crops. Water deficit and crop water stress are intrinsically linked to yields and food production. The significant trends in temperature increase might challenge the future of some of the rainfed crops in the basin, risking traditional crop

production and possibly leading to a shift to an increase in irrigation areas under climate change scenarios.

Figure 42. GAP yield for barley, olive and wheat in 2010.

Segura River basin

The evidence simulations cover the reference period of the five climate change scenarios defined in D2.2. For each scenario, variables and indicators referring to the WEFE nexus are calculated for this period to provide a broad and coherent picture of how the WEFE nexus performs and how trade-offs across the WEFE nexus behave. Although the developed models allow obtaining a large number of system variables, only the results obtained for the most relevant indicators (Table 6) are presented below, as well as the results of some additional variables that help contextualise the state of the system in the reference period.

Regarding the yield of irrigated crops (Figure 43, panel FD_20), despite the historical water deficit in the basin operating system, all climate models show a relatively high median crop yield between 120 and 160 t/ha. Despite the variability of specific climate models, yields are consistently high in all models, suggesting that the productivity of irrigated crops has remained robust during the reference period. However, for future scenarios, the solutions proposed for the system challenges should seek to minimise the water deficit for irrigation, which should increase the mean annual crop yield and decrease its variability.

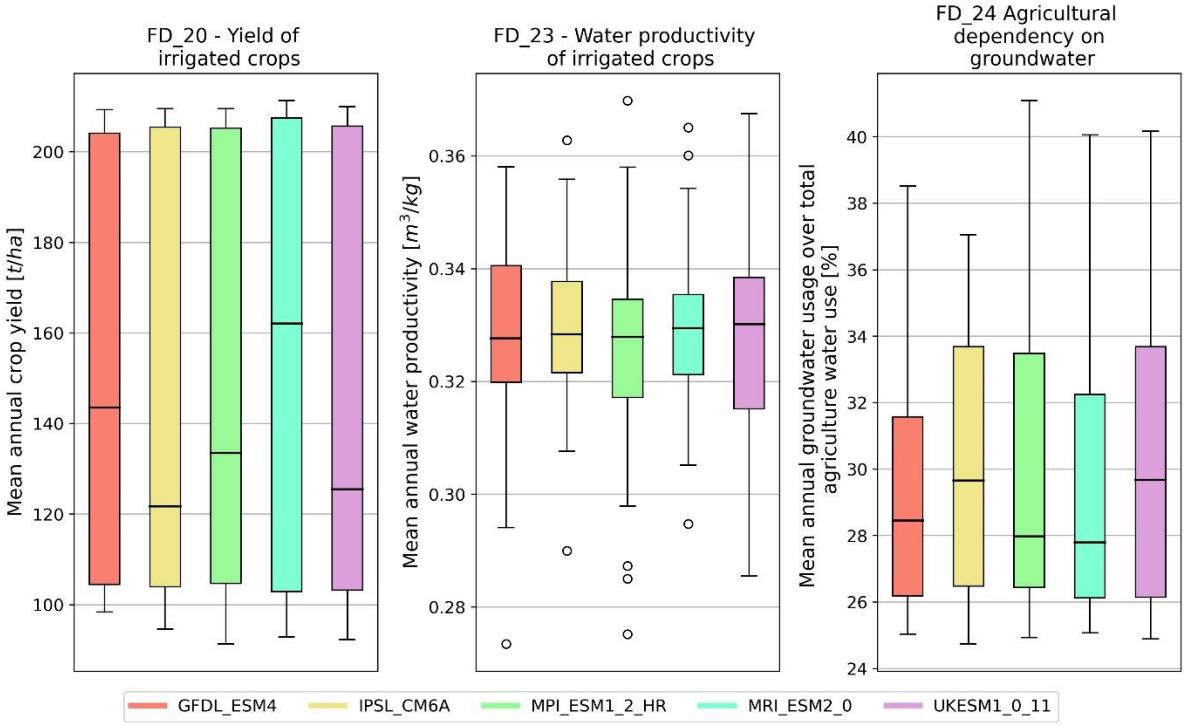

Figure 43. SAF Indicators for evaluating agricultural activity through irrigation in the Segura River basin and the scarcity challenge.

In Figure 43 (panel FD_23), water productivity varies slightly between models, with values ranging from approximately 0.31 to 0.34 m³/kg. Some models show a more significant variation, indicating that water use efficiency may be more uncertain under specific climate scenarios. Although irrigation efficiency in the basin is already high, adopting modern and technological production systems in key irrigation demands should increase efficiency in water use at the basin scale. Finally, in Figure 43 (panel FD_24) the dependence of irrigation agriculture in the Segura basin on the underground resource can be put into context. A comparison of this indicator in future climate change scenarios is helpful in indirectly evaluating the ecological component of the nexus, referring to the overexploitation of aquifers. By implementing solutions that guarantee an increase in the supply of other types of water resources that replace resources from non-renewable pumping from aquifers, agriculture's dependency on groundwater should decrease.

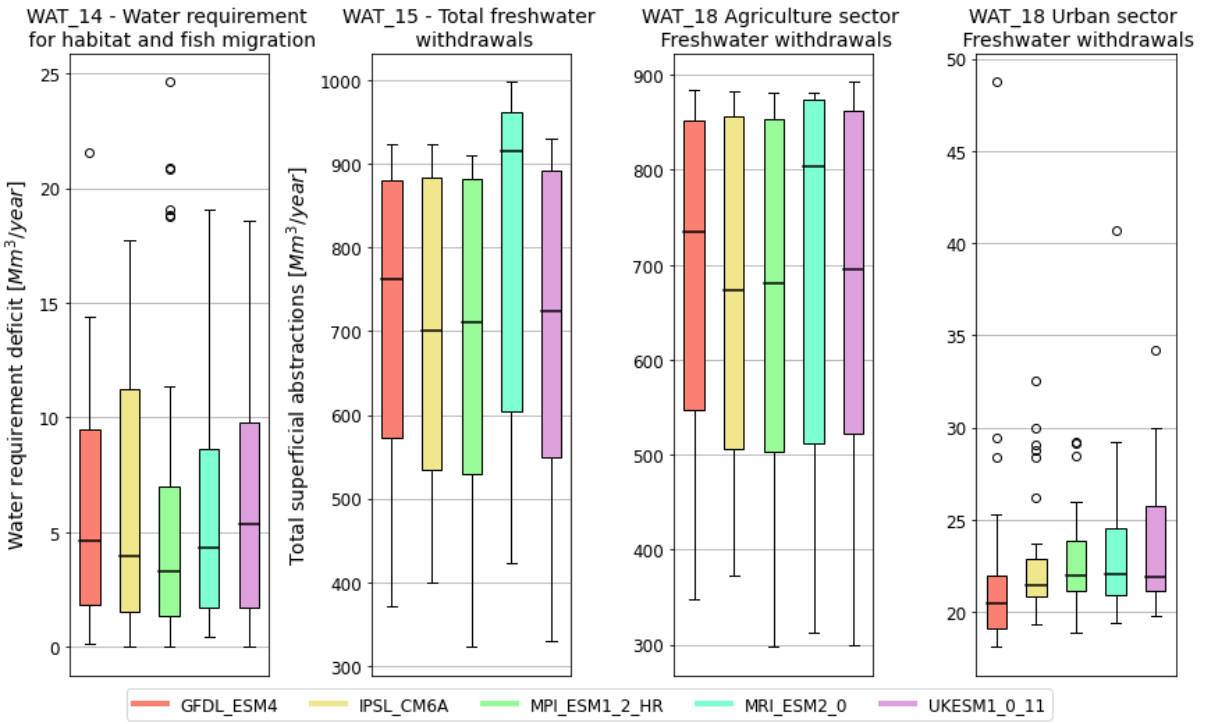

Figure 44 SAF Indicators for diagnosing superficial freshwater and the scarcity challenge in the Segura basin.

Considering that surface and underground water resources comprise 53% of the total available resources used in the basin, it is necessary to analyze indicators that describe their behaviour in various scenarios. Figure 44 (WAT_15) presents indicators that allow for the analysis of the use of surface water, discriminating them by urban and agricultural use in the Segura basin. In indicator WAT_18, it is easy to see the great weight of water used in irrigated agriculture. Regarding the ecological challenge in the system, WAT_14 describes the water requirement deficit for habitat and fish migration. This indicator considers the accomplishment of monthly ecological regime flows. The solutions formulated to improve the nexus governance are expected to ensure a decrease in this indicator.

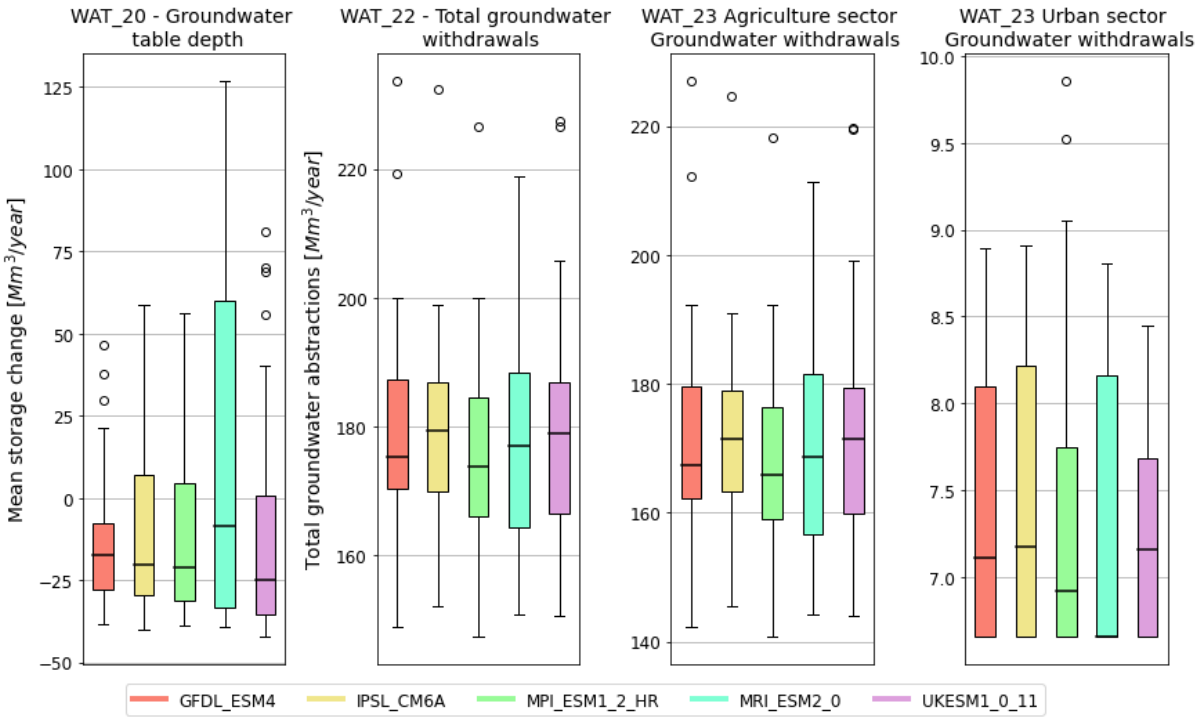

Figure 45 SAF indicators for the diagnosis of groundwater and the scarcity challenge in the Segura basin.

Figure 45 presents a series of indicators that contextualize the use of underground resources and the challenge of reducing the overexploitation of aquifers in the Segura basin. WAT_20 presents the average change in the total storage in the aquifers of the Segura basin, where it can be seen how the median of the total underground storage has been reduced between 10 and 25 hm³ compared to the storage at the beginning of the reference period. Water governance solutions within the nexus should seek to balance this negative shift in storage, thereby ensuring sustainable exploitation of the aquifers in the basin. On the other hand, from the other indicators (panels WAT_22 and WAT_23), we can again extract the great magnitude of water consumption for irrigation in the system and its annual variability.

Considering that some of the possible solutions proposed to improve the governance of the nexus in the Segura basin focus on the search for additional non-conventional resources, the indicators in Figure 46 were estimated to diagnose the current state of the use of these resources in the basin and thus be able to quantify their potential increase in future scenarios. Figure 46 WAT_25 presents the behaviour of water desalination used by urban and agricultural demands within the system. As can be seen, the volume desalinated annually presents a very low variability attributable to the system's maximum desalination capacity and restrictions for the reference period. This low variability behaviour can also be observed in WAT_28, which presents the volumes of treated municipal wastewater. In this case, the low variability of the resources is directly attributed to the high guarantee that the urban demands have within the system, which causes the volumes of wastewater to have a consistent behaviour over time. These two indicators show the consistency of two primary non-conventional water sources. This allows us to infer that increased desalination capacity can directly impact solving the system's challenges.

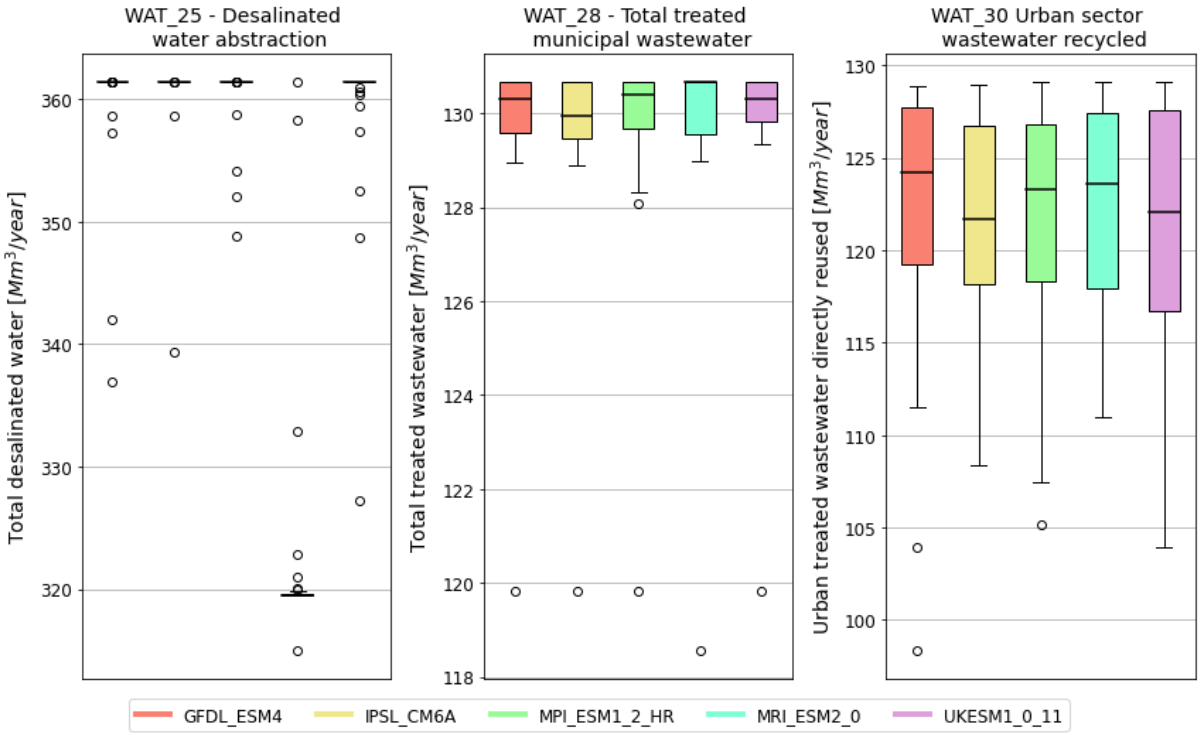

Figure 46 SAF indicators for evaluating non-conventional resources in the Segura basin.

For future scenarios and the evaluation of solutions, increases in desalination capacity will be projected from measures contemplated by the Segura River basin agency and from private initiatives formulated in the medium term. On the other hand, because wastewater treatment is closely related to the percentage of municipal water return in the basin (75% - 85% in the Segura basin), its capacity will increase in future scenarios based on prospecting future increases in urban demand and official wastewater treatment plans.

Concerning the energy and environmental component in the Segura basin, one of the main challenges is reducing energy consumption in agricultural irrigation and its corresponding GHG emissions. Currently, in Spain, 25% of the energy mix is still comprised of energy sources that generate GHG emissions, leaving the remaining percentage to renewable sources such as wind, hydraulic, and photovoltaic energy. Increasing the capacity of non-conventional sources such as desalination implies an increase in consumption, so seeking to increase energy production from renewable sources in the system can be a solution to face Segura's energy and environmental challenges. In Figure 47 FD_28, you can see the annual energy consumption variability, which is linked to the variability of the surface resource supply to irrigation demands. The fewer surface resources available, the more the system will depend on groundwater resources. For this reason, solutions focused on improving irrigation efficiency and adopting renewable energy for underground extraction can help reduce the temporal variability of available resources, both surface and underground, and mitigate the energy consumption of resource extraction.

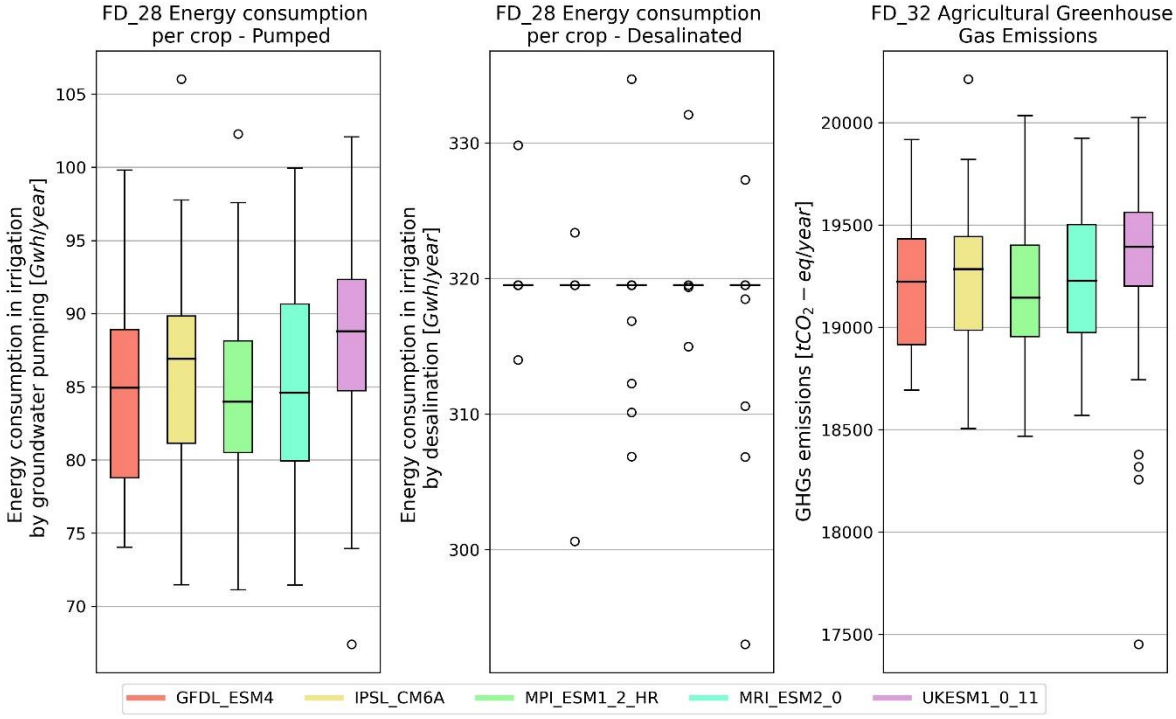

Figure 47. SAF indicators for evaluating energy consumption and GHGs emissions challenges in the Segura basin.

3.4.3 Summary of key evidence

The analysis of evidence for the reference period in the Tagus-Segura system highlighted the relevance of the connection between the two basins through the Tagus-Segura transfer. The variation in transferred volumes generates trade-offs in the components of the nexus of the two basins. The smaller the volume transferred, the greater the quality and quantity of resources available in the Tagus basin to face the challenges of scarcity and compliance with ecological flow regimes, as well as greater energy consumption and resource deficit in agricultural production in Segura. The proposed solutions to these challenges will focus on reducing the impact of transfer variation on the two systems; this will be sought by trying to provide resource independence to the Segura basin, looking for a balance between the generation of new resources and the increase in energy consumption, irrigation costs, and GHG emissions. Solutions for the Tagus basin will have to deal with the pressure of Madrid and its urban demand, the potential shift of rainfed agriculture to irrigation systems while keeping a good ecological status of the water resources.

3.5 Senegal

The Senegal River drains an area of 300,000 km² in western Africa (**¡Error! No se encuentra el origen de la referencia.**). The basin is shared by four countries: Guinea, Mali, Mauritania and Senegal. The headwaters are located in Guinea, the water tower of the Senegal River

basin (SRB), where the Bafing River runs north until it merges with the Bakoye in Mali. From there, the Senegal River runs north-west through a series of falls and gorges before arriving in Kayes. Downstream of Kayes, the hydraulic gradient is much lower and the river meanders through the plain while forming the boundary between Mauritania and Senegal until it discharges into the Atlantic Ocean. At Bakel, the Senegal receives the flows from the Faleme River, the last major tributary also flowing from Guinea.

Water in the SRB has been put to use by humans for transportation (navigation) and food production through flood recession agriculture. More recently, Senegal River flows have been used to generate hydroelectricity and three hydropower plants are now operational: (a) Manantali is a 200-MW power station supplied by an 11 km^3 multipurpose reservoir and (c) Gouina is 140-MW run-of-river power plant (b) Félou is a 62-MW run-of-river power plant located 60 km downstream of Gouina. Irrigated agriculture is mostly taking place downstream of Bakel, in Mauritania and Senegal, where the irrigation area is around 140 kha.

3.5.1 Overview of Challenges, Models, and Indicators

In the Senegal River basin (SRB), a preliminary analysis of the trade-off relationships reveals the existence of two coalitions of objectives: traditional food production (agriculture and floodplain fisheries) versus "modern" uses (hydropower, irrigated agriculture and river shipping). This trade-off is characterized by a strong political asymmetry: the former coalition involves politically and economically marginal communities, whereas the second one is advocated by the political and economic elites. In terms of vulnerabilities, the former coalition is particularly vulnerable to changes in allocation policies, whereas the latter is mostly affected by changes in supplies (e.g., climate change). Moreover, in terms of transboundary cooperation, a benefit sharing arrangement does exist for hydropower generation (riparian countries own shares of the power plants regardless of their location), but not for the agricultural sector.

Although the Senegal River basin is not yet approaching river basin closure, various alarming trends require the attention of water managers and policy makers: climate change and its impact on water demands and supply, increasing water demands due to sustained population growth, agriculture (irrigation and flood-recession agriculture), energy, navigation, etc.). The stakeholders responsible for managing water resources, and more generally those involved in the NEXUS, are faced with problems such as a lack of qualitative and quantitative information on water resources and water demands, and poor interaction between stakeholders within the basin, which complicate the identification of compromise solutions when managing trade-offs.

We rely on a hydroeconomic model of the SRB to reveal the evidence of the WEFE nexus. The model seeks to determine optimal allocation policies, e.g. reservoir releases, water withdrawals for offstream uses, throughout the system schematized in Figure 48.

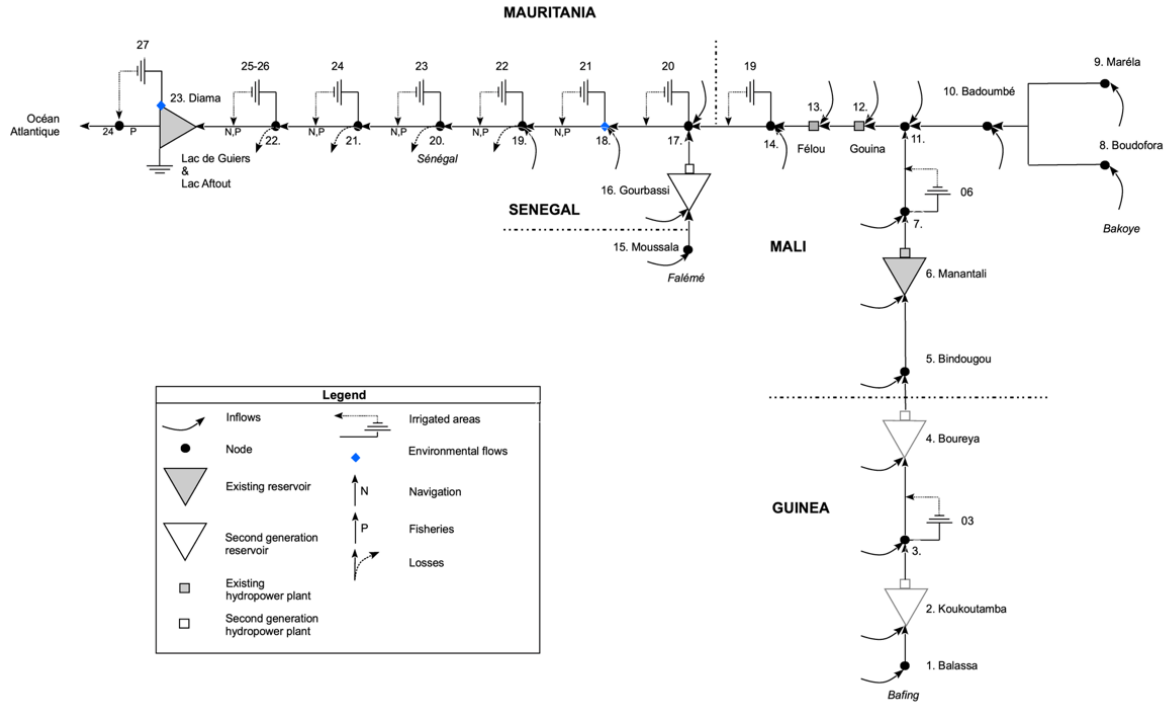

Figure 48. Schematization of the Senegal River basin.

In the reference scenario, this system comprises 3 hydropower plants (nodes 6, 12 and 13) , 2 reservoirs (nodes 6 and 23), 33 crops spread over 10 irrigation schemes for a total of 125 000 ha currently irrigated. Since both supplies and demands are highly seasonal, the allocation decisions are determined on a monthly time step for current hydrologic conditions.

Water allocation in the SRB is formulated as an optimization problem where the objective function corresponds to the expected sum of net benefits from water allocation subject to physical, operational, and legal constraints. The main economic activities are irrigated agriculture, hydropower generation, flood recession agriculture and fisheries. The development of river shipping is still in an early planning stage and economic appraisals have not yet been produced. Water withdrawals for municipal and domestic uses are considered as constraints. Economic data for agriculture, such as prices and crop budgets, come from either the recently updated river basin masterplan (SDAGE, 2022) or the surveys of agricultural households conducted at the beginning of the project. Energy prices correspond to the short-run marginal costs of the hydrothermal electrical systems of the West African Power Pool (WAPP, 2018).

Allocation policies are then simulated over the entire streamflow records (1904-2020) to assess performance indicators associated with the nexus for the reference scenario. Various relationships between relevant hydrologic attributes and WEFE indicators have been developed:

- Annual fish catch as a function of peak flow in Matam
- Inundated area as a function of peak flow in Bakel
- Cultivated area under flood recession agriculture as a function of peak flow in Bakel
- Total biomass production as a function of inundated area

– Reliability of navigation as a function of the flow at Richard Toll

Inundated area is detected using remote sensing products and a procedure explicitly developed within the framework of the GoNEXUS project. Various water indices have been successfully used in the Sahel to detect water bodies. The MNDWI, which overcomes the effects of bare soil, appears to be the most suitable for detecting water in Sahelian environments. The MNDWI formula is based on the normalized difference between the green and the SWIR band. A threshold for water detection was determined empirically from a variety of sources (direct examination of images as well as results from other studies). This work was carried out using Google Earth Engine with MODIS images, which have a spatial resolution of 250m and a temporal resolution of 8 days. The more precise Sentinel-2 data were also tested but are only available in the area from 2019. The work was carried out over the entire floodplain (between Bakel and Dagana), providing a series of maximum annual flood extensions between 2000 and 2022. The series shows high variability, with a minimum area flooded in 2017, with only 34,000 ha, and a maximum in 2003 with 368,271 ha. The second step consisted in determining a relationship between the monthly flow rates at Bakel (entrance of the valley).

Total biomass production is computed using WAPOR (https://data.apps.fao.org/wapor), the FAO managed portal on water productivity. It measures the production of biomass through the conversion of CO_2 by photosynthesis in the non-irrigated areas of the floodplain, from Bakel to the delta. For this indicator, we use a same procedure to define a relationship between discharge at Bakel (for September) and the average value of NPP over the potential flood zone during the months following the flood season (November to May). This is done to avoid the influence of rainfall on natural vegetation. We do not consider areas that have never been flooded (between 2000 and 2022), nor irrigated perimeters, to keep only vegetated areas that depend on flooding. The identified relationship between biomass production and river discharge in September is then used in simulation to assess the impact of altered flow regimes on biomass. When analysing future scenarios, we will assume that this relationship is still valid, i.e. floodplain plant communities will remain largely the same regardless of climate change. This assumption is motivated by the fact that floodplain plant species did exhibit resilience during the multi-year drought of the 80ies.

Figure 49 illustrates the modelling framework. This report deals with the reference scenario. However, for illustrative purposes, the framework also includes the three future scenarios identified during the dialogues (Full Business, Integrated Farming and Solar Revolution) even though they have not yet been analysed.

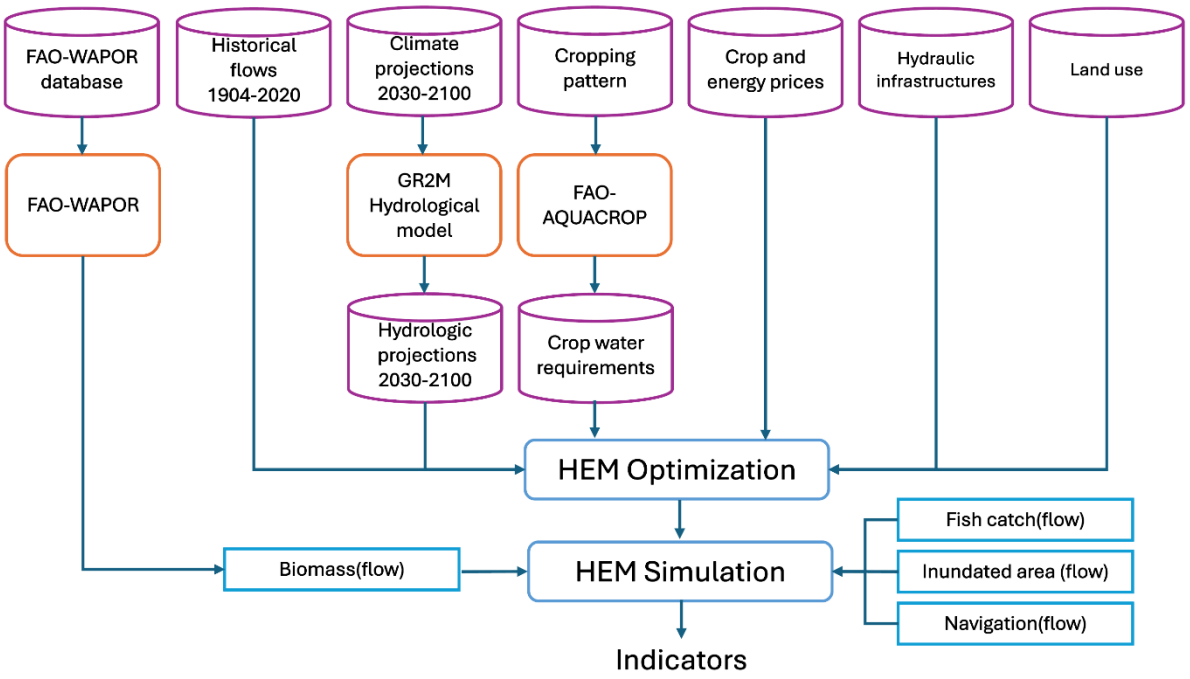

Figure 49. River basin modelling framework for the Senegal River basin.

3.5.2 Evidence simulations results

An overview of the WEFE nexus in the SRB can already be highlighted by focusing on a shortlist of six indicators: Irrigated area (ha), flooded area for flood recession farming (ha), annual fish catch (ton), hydropower generation (GWh), biomass production (gC/m²) and the reliability in ensuring minimum flows for river shipping (%). These six indicators are computed from simulations results associated with the reference scenario and a counterfactual one. The reference scenario corresponds to the current situation in the basin with three hydropower plants (one storage and two run-of-river) and total irrigated area of about 125 kha cultivated. In the counterfactual scenario, there is no reservoir so that the flow regime at the entrance of the floodplain is still largely natural.

Figure 51 displays the parallel coordinate plot for these two scenarios. As we can see, trade-offs exist essentially between two groups of activities: the first group includes "modern" activities such as irrigated agriculture, hydropower generation and navigation. The second group refers to the traditional food production sector, which includes flood recession agriculture and fisheries, and the sustainability of ecosystems captured through the biomass production indicator expressing the conversion of carbon dioxide into biomass driven by photosynthesis. When the relative performance in one group increases, then the performance in the other tends to decrease.

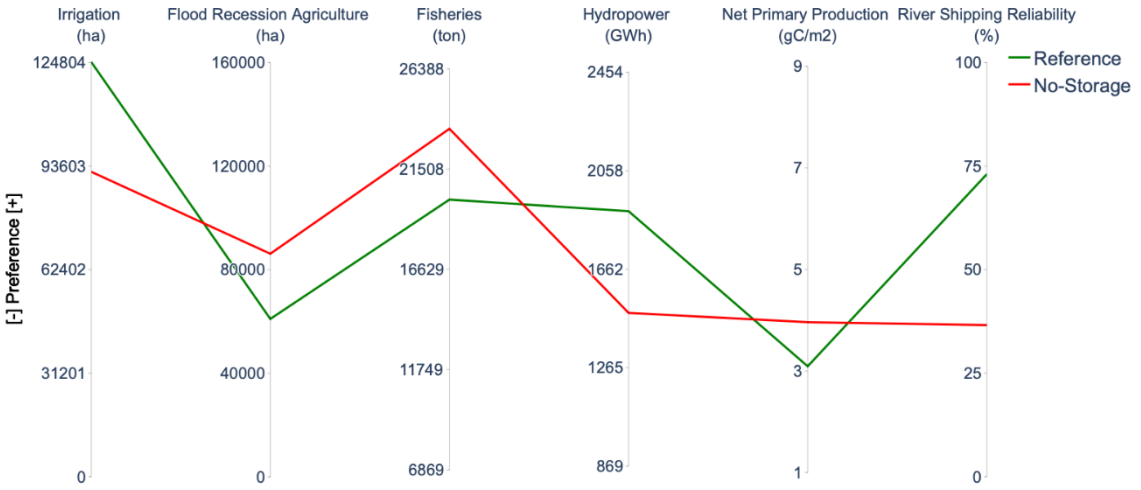

Figure 50. Trade-offs between competing uses (average values)

– The analysis of the trade-off relationship can be expanded to examine the year-to-year variability. Figure 51 Figure 52 displays the performance of the six major activities and their corresponding variability for the Reference scenario, while Figure 53 concentrates on the no-storage scenario. As we can see, the year-to-year variability of flood recession agriculture, fisheries, hydropower generation and navigation is substantial, indicating that the associated water users are exposed to significant hydrological risks. The number of irrigated hectares, on the other hand, remains constant regardless of the hydrological conditions in the basin. This is largely due to the Manantali reservoir and its ability to smooth the imbalance between supplies and demands. As a matter of fact, in the No-storage scenario, the area that can be irrigated is not only smaller but also much more variable. Not surprisingly, fisheries and flood recession agriculture perform better in the hypothetical scenario without the Manantali reservoir as the flow regime would be mostly natural.

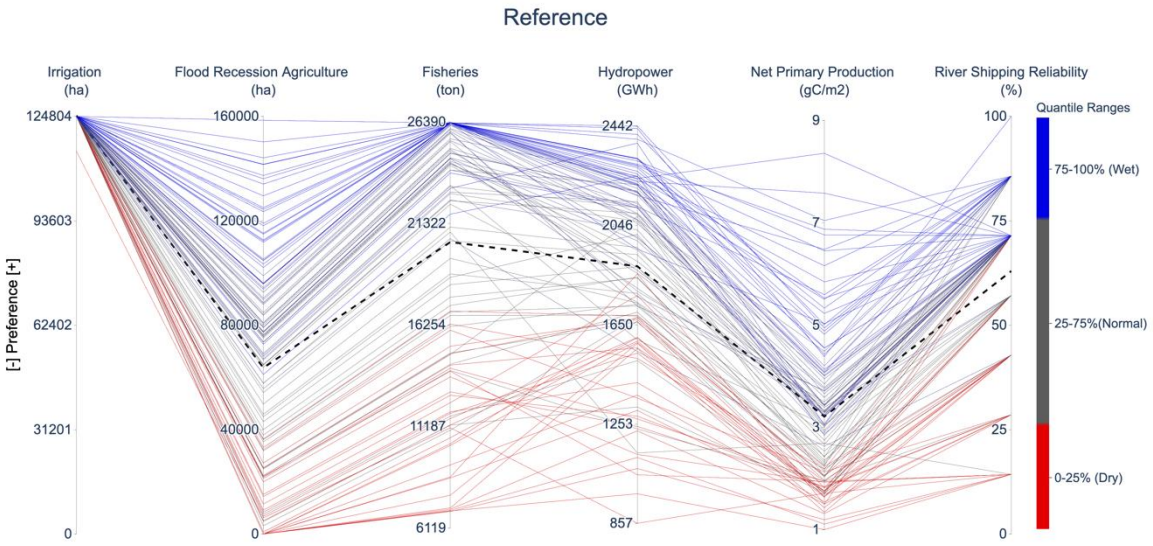

Figure 51. Trade-off for the reference scenario

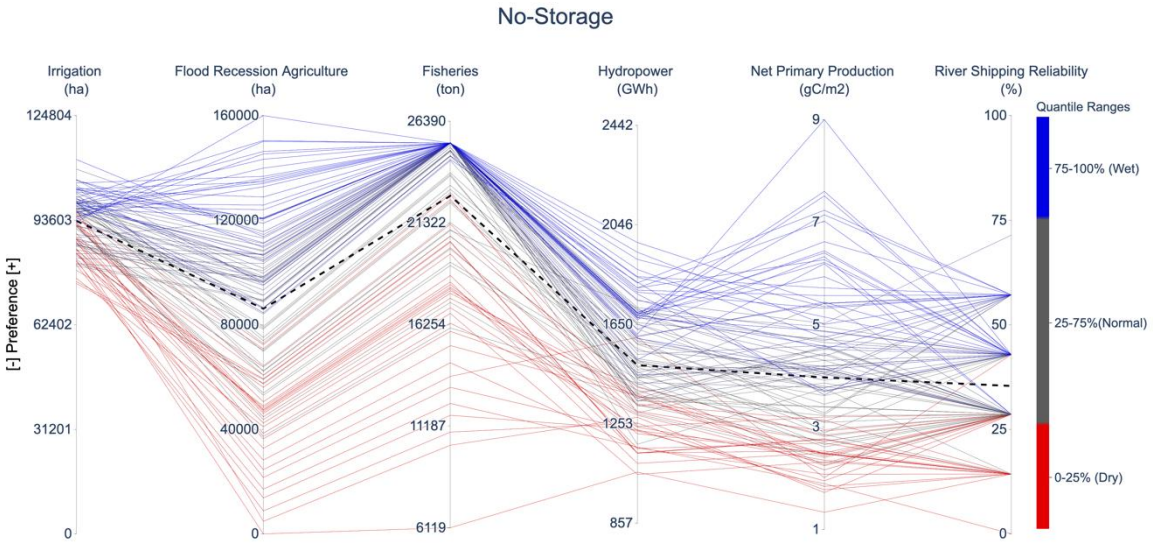

Figure 52. Trade-off for the no-storage scenario.

To better illustrate this main trade-off, we can look at the specific impact on different sectors.

– *Energy*. Figure 53 Figure 53displays the statistical distribution of the annual energy output for the Reference and No-Storage scenarios. For a given energy output, it gives the non-exceedance probability, i.e., the probability that the energy output is lower. The average energy production for the Reference and No-Storage scenarios, respectively, are around

1870 GWh and 1290 GWh. Notably, we can see that storage does increase energy generation about 96% of the time, underscoring the significance of water storage and regulation in enhancing the basin's energy security and reliability. In terms of firm energy (i.e., the amount of energy that can be guaranteed 90% of the time) the difference between the Reference and No-Storage scenarios is only 5%.

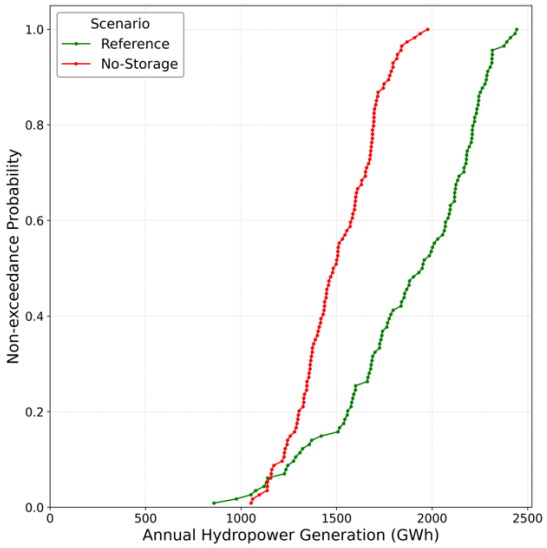

Figure 53. Statistical distribution - annual hydropower generation.

- *Irrigated agriculture*. Significant differences exist between the Reference scenario and the No-storage scenario. In the former, regulated discharges means that low flow augmentation ensures that current irrigation water demands are met regardless of the hydrologic conditions. Without regulation, the irrigated area varies between 80 and 110 kha depending on the annual volume of water available. Assuming an acceptable reliability level of 90%, only 85 kha could have been developed for irrigation without the Manantali dam.
- Traditional *livelihoods* and water uses, such as fishing and flood-recession farming, also exhibit distinct behaviours between the Reference scenario and the No-Storage scenario. Fish catches would be higher without the Manantali dam as the inundation of the floodplain would better replenish the fish stock by providing habitat for breeding and a nursery for various species. Then, during the dry season when the river gradually subsides, fish populations would be forced to leave the floodplain and concentrate in the main channel. Without the Manantali dam, 20 000 tons would already be caught 8 years out of 10, compared to 6 years out of 10 in the current situation. We can also see that the maximum fish catch is higher in the Reference scenario since fishing is possible in the Manantali reservoir (which does not exist in the No-storage scenario).
- Regarding *flood-recession* agriculture, the area cultivated each year is always lower in the Reference scenario following the reduction of flooding. The 50 kha objective from the river basin authority (Organisation de Mise en Valeur du Fleuve Senegal - OMVS) is exceeded 8 years out of 10 without storage, compared to 6 years out of 10 without storage.

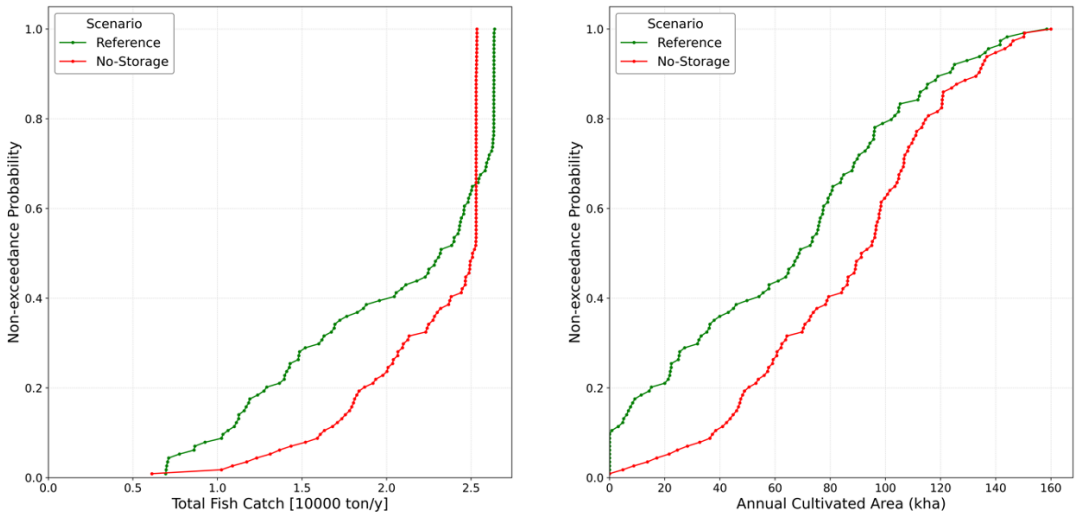

Figure 54. Statistical distribution of annual fish catch (left) and annual area for flood recession farming

– The *annual flooded area* is a particularly important ecological indicator in the Senegal River basin. The average flooded area in the Reference scenario is 200 kha, in contrast to the 370 kha a in the No-Storage scenario.

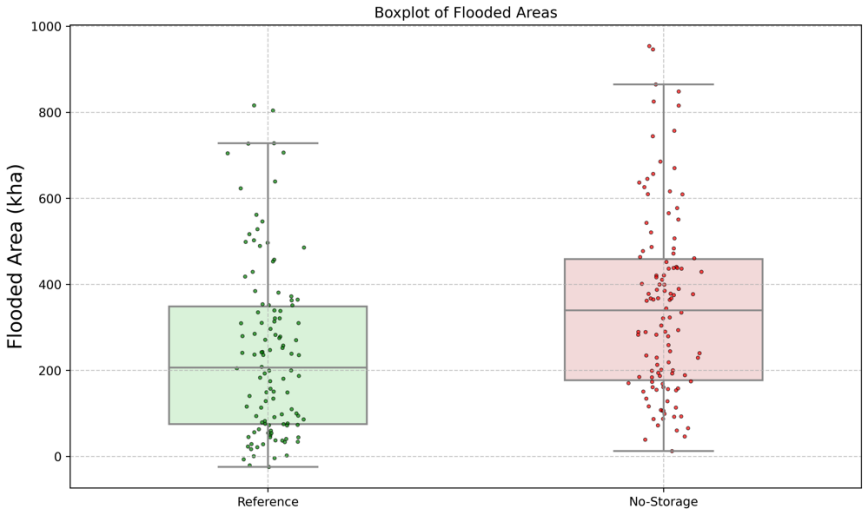

Figure 55. Flooded areas in Senegal River Valley.

Table 8Table 8 lists the WEFE indicators for both scenarios. Values associated with the Reference scenario will be used as a benchmark to assess the effectiveness of the proposed solutions with respect to the different aspect of the WEFE nexus in the Senegal River basin.

Table 8. WEFE indicators.

Sector	Indicator	Scenario	
		Reference	No-Storage
Water	Available water relative to max renewable available water at Bakel (%)	90	91
	Available water relative to max renewable available water at Outlet (%)	80	84
	Annual water withdrawal (hm^3)	2691	1969
	Annual water consumption (hm^3)	2789	1673
	Storage relative to annual inflow (%)	39	0
	Reliability in meeting minimum flow requirement for navigation (%)	63	35
Energy	Expected annual hydropower generation (GWh/y)	1873	1498
	Firm annual energy (GWh/y)	1292	1225
	Net benefits - energy (Million US$/y)	132	104
Water Energy	Energy footprint - ag sector (GWh/y)	78	53
	Fraction of renewable water resources used in the irrigation sector (%)	12	9
	Economic value of storage (Million US$/y)	34	0
	Opportunity cost of evaporation losses (Million US$/y)	5	0
Food	Crop self-sufficiency (%)	25	15
	Crop intensity (%)	77	58
	Flood recession area (ha)	63817	86137
	Irrigated area (ha)	124712	93272
	Gross production value - flood recession agriculture (Million US$/y)	13	18
	Gross production value - irrigated agriculture (Million US$/y)	3069	2074
	Gross production value - fisheries (Million US$/y)	41	46
	Fish catch (ton)	20275	22473
Water Food	Supply/demand ratio (water) (%)	100	73
Ecology	Net primary production (biomass) (gC/m^2)	4	4
Water Ecology	Inundated area (ha)	242232	351153

3.5.3 Summary of key evidence

Evidence of the interdependence between water, energy generation, food production and ecology is best illustrated by the presence of two coalitions of water-related activities: "modern" versus "traditional" uses. Modern uses include irrigated agriculture, hydropower generation and navigation, while traditional uses involve flood recession farming, floodplain fisheries and floodplain ecology. Making one coalition better off can only be achieved at the detriment of the other. In the second dialogue, we proposed solutions that would attempt at reconciling these two coalitions: implementing managed flood releases, developing a more diversify food production system and identifying the sustainable sequencing of new hydropower plants.

3.6 Danube

The Danube River is the second largest river in Europe with a length of 2 860 km and an area of 817 000 km^2. It is the world's most transboundary river, encompassing a population of 80 million, spread over nine countries. Between these countries, strong competing interests exist for the available water resources. The majority of the Danube River Basin lies within the European Union and is subject to relevant EU directives that should protect water resources and habitats (Water Framework Directive, Flood Directive, and Groundwater Directive for water, Nature Directives for habitats) but a substantial part of the headwaters of the tributaries of the Danube lies outside the EU and this makes water management over the Danube River Basin daunting. To strengthen international cooperation within its basin and to ensure sufficient water in terms of quantity and quality, the Danube River, the ICPDR (International Commission for the Protection of the Danube River) was established. Already currently water resources in the Danube are under stress and projected changes in climate and water demand will potentially aggravate the situation. In particular irrigation water demand and withdrawal are on the increase and together with the transition towards non-fossil energy resources (biofuels, hydropower, thermonuclear), this shall lead to increased water stress among the sectors and (aquatic) ecosystems that constitute the WEFE nexus.

3.6.1 Overview of Challenges, Models, and Indicators

Within the first round of dialogues for the Danube River Basin, three key challenges were identified, and fourteen points of interest identified by the stakeholders. These issues are addressed here by assessing relevant indicators and the three challenges are stated here:

- Challenge 1: **Water scarcity and increased flood risk** due to climate change, which may require changes in land management.
  As a consequence of climate change and dramatic changes in land management, there are quite significant changes in surface runoff, water retention and storage, hence floods and water scarcity. These changes are going to influence the recent land management practices.
- Challenge 2: **Water scarcity due to growing irrigation demand** as a consequence of a warmer and drier climate.

Agriculture is the major water user in the basin. In addition to climate change, other main drivers that influence the water nexus are the demographic changes and changes in agriculture (CAP, Farm-To-Fork). The pressure is increasing on water-intensive energy and food producers to look for alternative approaches due to the growing demand, particularly in water-scarce areas with large inter-sectoral competition for water.

- Challenge 3: **Vulnerability of riverine and terrestrial ecosystems (biodiversity)** due to water scarcity and land use changes driven by agriculture and energy.
  Agriculture and increasing energy demand transform(ed) the natural habitats and might need even more area and water for secure production, which can have direct and indirect impacts on rivers and land ecosystems.
  Water scarcity has direct and indirect impact on floodplains/wetlands, especially along freshwater bodies used for irrigation as well as the hydropower development has negative impact on the longitudinal connectivity of the water bodies, hence the ecosystems.

For the specific modelling of the Danube River Basin Case Study, the large-scale water resources model PCR-GLOBWB 2[4] (Sutanudjaja et al., 2018; Figure 56) has been adopted, which is also used for the global hydrological modelling in WP3, and which is applied at 5 arc minutes on a daily time step. This model setup is equally adopted for the Danube River Basin Case Study. In Tier 1 of WP3, PCR-GLOBWB is applied alongside the other dedicated models of the WEFE Nexus, being PROMETHEUS (Energy), CAPRI (Food) and GLOBIO (Ecosystems). Only in Tier 2 of WP3, these models will be loosely coupled and interactions within the WEFE nexus studied. These global simulations will then also be analysed for the Danube River Basin Scale in relation to the above challenges. In addition to these runs, PCR-GLOBWB will be used to evaluate specific scenarios and solutions that are tailored to address the challenges of the Danube River Basin on the basis of the indicators that have been identified in consultation with the stake holders (Table 9). A selection of these variables derived from the Tier 1 simulations is presented here, focusing on the PCR-GLOBWB output. To analyse the results at sub-basin level, four larger units have been identified, being the Upper and Lower Danube and the tributaries of the Sava and Tisza (Figure 57).

[4] In the remainder, the version number has been omitted and the model is referred to as PCR-GLOBWB.

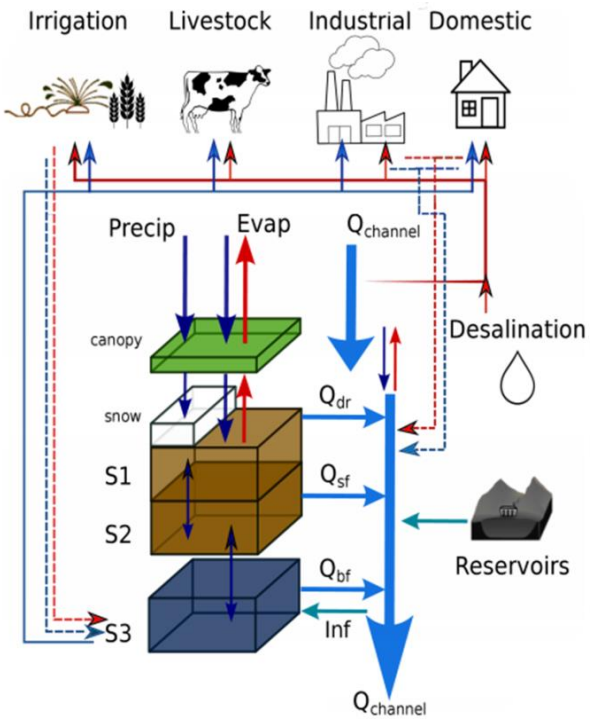

Figure 56. Model structure of the large-scale water resources model PCR-GLOBWB 2 (Sutanudjaja et al. 2018). Central in the schematic the vertical water balance is depicted that is evaluated for different land cover types within each cell, considering the canopy and two soil layers (S1 and S2), that interact with the groundwater store (S3). The propagation of the discharge $Q_{channel}$ along the drainage network over the cells, is depicted to the right, and within each cell, the discharge is fed by the runoff from the land surface (Q_{dr}, Q_{sf}, Q_{bf}) or lost because of riverbed infiltration (Inf). The resulting flood wave is modified by the regulating effect of lakes and reservoirs. At the top, the different sectors withdrawing water to meet human demands are depicted. Water withdrawals are shown as the solid lines and are taken from the groundwater store (blue) or the available surface water or supplied by desalination (red). Return flows (dashed lines) mostly flow back to the surface water system, with the exception of irrigation water that can enhance the deep percolation to the groundwater

For the specific modelling of the Danube River Basin Case Study, the large-scale water resources model PCR-GLOBWB 2[5] (Sutanudjaja et al., 2018; Figure 56) has been adopted, which is also used for the global hydrological modelling in WP3, and which is applied at 5 arc minutes on a daily time step. This model setup is equally adopted for the Danube River Basin Case Study. In Tier 1 of WP3, PCR-GLOBWB is applied alongside the other dedicated models of the WEFE Nexus, being PROMETHEUS (Energy), CAPRI (Food) and GLOBIO (Ecosystems). Only in Tier 2 of WP3, these models will be loosely coupled and interactions within the WEFE nexus studied. These global simulations will then also be analysed for the Danube River Basin Scale in relation to the above challenges. In addition to these runs, PCR-GLOBWB will be used to evaluate specific scenarios and solutions that are tailored to address the challenges of the Danube River Basin on the basis of the indicators that have been identified in consultation with the stake holders (Table 9). A selection of these variables derived from the Tier 1 simulations is presented here, focusing on the PCR-GLOBWB output. To analyse the results at

[5] In the remainder, the version number has been omitted and the model is referred to as PCR-GLOBWB.

sub-basin level, four larger units have been identified, being the Upper and Lower Danube and the tributaries of the Sava and Tisza (Figure 57).

Indicators are aggregated for distinct time slices taking into account the temporal variability when applicable that are centred on a 30-year normal period. These time slices are the baseline for the year 2000 (1985-2014), and the future periods 2050 (2035-2064) and 2080 (2065-2094)[6]. While all three combinations of SSP-RCPs have been evaluated, the emphasis is placed on SSP3-RCP7.0, using the mean or median for the available ensemble of five bias-corrected GCMs.

Table 9. List of indicators for the Danube River Basin Case Study.

ID or Name	Additional information	Unit	Scale
Water	Unless otherwise indicated, all variables are reported by PCR-GLOBWB; all values have a monthly time resolution (average, total)		
WAT_1 River Discharge	Amount of flow through the river channel	m^3/s	Multiple purposes
WAT_4 Reservoir volume	Storage per reservoir	m^3	Reservoirs
WAT_15 Total freshwater withdrawals	Total of all freshwater withdrawals from all resources in PCR-GLOBWB.	m^3	Cells
WAT_17 Surface water withdrawn	Total of all fresh water withdrawals from surface waters in PCR-GLOBWB.	m^3	River cells
WAT_22 Groundwater withdrawal	Total of all groundwater withdrawals in PCR-GLOBWB.	m^3	Cells

[6] Optionally, 2030 (2015-2044) has also been included.

Figure 57. Subdivision of the Danube River Basin into four main sub-basins (Upper Danube 256 000 km², Lower Danube 296 000 km², Sava 98 000 km² and Tisza 148 000 km²).

3.6.2 Evidence simulations results

Validation

The simulations with PCR-GLOBWB will be applied with different meteorological forcings and under different conditions to the future. To avoid that any structural bias would be introduced by calibration in the future projections, PCR-GLOBWB is applied with the default parameterization. The skill of the model to simulate the hydrology may be affected by this choice. Discharge is a commonly available measurement that encompasses the various hydrological processes that lead to the conversion of the effective precipitation into streamflow over the basin area. Hence, discharge measurement at three major stations on the Danube and the Tisza have been used to assess the model skill by means of the Kling-Gupta efficiency statistic (KGE, Gupta et al., 2009) that weighs the bias in the average value, the coefficient of variability and the correlation (Table 10). A KGE of 1 means perfect skill, a value of -∞ means no skill at all. The KGE was determined on the basis of monthly values over the period 1960-2010, the actual period being limited by data availability. Overall, the model is quite skilful, even without calibration although the average annual discharge is somewhat overestimated by the model and the variability underestimated. For the Tisza and Lower Danube, the correlation between observations and simulations is not as good as one would expect. That the overall values are well simulated is supported by the hydrographs, for which only the one at Ceatal Izmail, the most downstream station, is shown (Figure 58). Overall, the river regime is well-approximated by the simulations, although the high flows are somewhat overestimated.

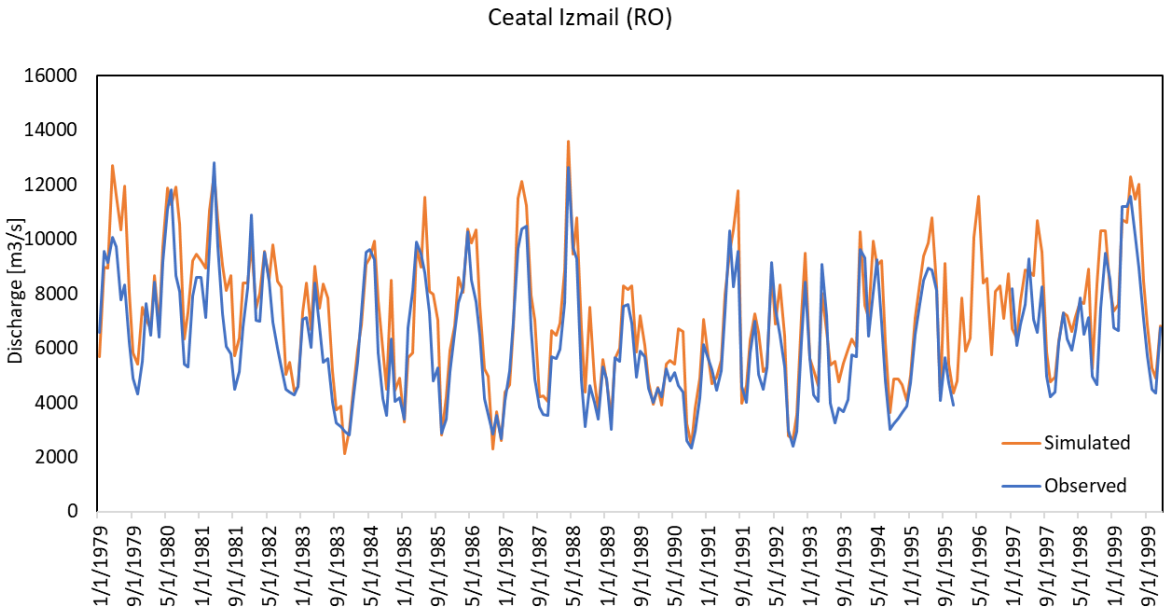

Figure 58: Hydrograph of the observed discharge from the GRDC inventory (Table 10) and the values simulated by PCR-GLOBWB

Table 10: Validation results for the Upper Danube (Bratislava), Danube (Ceatal Izmail) and Tisza (Szeged). The Kling-Gupta efficiency (KGE, Gupta et al., 2009) is used to express skill. A KGE of 1 means perfect skill, a value of -∞ means no skill at all. The cutoff for any skill in the original version of the KGE = -0.41. To constrain the range with skill from 0-1, the values have been scaled accordingly and given as the corrected values according to Knoben et al. (2019).

				Average Discharge [m3/s]		Standard deviation Discharge [m3/s]		Correlation coefficient [-]	Kling-Gupta efficiency [-]	
River	Station	Area [km2]	GRDC code	Simulated	Observed	Simulated	Observed	[-]	Original	Corrected
Danube	Bratislava (SK)	131331	6142200	2529	2067	816	688	0.921	0.698	0.787
	Ceatal Izmail (RO)	807000	6742900	7179	5976	2392	2699	0.683	0.608	0.723
Tisza	Szeged (HU)	138408	6444100	1182	860	554	528	0.841	0.590	0.710

Water balance

The water balance gives a first indication of the available renewable water resources and how they are affected by climate change. Climate change (RCP7.0, ensemble mean). For all sub-basins, the air temperature increases over time. With the higher temperatures, the potential evaporation also increases substantially, with similar relative changes for all sub-basins. The precipitation remains relatively the same but decreases slightly for the Danube as a whole at the end of the 21st century.

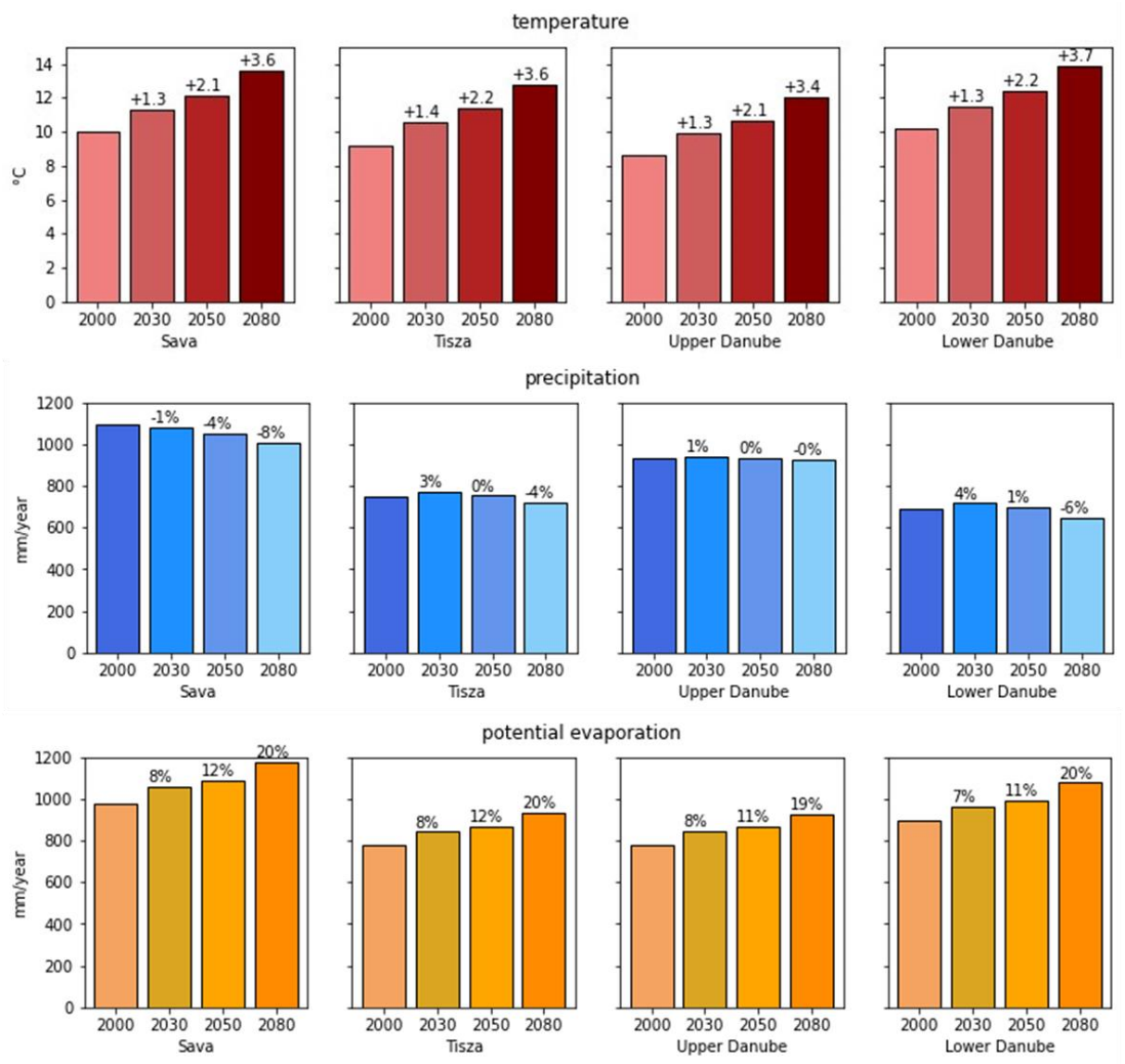

Figure 59. Climate change expressed as the basin-averaged ensemble mean for the selected period. Shown are the air temperature, precipitation and potential evaporation. The changes are relative to the values for 2000.

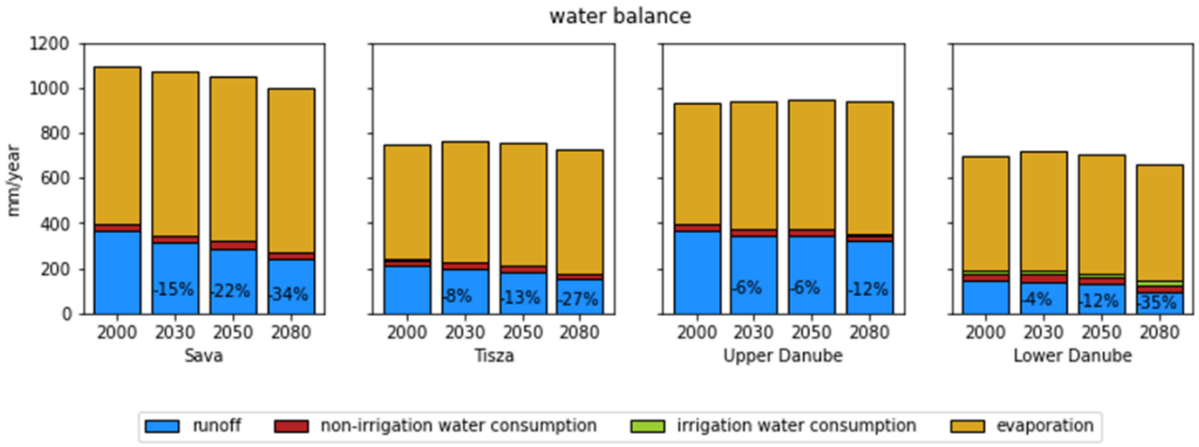

Figure 60. Water balance for the ensemble mean of SSP3-RCP7.0 for the sub-basins of the Danube River. The percentual change gives the relative change in the runoff relative to the year 2000.

As the precipitation remains nearly constant, the total amount of water expressed as water slice does not change much over the 21st century (Figure 60). However, due to the higher temperatures and larger potential evaporation, more of the precipitation is lost to evaporation (including transpiration) and less remains for runoff. Also, consumption of water (i.e., withdrawals minus return flows) for human purposes is small and constitutes a minor amount of the water balance on average. All-in-all, the runoff decreases for all sub-basins over the 21st century. The largest decreases occur over the warmer parts of the Danube (Lower Danube and Sava) with a decrease of 35% towards the end of the 21st century, whereas the decrease of 12% is less pronounced for the wetter and cooler Upper Danube.

Water demand and withdrawal

The diminishing runoff of Figure 60 implies that the amount of renewable water resources per sub-basin is decreasing. Only the Lower Danube also receives water from upstream and this is the largest share of renewable water available on average (Figure 61). Overall, the conclusion would be that there is sufficient water to meet the human demands, and the consumption is a minor amount of the total water balance (Figure 60). Yet, more water is withdrawn than what is consumed and this may lead to water stress among the sectors of the WEFE nexus if the demand is high compared to the available water. For the historic period (2000), it can be observed that for all sub-basins the demand can be fully met and that this is largely taken from the available surface water (Figure 61).

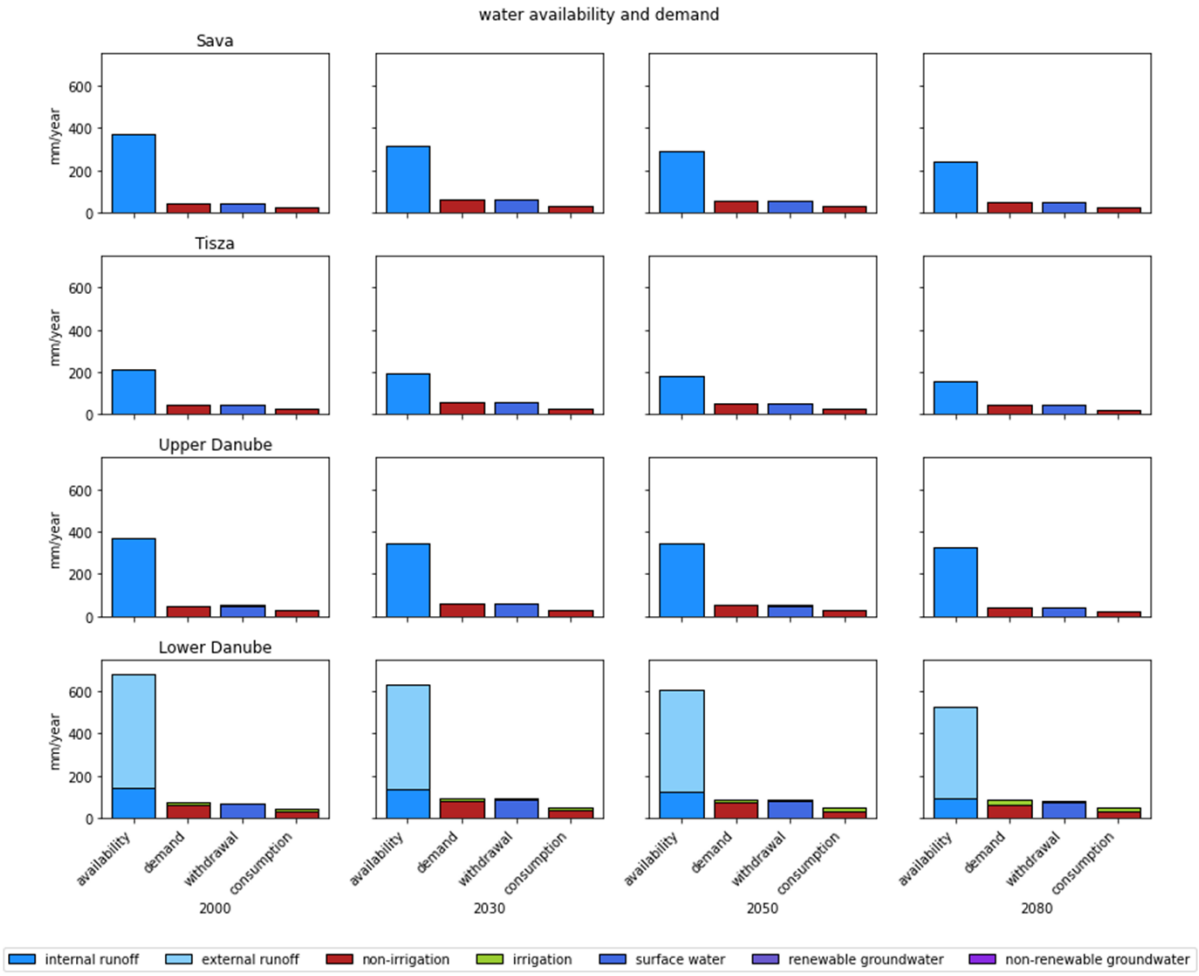

Figure 61: Renewable water resources, water demand, withdrawal and consumption. The renewable water resources are given by in terms of the renewable internal and external runoff, while the withdrawals are split according to their provenance (surface water, renewable and non-renewable groundwater). Demand and consumption are split into two groups, being irrigation and non-irrigation, the latter comprising households, industry (manufacturing and energy production) and livestock.

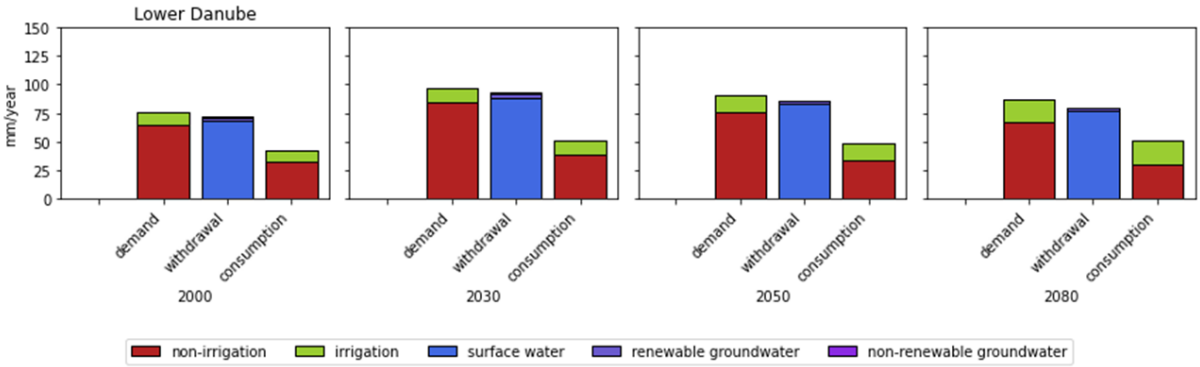

Figure 62: Water demand, withdrawal and consumption. As above, but rescaled and shown for the Lower Danube only.

Among all sectors, non-irrigation water demand is the largest over all periods and for all the SSPs, but the water demand increases and the distribution changes. For example, in SSP3 in combination with RCP 7.0 the total water demand increases in the order of 30% by 2030 relative to 2000 (Figure 61; for clarity, the demand, withdrawals and consumption are shown rescaled for the Lower Danube only in Figure 62). For all sub-basins, the irrigation demand increases more than the other sectors (non-irrigation comprising the domestic, industrial and livestock sectors), as a result of two developments: first, the population is decreasing in the second half of the 21st century and this lowers in particular the non-irrigation water demand; second, the warmer climate with more evaporation and the corresponding increase in irrigated area, increases the irrigation water demand (Figure 63). The increase in irrigated area is small in absolute terms but important; while the irrigated area decreases after 2030, the higher irrigation water requirement per unit area leads to an overall increase in the total irrigation water demand.

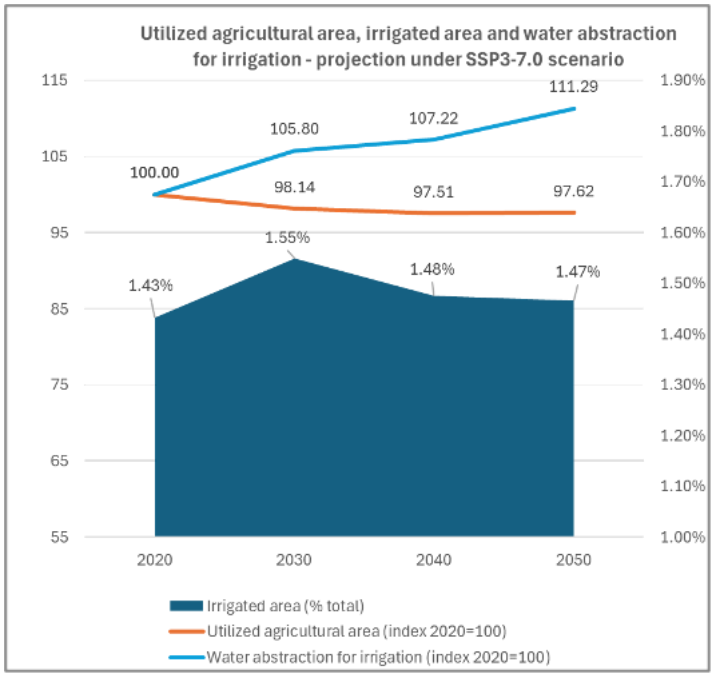

Figure 63. Temporal change in total agricultural area (normalized), the irrigated area (percentage of total area) and the irrigation water abstraction (normalized). Data from the Tier 1 simulation by CAPRI for SSP3-RCP7.0.

From irrigation, a larger share of the withdrawals is consumed and as a consequence irrigation increases relative to the non-irrigation sector if consumption is considered (Figure 62). While the availability of renewable water on average is high, local shortages can occur during low flow periods, particularly in the Lower Danube where the demand is close to the internally renewable water resources. For the other sub-basins the situation is less dire but there too the water demand increases while the availability of renewable water decreases. In terms of the water withdrawals, it is evident that most water is taken from the surface water with minor fractions being taken from the renewable surface water and the non-renewable groundwater. This reflects the average availability of surface water, with little variations between

the periods (Figure 62). For the Lower Danube, the simulated withdrawals are not always sufficient as the groundwater pumping capacity of PCR-GLOBWB is capped at reported values that have been projected in the future. As a consequence, a water gap opens and this becomes larger with time and implies that not all human demands can be met and competition between the sectors of the WEFE nexus for the available resources will be large.

Discharge

The runoff that accumulates and is routed along the drainage network, gives the discharge that has been validated in Table 10.Eventually, all the net runoff (runoff minus consumption) propagates downstream but the temporal signal varies, dependent on the residence time in the slower stores of the hydrological system (lakes and reservoirs; groundwater) and the travel time of the flood wave. High and low flows (see Figure 58) are of particular concern as they are respectively linked to flood events or to situations in which low stands may impair surface water intake, obstruct river navigation or limit reservoir operations. Flow duration curves (FDCs) have been constructed that give the exceedance probability of the discharges in ascending order.

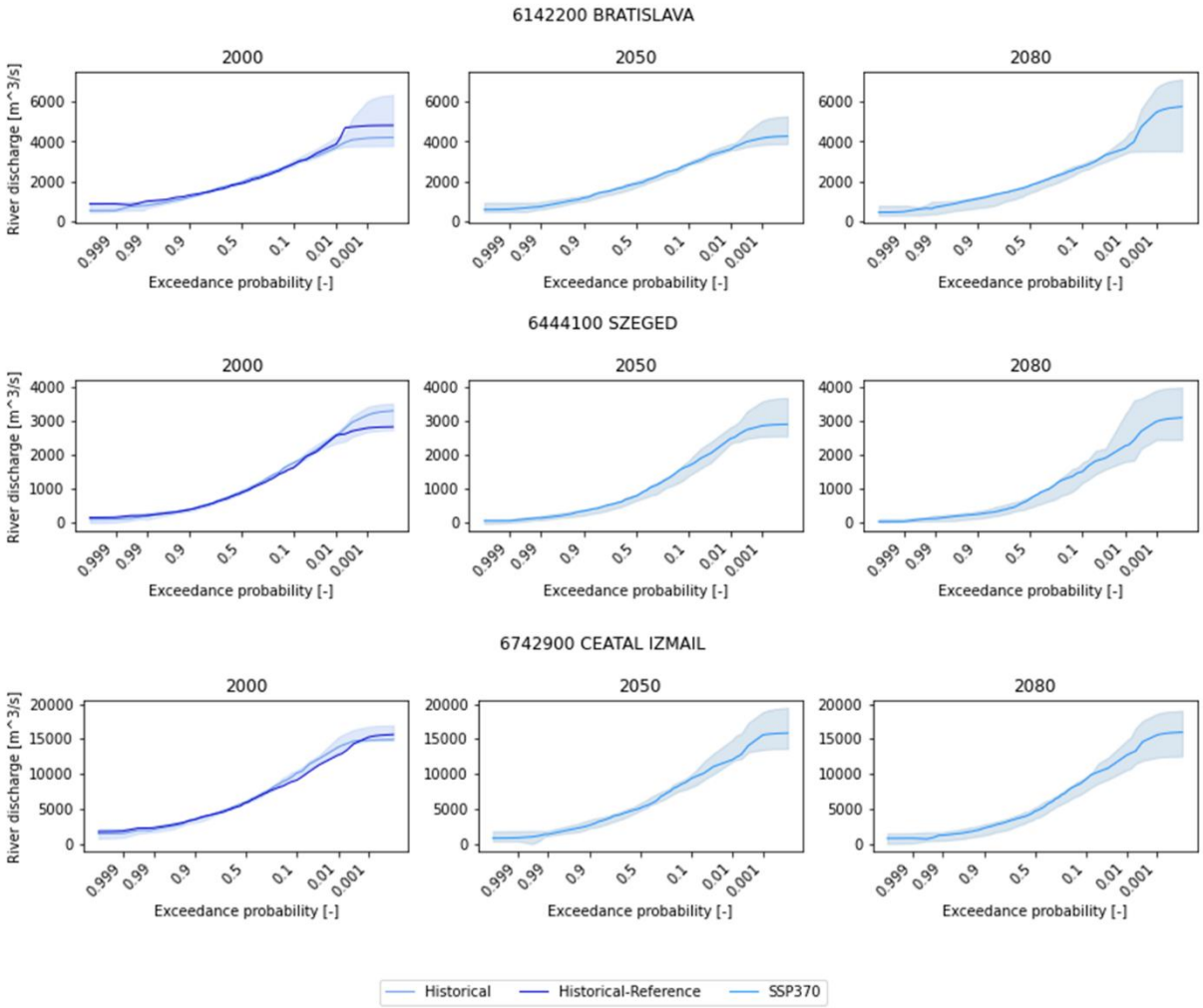

Figure 64. Flow duration curves for stations on the Upper Danube (Bratislava), Tisza (Szeged) and Lower Danube (Ceatal Izmail) (see also Table 10). The period-of-length flow duration curves are based on 30-years of monthly

discharges centred on the year given. The shaded area spans the FDC of all five GCMs of RCP7.0, the light-blue line is the median while the dark blue line for the Historical Reference is based on the observed climate over the historical period.

For the historical period, the bias-corrected GCMs simulate discharges that are close to those for the reference historical climate for the more common discharges but that can deviate substantially for the less frequent tails. This concerns both the ensemble median as the range of the GCMs. For the Upper Danube and Tisza, the agreement spans the range 1-99% but for the Lower Danube, which includes nearly the total drainage area for the Danube, the deviation for the higher discharges is large for the upper 10%.

The projected FDCs show an increase in the range that becomes wider further in the future and that show greater uncertainty for the higher discharges. This increased uncertainty is a direct result of differences in sensitivity of the GCMs to greenhouse gas emissions and the reduced influence of the bias-correction that keeps the simulations in check for the year 2000. Still, the FDCs are relatively well-constrained for the more frequent discharges (exceeded less than 10% of the time on average). Thus, conclusions on the low flows can be viewed as more certain than those on the high flows.

The decrease in runoff that was observed in the water balance for all sub-basins, is also evident in the FDCs. The mean discharge decreases and the change is the largest for the downstream station on the Lower Danube (Ceatal Izmail). This is not only reflected by the mean but also by an increased variability in the discharge, as the FDCs become more curved, with more frequent low flows and some infrequent but high discharges. This shift in the hydrological regime can be observed for all three stations but they reflect the findings of the water balance that the decrease in the runoff is the higher for the Lower Danube (and the Sava, not shown), followed by the Tisza and then the Upper Danube. This increased variability with more frequent low flows also implies that in the future the environmental flow requirements for streamflow will be violated more often. All stations show an increased occurrence of low flow events, which explains partly the reduced availability of surface water in the future and will have implications for the navigability of the Danube and its main tributaries in the future. At the other end, the sharp increase in high flows is evident for the station on the Upper Danube (Bratislava) by 2080. This is likely due to a change in the amount and timing of the snow melt, making the area more sensitive to flooding.

Reservoir capacity

In the Tier 1 simulations for the Danube, reservoirs were simulated with the standard reservoir operations and parameterization of PCR-GLOBWB (Sutanudjaja et al., 2018). This means that all reservoirs are treated as hydropower reservoirs of which the primary objective is to store water and that the release is directly proportional to the amount of storage. The parameterization is based on the GRanD database (Lehner et al., 2011), that includes the largest reservoirs in the world that were constructed up to 2010. No projected reservoirs were added for the future yet, and the storage in all simulations remains near constant over time (not shown). Still, the amount of reservoirs constructed over the historic period increases substantially, with both the number of reservoirs and the overall capacity increasing more than eightfold over the period 1960-2000. No new reservoirs were added according to the GRanD dataset after that date (Figure 65).

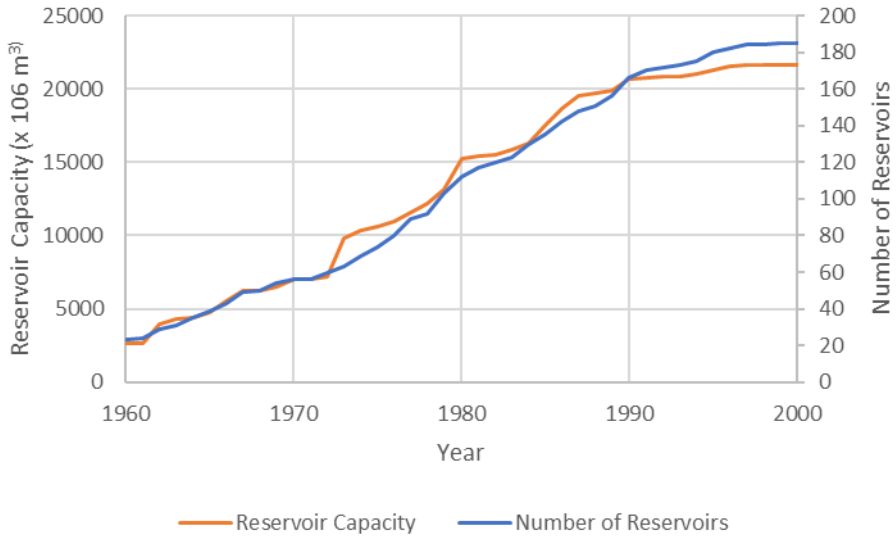

Figure 65: Historic development of the number of reservoirs and the total capacity for the Danube River Basin over the historical period 1960-2000 (from GRanD).

The reservoir capacity is substantial in terms of the total discharge, being in the order of 10% of the total discharge at the outlet of the Danube River Basin. It can therefore be postulated that the impact of reservoir construction is relevant in terms of buffering streamflow for human water needs, including water supply and energy production, but at the same time will have detrimental effect for freshwater biosystems along the river as a result of regulation and fragmentation.

3.6.3 Summary of key evidence

Three major challenges were identified for the Danube. Here, the indicators are presented at a high level of aggregation, giving the overall tendency in the development for the Danube River Basin under the impact of climate change and socio-economic development, with particular focus on SSP3-RCP 7.0.

The evidence shows that in the future the Danube River Basin will become more water scarce, with substantially more low flows and greater stress among the different sectors of the WEFE nexus. This is primarily driven by climate change. Hence, human water demands are generally met but periods of water gaps become more frequent and will negatively affect the availability of stream flow to meet the environmental flow requirements and will decrease navigability (Challenges 1 and 3). At the same time, the river regime becomes more variable, with low frequency high flows increasing in magnitude, particularly towards the end of the 21st century for the Upper Danube, although this change is relatively uncertain. This would imply that the flood hazard could increase here and further downstream of the Danube.

Socio-economic changes are particularly evident in the changing water demand, with non-irrigation water demand falling over the 21st century as a result of the projected population

decline after the mid of the century. This decrease in water demand is partly compensated for by the increase in irrigation water demand. Partly, the irrigated area increases and falls again in line with the projected population trend. At the same time, higher irrigation water demand per unit area as a result of climate change leads to an overall increase in the total irrigation water demand over the Danube River Basin. This increase is the greatest for the sub-basins that have Mediterranean and Continental climates as the Sava, Tisza and particularly the Lower Danube. These are also the sub-basins that are already water scarce and will become more so in the future. In particular, the Lower Danube is vulnerable to water scarcity as the relative availability of internal renewable water resources compared to the increased water demand is decreasing and the dependence on external water from the other sub-basins is increasing, thus increasing the vulnerability of all the sectors of the WEFE nexus in periods of lower discharges. Partly, groundwater compensates for the decreased surface water availability but its availability is limited and insufficient to avoid the occurrence of possible water gaps in the future. This has negative consequences for food production within the Danube River Basin (Challenge 2).

Reservoir construction can help to increase water availability in the future and increase the production of renewable energy resources by hydropower. However, already the Danube River Basin is fragmented and reservoir construction in combination with larger withdrawals from surface water resources, will have negative consequences on the streamflow from an environmental perspective and require the evaluations of solutions that minimize the negative trade-offs of water dependence in the WEFE nexus (Challenge 3).

4 Conclusions and summary of key evidence across case studies

Due to the variance across the basin case studies in terms of factors such as the most important WEFE challenges identified, modelling toolchains, and prior experience of the modelling teams in the case study basin, there is quite a broad range of reference evidence reported in this deliverable. The summary of key evidence for each case study basin, reported respectively in the above sections 3.1.3, 3.2.3, 3.3.3, 3.4.3, 3.5.3, and 3.6.3, show how, expectedly, the WEFE evidence is specific to the considered river basin. While for the evidence specific to each case studies we refer the reader to the above sections, we could identify a few considerations, which are common across the evidence resulting from simulation in all case studies.

The first consideration is that, wherever water is used across different sectors and across different riparian states, there is an inevitable competition for the allocation of the resource. Favouring allocation to one stakeholder generally implies an impact for the use by one or more other stakeholders. This is not a novel result that can be ascribed to GoNEXUS, but this project has demonstrated that advanced modelling tools and a systematic taxonomy of indicators help to identify and, especially, quantify the trade-offs. The importance of a detailed

quantification, in terms of both spatio-temporal resolution and breadth of accounted sectors, is key to support basin authorities and stakeholders in defining the evidence that can inform the search for and implementation of solutions. In this respect, all the case studies considered showed that, informing the modelling activities through a participatory approach based on stakeholders' dialogues leads to more effective results.

With regard to impact of future climatic and socio-economic drivers, a common thread across the case studies is that the largest impact is created by climatic extremes, be these prolonged dry spells causing long periods of low flow conditions or flood conditions, or heat wave spells. Most of the water use compartments are generally able to cope with changes in average regime but turn into critical conditions during periods of extreme forcing, which exacerbate the WEFE interdependencies. This is the case for drought and low flow conditions as well as for floods. The former are predicted to become more frequent, the latter present, in general, a dual response to climate change forcing with high frequency (low return period) flood magnitudes decreasing and low frequency (high return periods) flood magnitudes increasing.

This more variable behaviour of extremes than in the reference scenarios is consistent with another common feature of climate change scenarios impacts, which concerns the increased variability. Such variability is generally driven by the climate change forcing, while water demand across sectors seem to follow the impact of such variability. Regional differences related to population dynamics – e.g. growth in river basins located in regions of the global South and contraction in Europe – as well as possible solutions (discussed in the forthcoming D5.7) can mitigate or exacerbate the effect of the increased variability. However, one can likely conclude out of the simulations across all case studies that both natural water systems and anthropic infrastructures and management strategies will have to cope with the increased variability, either accepting the related risk or planning and implementing solutions to mitigated it.

A positive news seems to concern the dependence of the evidence on the trend signal used by the forcing scenarios. The common traits of the evidence discussed here above seem to be largely independent from the models that generated the climate forcing scenarios. Variability and influence on extremes represent a common thread across the impact caused by the forcing scenarios with quantitative differences that are not highly significant.

Two final considerations seem to emerge from the simulated evidence. The first concerns the impacts, which can be properly investigated, analysed and quantified across the different sectors only if an effort is done in search of the most predictive indicators. These are in some cases different from those conventionally used and a participatory approach based on dialogues is essential to maximise the chances of defining the most effective general and sectoral indicators. The second concerns the solution that will be the object of the next round of simulations. The evidence emerged from the simulations presented in this deliverable have highlighted the importance of models that explicitly address trade-offs and that quantify them. Only if models are capable of quantifying the trade-offs it will be possible to measure the impact of solutions and, thus, aim to infrastructural and management changes that allow mitigating the impacts of climate and socio-economic changing forcing. This is one of the strengths of the model toolbox of GoNEXUS, which will be challenged in the upcoming deliv-

erable D5.7, in which the reference evidence will be expanded, and tested against the solutions developed in WP7 to address the relevant most impactful WEFE challenges in each case study.

5 References

Denaro, S., D. Anghileri, M. Giuliani, and A. Castelletti (2017), Informing the operations of water reservoirs over multiple temporal scales by direct use of hydro-meteorological data, Advances in Water Resources, 103, 51–63

England, J. F. J., Cohn, T. A., Faber, B. A., Stedinger, J. R., Thomas, W. O. J., Veilleux, A. G., Kiang, J. E., and Mason, R. R. J. (2018). Guidelines for Determining Flood Flow Frequency -Bulletin 17C. Techniques and Methods Book 4, Chapter B5, U.S. Geological Survey. Version 1.1, May 2019

Garcia-Molla, M., Sanchis-Ibor, C., Macian-Sorribes, H., Avella-Reus, L., & Pulido-Velazquez, M. ,2016: Los mercados de agua en la demarcación hidrográfica del Júcar (in Spanish). In J. A. Gomez-Limon & J. Calatrava-Leyva (Eds.), Los mercados de agua en España: presente y perspectivas (p. 480). Almeria, Spain: Cajamar Caja Rural.

Garcia-Molla, M., Sanchis-Ibor, C., Macian-Sorribes, H., Avella-Reus, L., & Pulido-Velazquez, M. (2016). Los mercados de agua en la demarcación hidrográfica del Júcar. In J. A. Gomez-Limon & J. Calatrava-Leyva (Eds.), Los mercados de agua en España: presente y perspectivas (p. 480). Almeria, Spain: Cajamar Caja Rural.

Giuliani, M., J.R. Lamontagne, M.I. Hejazi, P.M. Reed, and A. Castelletti (2022), Unintended consequences of climate change mitigation for African river basins, Nature Climate Change, 12, 187–192

Gupta, H. V., Kling, H., Yilmaz, K. K., and Martinez, G. F.: Decomposition of the mean squared error and NSE performance criteria: Implications for improving hydrological modelling, J. Hydrol., 377, 80–91, https://doi.org/10.1016/j.jhydrol.2009.08.003, 2009.

IPCC: Annex I: Glossary [van Diemen, R., J.B.R. Matthews, V. Möller, J.S. Fuglestvedt, V. Masson-Delmotte, C. Méndez, A. Reisinger, S. Semenov (eds)]. In IPCC, 2022: Climate Change 2022: Mitigation of Climate Change. Contribution of Working Group III to the Sixth Assessment Report of the Intergovernmental Panel on Climate Change [P.R. Shukla, J. Skea, R. Slade, A. Al Khourdajie, R. van Diemen, D. McCollum, M. Pathak, S. Some, P. Vyas, R. Fradera, M. Belkacemi, A. Hasija, G. Lisboa, S. Luz, J. Malley, (eds.)]. Cambridge University Press, Cambridge, UK and New York, NY, USA. https://doi.org/10.1017/9781009157926.020 , 2022

Knoben, W. J. M., Freer, J. E., and Woods, R. A.: Technical note: Inherent benchmark or not? Comparing Nash–Sutcliffe and Kling–Gupta efficiency scores, Hydrol. Earth Syst. Sci., 23, 4323–4331, https://doi.org/10.5194/hess-23-4323-2019, 2019.

Lehner, B., Reidy Liermann, C., Revenga, C., Vörösmarty, C., Fekete, B., Crouzet, P., Döll, P., Endejan, M., Frenken, K., Magome, J., Nilsson, C., Robertson, J., Rödel, R., Sindorf, N., and Wisser, D.: High- resolution mapping of the world's reservoirs and dams for sustainable river-flow management, Front. Ecol. Environ., 9, 494–502, 2011.

Macian-Sorribes, H. (2017). Design of optimal reservoir operating rules in large water resources systems combining stochastic programming, fuzzy logic and expert criteria [Tesis doctoral no publicada]. Universitat Politècnica de València. https://doi.org/10.4995/Thesis/10251/82554

Mezger, G., L. De Stefano, and M. González del Tánago (2022). Analysis of the Evolution of Climatic and Hydrological Variables in the Tagus River Basin, Spain. Water. 14. 818. 10.3390/w14050818.

Pellicer-Martinez, F. and Martínez-Paz, J.M. (2015), Transferability of the parameters of the lumped models. Water Environ J, 29: 43-50. https://doi.org/10.1111/wej.12091

Perni, A. & J. Martínez-Paz, (2017) Measuring conflicts in the management of anthropized ecosystems: Evidence from a choice experiment in a human-created Mediterranean wetland. Journal of Environmental Management. 203, Part 1. 40 - 50. 10.1016/j.jenvman.2017.07.049.

Sutanudjaja, E. H., van Beek, R., Wanders, N., Wada, Y., Bosmans, J. H. C., Drost, N., van der Ent, R. J., de Graaf, I. E. M., Hoch, J. M., de Jong, K., Karssenberg, D., López López, P., Peßenteiner, S., Schmitz, O., Straatsma, M. W., Vannametee, E., Wisser, D., and Bierkens, M. F. P.: PCR-GLOBWB 2: a 5 arcmin global hydrological

and water resources model, Geosci. Model Dev., 11, 2429–2453, https://doi.org/10.5194/gmd-11-2429-2018, 2018.